INFLUENCE OF THE DISTRIBUTOR AND THE PLENUM CHAMBER VOLUME ON FLUIDIZED BED HYDRODYNAMICS

by

KIARASH VAKHSHOURI

B.Sc., Sharif University of Technology, 2006

A THESIS SUBMITTED IN PARTIAL FULFILLMENT OF
THE REQUIRMENT FOR THE DEGREE OF
MASTER OF APPLIED SCIENCE

in

THE FACULTY OF GRADUATE STUDIES
(CHEMICAL ENGINEERING)

THE UNIVERSITY OF BRITISH COLUMBIA
(Vancouver)

June 2008

Abstract

Hydrodynamic experiments were conducted in a three-dimensional fluidized bed with a specially designed plenum chamber. The air supply system and plenum chamber are axially symmetric to minimize the influence of geometry. Glass beads of mean diameter 157 μm and FCC particle of mean diameter 70 μm were bed materials. Pressure fluctuations were measured in the bed, plenum chamber and across the distributor for two low-pressure-drop distributors, one with a single orifice, and one with 33 orifices having the same total open area as the single-orifice distributor. Velocity fluctuations ware also measured for the single orifice distributor by means of a custom-made hot-wire anemometer.

For the single-orifice distributor, the frequency spectrum of the distributor pressure drop fluctuations (differential pressure transducer) revealed multiple peaks, as reported by Kage et al. (2000). The sharpest peak is believed to represent the bubbling frequency. It was found that the bubbling frequency increased slightly with decreasing plenum volume. This is likely because of forming larger bubbles while using large plenum chamber volumes. The same trend was reported by Kage et al. (2000). The lower peak in the frequency spectrum of the distributor pressure drop fluctuations represented bubble eruptions at the bed surface, since it matches Baskakov et al. (1986) model suggested for bubbles bursting at the bed surface. For the multi-orifice distributor, effects of gas superficial velocity and bed depth on frequency spectra were found to be similar to those of from the single-orifice distributor. Decreasing plenum volume caused the broad frequency spectrum of the plenum pressure fluctuations to move slightly towards higher frequencies.

A model was developed to simulate bubble formation at a single orifice in a gas-solid fluidized bed. Two-stage bubble formation was assumed: an expansion stage, referring to a stage where the bubble grows spherically while it remains at the orifice, and a detachment stage where the bubble continues to grow while lifted off the plate, but still connected to the orifice by a small neck. The model was able to predict the variation of plenum pressure, bubble volume, and orifice flow rate with time correctly in the similar manner as previously reported by some researchers for gas-liquid system (McCann and Prince, 1969, Ramakrishnan et al., 1969, Tsuge & Hibino, 1983).

Table of Contents

List of Tables

List of Figures

Nomenclature

A	=cross-sectional area of column (m^2)
A_s	=cross-sectional area of hot-wire anemometer (m^2)
c	=velocity of sound in gas (m/s)
c_s	=specific heat of hot-wire sensor (J/kg.K)
C_D	=drag coefficient of bubble (-)
d_{Bo}	=diameter of bubble formed at orifice (m)
d_h	=grid hole diameter (m)
d_s	=sensor diameter (m)
d_p	=average particle diameter (m)
d_{pi}	=average screen aperture size (m)
D	=column diameter (m)
D_o	=orifice diameter (m)
E	=anemometer output voltage (V)
f	=frequency (Hz)
g	=acceleration due to gravity (m/s^2)
G	=volumetric flow rate through orifice (m^3/s)
h	=coefficient of convective heat transfer ($W/m^2.K$)
H	=bed height (m)
H_o	=static bed height (m)
H_{mf}	=bed height at minimum fluidization (m)
I	=electrical current (A)
J	=constant in Equation 1.2 (-)
k_s	=sensor thermal conductivity (W/m.K)
L	=orifice plate thickness (m)
L_h	=grid hole pitch (m)
L_{sl}	=length of slug (m)
m_b	=mass of particles inside bed (kg)
m_g	=mass of gas inside plenum chamber (kg)
M	=virtual mass for ascending bubble (kg)
N	=total number of grid holes (-)

N^* =number of unplugged grid holes (-)

N_c, N_c' =capacitance number (-)

P =pressure (Pa)

$p(x)$ =probability density function (-)

P_{atm} =atmospheric pressure (Pa)

P_b =pressure at bottom of bed (Pa)

P_{bubble} =pressure inside the bubble (Pa)

P_e =pressure at gas inlet to plenum chamber (Pa)

P_h =hydrostatic pressure at orifice plate, $P_{atm} + \rho_{bulk}.g.H$ (Pa)

P_p =pressure inside plenum chamber (Pa)

Q_o =instantaneous gas flow rate through orifice (m^3/s)

Q_e =volumetric gas flow rate entering plenum chamber (m^3/s)

r =radius of bubble at any instant (m)

r_o =radius of orifice (m)

R =universal gas constant, (8.314 J/mol. K)

R_s =electrical resistance of sensor (Ω)

s =vertical distance moved by bubble centre (m)

t =time (s)

T =absolute temperature (K)

T_s =sensor temperature (K)

T_f =fluid temperature (K)

T_{sl} =slug spacing factor (-)

U =superficial gas velocity (m/s)

U_f =fluid velocity (m/s)

U_h =velocity of gas through grid hole (m/s)

U_M =superficial gas velocity at which all orifices become operative (m/s)

U_{mf} =minimum fluidization velocity (m/s)

U_t =terminal velocity of particle (m/s)

U_{tf} =average "throughflow" velocity of gas through upper bubble boundary (m/s)

V =bubble volume at time t (m^3)

V_o =residual volume of bubble when bubble detaches, $4\pi r_o^3/3$ (m^3)

V_b =final volume of gas bubble after total detachment (m^3)

V_p =plenum volume (m^3)

x_i =mass fraction of particles in i^{th} size interval (-)

Greek Characters

α =viscosity-dependent parameter in Equations 5.16 and 5.17 (-)

ΔP_{dist} =distributor pressure drop (Pa)

ΔP_b =pressure drop across fluidized bed (Pa)

γ =ratio of specific heats (-)

ε =bed voidage (-)

ε° =emissivity (-)

ε_o =loose-packed bed voidage (-)

ρ_b =bulk density of particles (kg/m^3)

ρ_{bulk} =bulk density of dense phase in gas-solid fluidized bed (kg/m^3)

ρ_g =gas density (kg/m^3)

$\rho_{g,h}$ =density of gas entering grid hole at plenum conditions (kg/m^3)

ρ_l =liquid density (kg/m^3)

ρ_{mf} =density of incipient fluidized bed (kg/m^3)

ρ_p =particle density (kg/m^3)

ρ_r =resistivity (Ω.m)

ρ_s =density of hot-wire material (kg/m^3)

σ =Stefan-Boltzmann constant (5.6704×10^{-8} $kg/m^2.K^4$)

μ_{bulk} =effective bulk viscosity of gas-solid fluidized bed (kg/m.s)

μ_g =gas absolute viscosity (kg/m.s)

$\xi_d(t)$ =orifice discharge coefficient (-)

Superscripts

$\bar{}$ (over-bar) =time-average value

$\sim$ (over-tilde) =fluctuation about the mean

Subscripts

fe =final value after expansion stage

Acknowledgments

I would like to express my sincere gratitude to Professor John Grace for his excellent guidance, support and distinguished supervision which allowed me to complete this work. His door was always open to me whenever I needed his help and guidance. I also appreciate the dedication and respect he showed me.

I am very grateful to Mr. Siamak Elyasi who taught me LabVIEW programming and guided me with his ideas during this project. I would like to thank my friend and lab mate, Muammar Omar, who was always there to help me during the experiments and was an endless source of encouragement.

I would like to thank the Department of Chemical and Biological Engineering for providing a simulating and instructive environment for carrying out my studies. The financial support of Natural Sciences and Engineering Research Council and the Faculty of Graduate Studies of the University of British Columbia are also gratefully acknowledged.

Finally I want to express my special thanks to my family for their patience, encouragement and continuous support which made the difficult times more bearable.

Chapter 1: Introduction

1.1 Fluid-Solid Systems

Fluid-solid systems have been used in many physical processes like adsorption, absorption, filtration, particle coating and drying operations, as well as heat exchangers, quenching, etc. Various techniques have been developed to assure intimate contact between solids and fluid. Solids may be reactants, such as in calcination of limestone and roasting of sulfide ores. The solids may also be catalysts, as a heat carrier or to adsorb a gaseous species in order to improve conversion or selectivity and obtain better reactor performance. Such systems are used in synthesis reactions, reforming and cracking of hydrocarbons (Kunii and Levenspiel, 1969). Fluid-solid systems also play an important role in other areas such as electric power generation, food processing, biotechnology, pharmaceuticals and mineral processing.

1.2 Operating Regimes of Gas-Fluidized Beds

A fluidized bed is formed by passing a fluid, usually a gas, through a bed of particles supported on a distributor. Although, even after passing the minimum fluidizing velocity, particles touch each other, the friction between particles is so small that this system acts like a liquid with a density of the bulk density of powders (Geldart, 1986). Fluidized beds have been extensively used for contacting solid and fluids because of their special characteristics such as excellent mixing resulting in radial and axial isothermal conditions, and high heat and mass transfer due to the motion and their fluid-like state of the particles.

Several flow patterns/regimes have been identified with increasing gas velocity (i.e., fixed bed, delayed bubbling or particulate fluidization, bubbling, slugging, turbulent fluidization, fast fluidization and dilute pneumatic conveying) as shown in Figure 1.1. For bubbling fluidization, it is difficult to describe the flow of gas due to random bubble generation and eruption. Moreover, bubble size can affect fluidization performance. For example, for large bubbles, gas-solid contacting decreases. There are several design factors which can influence the bubble size and fluidization performance such as distributor design as discussed below.

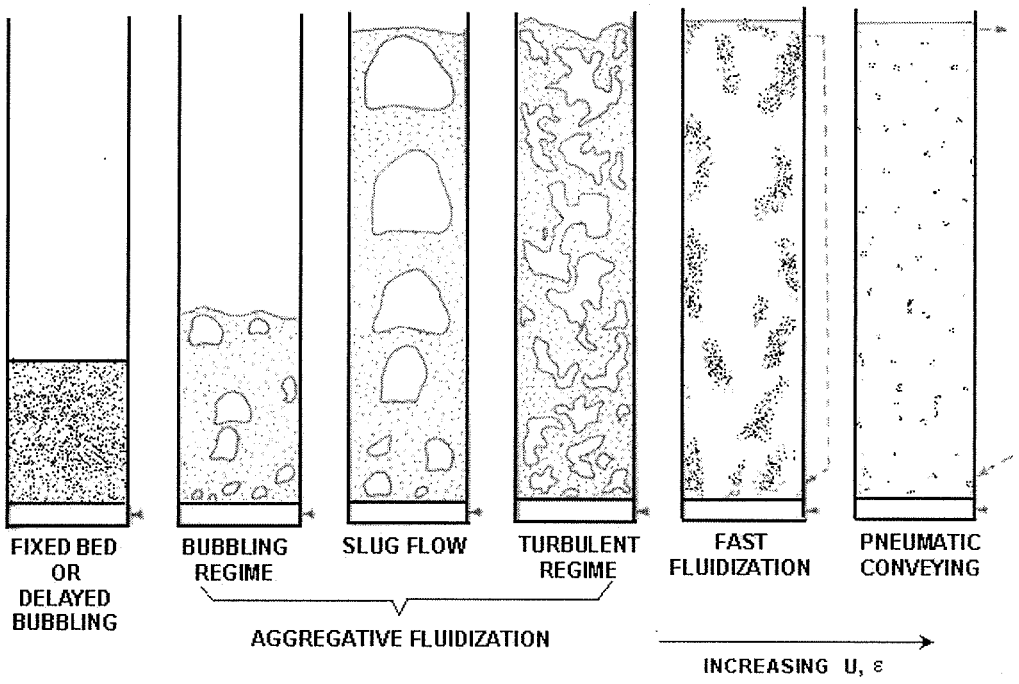

Figure 1.1. Flow patterns in gas-solid fluidized beds (modified from Grace, 1986).

1.3 Importance of Distributors in Fluidized Beds

The performance of the gas distributor often determines the success or failure of a fluidized bed. Careless design of gas distributors or their malfunction in operation is usually responsible for serious difficulties encountered in fluidized beds (Geldart and Baeyens, 1985). In solid processing, the major concerns are to achieve rapid dispersion of solids feed and prevent segregation and settling of denser particles on the distributor which can cause variable temperature and rapid defluidization of the entire bed. Uniform gas distribution and small bubbles at the grid are major concerns in applications where high conversions are required. Therefore successful design of the distributor, including the pressure drop ratio, hole size, geometry, spacing, and dead zones, can play a key role in improving fluidization processes.

1.3.1 Distributor Pressure Drop

Low pressure drop distributors are known to cause poor fluidization (Svensson et al., 1996); that is some parts of the bed receive much less gas than others, and may be defluidized temporarily or permanently, while in other parts channeling occurs and gas forms semi-

permanent spouts. On the other hand, high pressure drop distributors, although they may result in more even gas distribution, consume more power in terms of air compressors and fans.

Agarwal et al. (1962) proposed that ΔP_{dist} should be about 10% of the bed pressure drop and never less than 3400 Pa (35 cm H_2O), whilst Whitehead (1971) suggested higher values of $\Delta P_{dist}/\Delta P_b$, such as 0.3 for even gas distribution. Hiby (1964) assumed a bubbling fluidized bed with even gas distribution (Figure 1.2 a); at the same flow rate the system was then disturbed, with some holes ceasing to operate and velocity in that region falling to U_1 and in region 2 rising to U_2 (Figure 1.2 b). As a consequence solids were displaced from region 2 to region 1 so $\Delta P_b(2) < \Delta P_b(1)$. On the other hand, $\Delta P_{dist}(2) > \Delta P_{dist}(1)$ because the velocity has risen in region 2. Hiby concluded that if the rise in the local distributor pressure drop is less than the fall in the same local bed pressure drop (i.e. $\Delta P_{dist}(2) + \Delta P_b(2) > \{\Delta P_{dist} + \Delta P_b\}_{\text{Original Condition}}$), the perturbation will be damped. Therefore he suggested $d(\Delta Pdist)/dU$ as a controlling factor for design considerations. Hiby's analysis led to a criterion for $\Delta P_{dist}/\Delta P_b$ of 0.15 for low values of U/U_{mf} and 0.015 at high velocities.

Geldart and Kelsey (1968), using a two-dimensional fluidized bed, concluded that the aspect ratio (bed height/bed width) influences the critical value of $\Delta P_{dist}/\Delta P_b$ for even gas distribution and stable fluidization (all holes in operation). They recommended that four factors be considered for distributor design; $\Delta P_{dist}/\Delta P_b$, $d(\Delta Pdist)/dU$, geometry, and open area fraction of orifices.

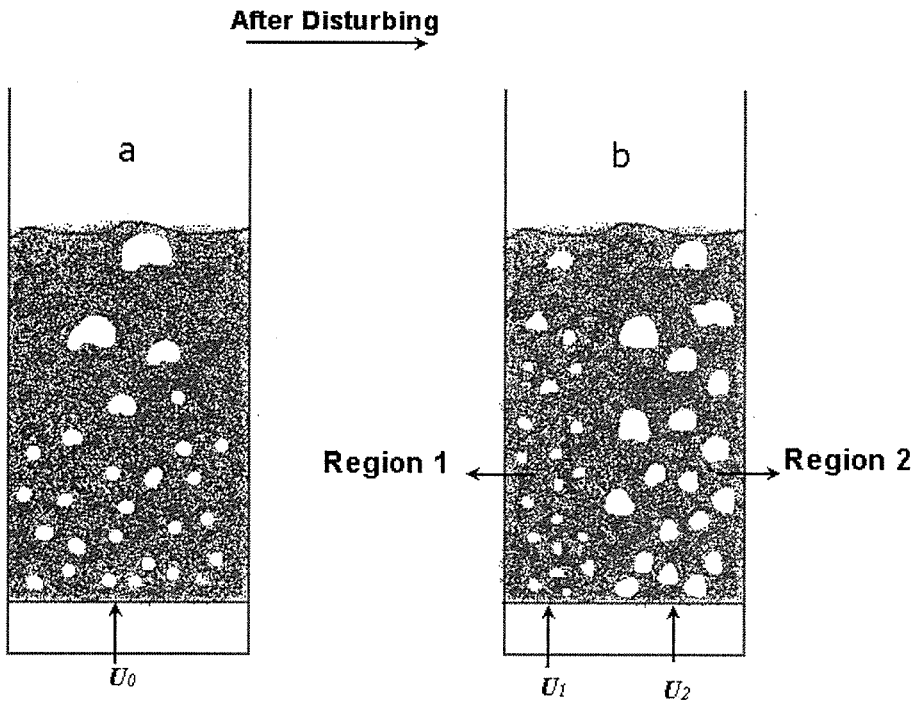

Figure 1.2. Bubbling bed with (a) even distribution (b) mal-distribution.

All orifices located in a distributor may not operate permanently at low superficial velocity. Sathiyamoorthy and Sridhar Rao (1981) determined U_M, the superficial gas velocity at which all the orifices in a distributor become operative for a uniformly fluidized bed;

$$U_M = U_{mf}\left(2.65 + 1.24\log_{10}\left(\frac{U_t}{U_{mf}}\right)\right) \tag{1.1}$$

The distributor to bed pressure drop ratio ($\Delta P_{dist}/\Delta P_b$) can be calculated from U_M and U_{mf}:

$$\frac{\Delta P_{\text{dist}}}{\Delta P_b} = J\left(\frac{U_{mf}}{U_M - U_{mf}}\right)^J \tag{1.2}$$

The authors suggested that J equals 2 after some data regression and proposed the rule of thumb that for fine particles $\Delta P_{dist}/\Delta P_b$ should be chosen as 0.12 and for coarse particles as 0.24 to achieve stable fluidization. They also mentioned that four factors can affect the operation of orifices; bed depth, flow-rate, bed material, and distributor geometry (Sathiyamoorthy and Rao, 1977).

Qureshi and Creasy (1979) reviewed the literature for data on successful and unsuccessful commercial fluidized beds and concluded that D/H_{mf} can influence the fluidization. For stable fluidization operation they suggested;

$$\frac{\Delta P_{dist}}{\Delta P_b} \geq 0.01 + 0.2\left(1 - \exp\left(-0.5\frac{D}{H_{mf}}\right)\right) \tag{1.3}$$

Since for low D/H_{mf} this equation gives very small values, Geldart and Baeyens (1985) suggested a more conservative approach for $H_{mf}/D < 0.5$;

$$\frac{\Delta P_{dist}}{\Delta P_b} \geq \exp\left(-3.8^{H_{mf}/D}\right) \tag{1.4}$$

After estimating pressure drop ratio, other factors for the distributor should be specified such as orifice size and spacing; however as Geldart and Kelsey (1968) mentioned the bubble size is more affected by pressure drop over the distributor than orifice size and spacing.

1.3.2 Geometry, Size and Lay-out of Orifices

Various types of distributor are used in industrial fluidized beds with their own advantages. A common one is a simple perforated plate. This is inexpensive and easy to scale up or down. A common disadvantage is bed weepage to the plenum chamber below. In order to overcome this issue bubble caps and laterally directed nozzles have been used, but they are more expensive and difficult to clean and modify. In some fluidized beds, sparger and conical grids have been used, but they are less common (Karri & Werther, 2003).

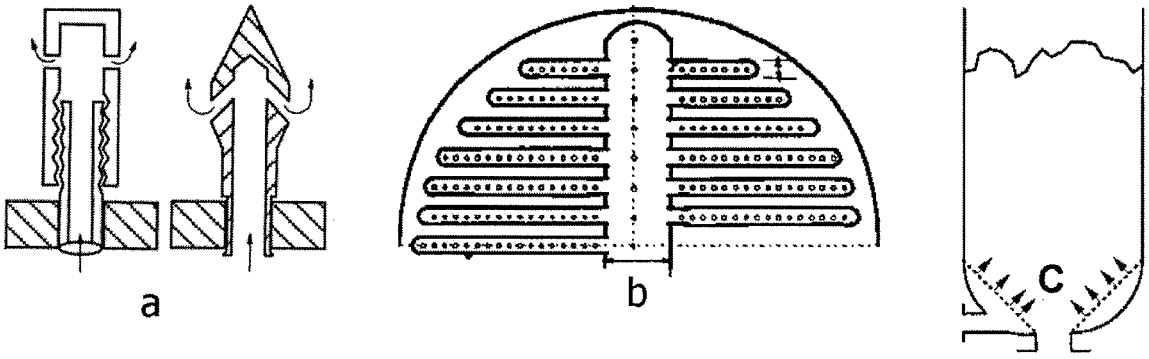

Figure 1.3. Different types of distributor: (a) bubble caps, (b) sparger, and (c) conical grids (Karri & Werther, 2003).

If holes are larger than about $5d_p$, the bed will drain into the windbox (Geldart and Baeyens, 1985). However, this limitation can be avoided by using a mesh under the plate or using bubble caps and horizontal holes (Geldart and Baeyens, 1985). To increase the gas residence time in the fluidized bed, it is desirable to have large number of small gas bubbles, which can be achieved by maximizing N, the number of holes, at the expense of having small holes (d_h) which may have some mechanical, cost and scale-up constraints. Karri and Werther (2003) suggested more than 10 holes per m^2 to prevent dead zones.

It is common to lay out the holes in triangular or square pitch in order to increase the uniformity of fluidization. A triangular pitch will result in more holes per unit area. Pitch should be defined in such a way to minimize dead zones and also provide even gas distribution. The relationship between the grid hole pitch, L_h, and the number hole density depends on whether the holes are laid out in a triangular or square pitch (Figure 1.4 a and b). Beside these layouts, different orifice spacing and layout have been used by researchers to determine their effects, such as the circular layout tested by Fan et al. (1981) (Figure 1.4 c).

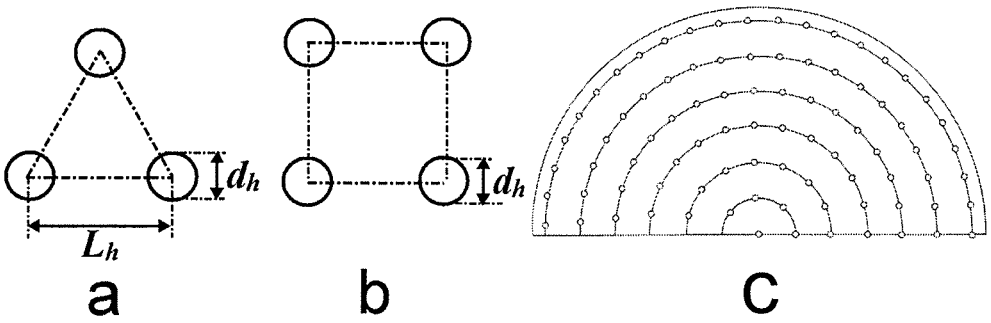

Figure 1.4. Different orifice layouts: (a) Triangular, (b) Square, and (c) Circular.

In addition to the above factors, there are some less important parameters which should be considered in distributor design, especially in large scale fluidized beds. The distributor should have sufficient strength to resist deformation under operating conditions and to support the static bed. It must also be able to withstand stresses caused by thermal expansion, operate for long periods without blocking and be easy to unblock, prevent weeping to the windbox, and minimizing erosion of the plate and attrition of the particles.

1.3.3 Boundary Conditions at the Distributor in CFD Simulations

In most CFD (Computational Fluid Dynamics) modeling and numerical simulations, researchers have assumed a uniform velocity boundary condition at the distributor. This is only a valid approximation in the case where the ratio of distributor pressure drop to bed pressure drop is high. As mentioned before when $\Delta P_{dist}/\Delta P_b$ is a necessary condition for gas to be distributed uniformly resulting in a uniform velocity profile boundary condition.

Peirano et al. (2002) noted that for a low pressure drop distributor, assuming a uniform velocity profile at the distributor is not accurate for CFD simulation. They performed numerical simulations considering fluidized bed and the air supply system together because air supply system can affect fluidized bed hydrodynamics for low-pressure-drop distributors, as suggested aslo by Svensson et al. (1996) and Johnsson et al. (2002). Figure 1.5 shows that for a low-pressure-drop distributor (part b), the velocity profile is less uniform compared with a high pressure drop distributor (part a).

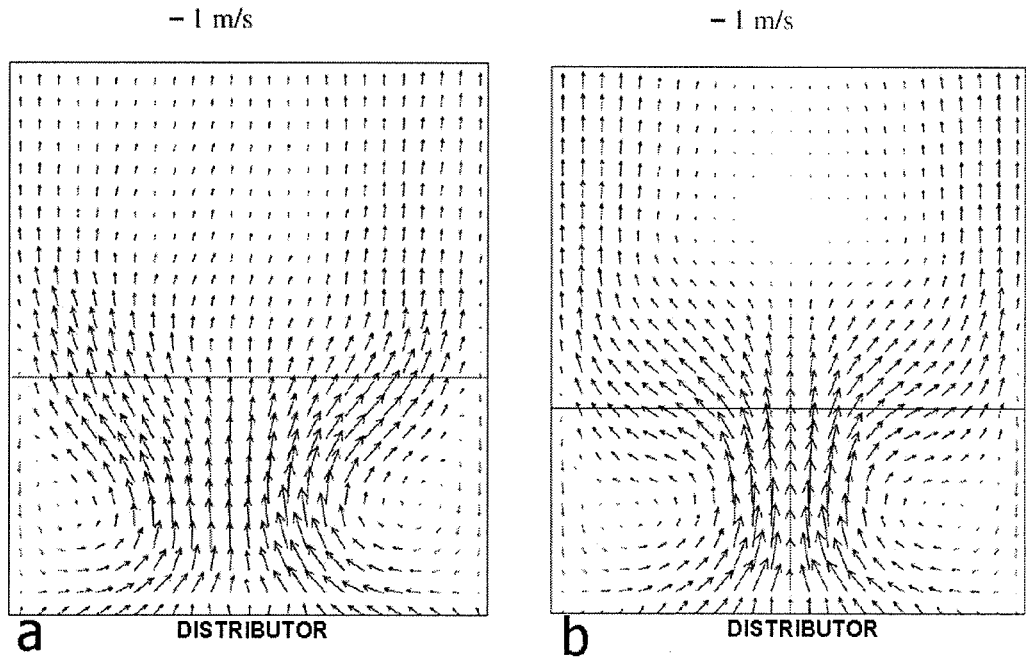

Figure 1.5. Time-averaged gas velocity field for (a) high-pressure-drop distributor and (b) low-pressure-drop distributor (bed height is indicated by the horizontal line). From Peirano et al. (2002).

The effects of air supply system and plenum chamber volume have been less investigated in the literature, but, as mentioned by Sasic et al. (2005), they can influence fluidization regimes. The following is a brief literature review of different sources of pressure fluctuations, especially for the plenum chamber.

1.4 Pressure Fluctuations in Gas-Solid Fluidized Beds

The dynamics of gas-solid fluidized beds can be significantly determined by pressure fluctuations. Recently Bi (2007) reviewed the literature focusing on the complex pressure fluctuation phenomenon in gas-solid fluidized beds and categorized the sources of pressure fluctuations into six sources.

The first source can be referred to the surface fluctuations due to bubble eruption at the surface. These are more pronounced when slugging occurs. Table 1.1 summarizes the equations giving the sloshing frequency.

Table 1.1. Summary of oscillation frequency caused by surface fluctuations

Authors	Equation	Origin of Theory	Application
Baskakov et al. (1986)	$f = \frac{1}{\pi}\sqrt{\frac{g}{H_{mf}}}$	Oscillation of an ideal liquid in U-tube	Deep beds; only one bubble erupts at a time
Sun et al. (1994)	$f = Cons.\sqrt{\frac{g}{D}}$	Liquid bed sloshing at surface	Deep beds
Van der Schaaf et al. (1999)	$f = \frac{1}{2}\sqrt{\frac{g}{\pi D}}$	Sloshing of a fluid in a cylindrical container	Deep beds

The second source of pressure fluctuations is due to the passage of bubbles and slugs. Table 1.2 summarizes the equations proposed for this source of fluctuations.

Table 1.2. Summary of oscillation frequency caused by bubble passage

Authors	Equation	Origin of Theory	Application
Baeyens and Geldart (1974)	$f = \frac{0.35}{Cons.}\sqrt{\frac{g}{D}}$	Equal-sized slugs	Slugging beds
(Kehoe & Davidson, 1973)	$f = \frac{U - U_{mf} + 0.35\sqrt{gD}}{L_{sl} + T_{sl}D}$	Change in hydrostatic head with passing slug	Slugging beds

The third source of pressure fluctuations in gas-solid fluidized bed is the self-excited oscillation of fluidized bed particles, known as mechanical vibration of particles, mostly observed in shallow fluidized beds (Hiby, 1967). Tamarin (1964) used the Buckingham π-theorem and introduced a modified Froude number, suggesting the first equation for frequency of self-excitation of particles. Hiby (1967) proposed a resonant frequency equation for particles in shallow fluidized beds ($H<10d_p$) by combining the action of gravity and a quasi-elastic lifting force. The weighted mean of natural frequencies of all particle layers was taken as the oscillation frequency of the bed. Verloop and Heertjes (1974) later modified Hiby's model assuming that all particles have the same frequency and that fluid and particles move in phase. Roy et al. (1990) reported that when a fluidized bed is subjected to an external disturbance, particles can sustain oscillations. They treated the fluidized bed as an organ pipe with a fixed boundary at the bottom (distributor) and a free boundary at the top surface. Table 1.3 summarizes natural frequency equations related to self-oscillations of particles.

Table 1.3. Summary of oscillation frequency caused by self-oscillation of particles

Authors	Equation	Origin of Theory	Application
Tamarin (1964)	$f = 0.342\frac{\sqrt{gD}}{\sqrt[3]{V_b}}\left(\frac{U}{U_{mf}}-1\right)^{0.55}$	π-theorem	Bubbling beds
Hiby (1967)	$f = \frac{2}{\pi}\left(\frac{3}{H_{mf}}\frac{(1-\varepsilon)}{3\varepsilon}\left(1-\frac{150\mu_g U_{mf}}{3\varepsilon^2\rho_p g d_p^2}\right)\right)^{\frac{1}{2}}$	Force balance on particle	Homogenous fluidization, Shallow beds
Verloop and Heertjes (1974)	$f = \frac{1}{2\pi}\sqrt{\frac{g(2-\varepsilon)}{H\varepsilon}}$ for laminar flow $f = \frac{1}{2\pi}\sqrt{\frac{g(1-\varepsilon)}{H\varepsilon}}$ for turbulent flow	As Hiby, entire bed moves in phase	Homogenous fluidization, Shallow beds
Roy et al. (1990)	$f = \frac{U_{so}}{4H}\sqrt{\frac{\rho_g}{\gamma\varepsilon(\rho_p(1-\varepsilon)+\rho_g\varepsilon)}};\ U_{so}=\sqrt{\gamma RT}$	Organ pipe with one fixed and one free boundary	Isothermal fluidization

Oscillation because of bubble/jet formation may be another source of pressure fluctuations. Davidson & Schuler (1960) investigated the formation of gas bubbles at an orifice in a low-viscosity liquid, defining the upward motion of a forming bubble by balancing the

buoyancy force against the rate of upward momentum of liquid surrounding the bubble and proposed an equation for bubble volume from which the bubbling frequency can be estimated:

$$f = g^{3/5}\left(\frac{6G}{\pi}\right)^{-1/5} \tag{1.5}$$

To consider gas flow through a bubble forming in a gas-solid fluidized bed, Nguyen and Leung (1972) did some experiments and proposed a correlation for bubble volume:

$$V_b = 0.53\frac{G}{f} \tag{1.6}$$

This equation can be used to modify the Davidson and Schuler (1960) equation. Later, Nelson et al. (1993) measured bubbling frequency by placing one pressure tap just above each hole located in the distributor. They used a peak detection procedure to determine the bubbling frequency based on the orifice-windbox pressure difference signal. They recommended using the number of unplugged grid holes, instead of the total number of grid holes, to calculate bubbling frequency leading to:

$$f = g^{3/5}\left(\frac{6}{\pi}\right)^{-1/5}\left(\frac{AU}{N^*}\right)^{-1/5} \tag{1.7}$$

Another source of pressure fluctuations may be due to bubble coalescence and splitting (Fan et al., 1981). The last source of pressure fluctuations in a gas-solid fluidize bed could be because of self-excited oscillation of gas in the plenum chamber when the resistance of the distributor is low as described below.

1.5 Importance of Plenum Chamber and Air-Supply System

Lirag and Littman (1971) were among the first researchers to find a strong correlation between measured pressure fluctuations in the bed and in the air-plenum of a bubbling fluidized bed, but they did not specify the air-feed system. They suggested bubbles escaping at the surface of the bed as the source of pressure fluctuations, and by using statistical methods (autocorrelation, power spectral density, and probability function) they concluded that there was a periodic component in the fluctuations. The frequency of this periodic component was generally lowered by raising the bed depth and increasing the particle size (because of more coalescence). They calculated the average bubble size by using the plenum chamber frequency

and compared with the Kato and Wen (1969) correlation, resulting in reasonable agreement with the measured frequency.

The first equation for natural frequency taking into account the plenum chamber characteristics was proposed by Davidson (1968). He assumed that isentropic compression and expansion of the air inside the plenum gives the stiffness of a "spring" and the mass of the particle bed provides the inertia (piston-like behavior) leading to:

$$f_n = \frac{1}{2\pi}\sqrt{\frac{\gamma \bar{P}_p A^2}{m_b V_p}} \tag{1.8}$$

By increasing the bed depth, this equation would give lower frequency, but Davidson (1968) did not provide any data for validation. Wong and Baird (1971) later modified the Davidson piston-like model by considering the effect of permeability on gas flow through the particles. They used a pulsed gas fluidized bed and modified Davidson's equation to:

$$f_n = \frac{1}{2\pi}\sqrt{\frac{\gamma \bar{P}_p A^2}{m_b V_p}}\left(1-\frac{\gamma \bar{P}_p U_{mf}^2 A^2}{4 m_b g^2 V_p}\right)^{\frac{1}{2}} \tag{1.9}$$

This equation predicts a lower frequency than the Davidson's model, especially for coarse particles, resulting from their higher permeability.

Moritomi et al. (1980) also found a strong correlation between the flow fluctuations in the air-feed system and the air-plenum pressure fluctuations. They used a rotational valve to generate defined flow pulsations to determine the pressure response of the plenum chamber. The pressure response was classified into five modes; 1) pulsed fluidization, 2) forced oscillation control, 3) free bubbling fluidization, 4) intrinsic fluctuation control, 5) transition mode. Moritomi et al. (1980) also proposed an equation for intrinsic resonant frequency of the fluidized bed:

$$f = \frac{1}{2\pi}\sqrt{\frac{\bar{P}_p A}{\rho_{mf} H_{mf} V_p}} \tag{1.10}$$

Fan et al. (1984) proposed a dynamic model, based on the assumption that fluctuations of bed height are affected by both present and time-delayed fluctuations of the gas flow rate

through the distributor. They treated the fluidized bed as a second-order vibration system and suggested an equation for natural frequency identical to that of Moritomi et al. (1980):

$$f_n = \frac{1}{2\pi}\sqrt{\frac{\overline{P}_p A^2}{m_b V_p}} = \frac{1}{2\pi}\sqrt{\frac{\overline{P}_p A}{\rho_{mf} V_p}}\frac{1}{\sqrt{H_{mf}}} \tag{1.11}$$

Baird and Klein (1973) compared their experimental bed oscillation frequencies with Davidson's model for variable plenum chamber volume. They found that the major frequency decreased with increasing plenum volume. They observed random irregular pressure fluctuations for small plenum chamber volumes (less than 0.0020 m^3), and relatively more regular, higher amplitude pressure fluctuations for a large windbox.

Kage et al. (1991, 1993, and 2000) used the power spectral density to characterize pressure fluctuations in a plenum chamber, identifying three peaks. One was found to be in agreement with the Davidson (1968) and Moritomi (1980) theory for natural frequency of the plenum chamber. The second peak matched the bubble eruption frequency as confirmed by camera recordings from the top of the fluidized bed. They concluded that the third peak was related to bubble generation, which was confirmed by an optical fiber probe placed at different radii inside the fluidized bed. Based on the experiments, they also noted that for a large plenum chamber, bubble generation is controlled by the natural frequency proposed by Moritomi et al. (1980).

Svensson et al. (1996) changed the number of orifices in the distributor to vary the distributor pressure drop and observed a transition of bed dynamics from a multiple bubble regime for a high-pressure-drop distributor to a single bubble regime for a low pressure drop distributor. The former case gave a broad frequency spectrum with low-amplitude pressure fluctuations, whereas in the later case the frequency spectrum showed a single sharp peak with higher amplitude of pressure fluctuations. In this regime the plenum chamber and fluidized bed are coupled (Svensson et al., 1996, and Sasic et al., 2004).

Sierra and Tadrist (2000) used a similar treatment as Hughes et al. (1955) and treating a gas-solid fluidized bed as an electric circuit, with the plenum acting as a capacitor and the distributor as a resistor. This electrical low-pass filter has a cut-off frequency of

$$f_c = \frac{1}{4\pi}\frac{\gamma \bar{P}_p A}{V_p}\left(\frac{U}{\Delta P_{dist}}\right) \tag{1.12}$$

This indicates that if the oscillations originating in the plenum chamber have a higher frequency than the cut-off frequency, they will be attenuated significantly by the gas distributor during transmission.

1.6 Scope of Work

This thesis investigates the effect of plenum chamber on the hydrodynamics of a fully cylindrical fluidized bed. Two low-pressure-drop distributors were used, a multi-orifice distributor and a single-orifice. The single-orifice distributor was used to determine the bubble formation in a gas-solid fluidized bed, taking into account the effect of the plenum chamber volume. The study involves measurements of absolute and differential pressure fluctuations. For the single-orifice distributor, velocity fluctuations were also measured by a custom-made hot-wire anemometer. Two types of particles were used in these experiments, representing groups A and B of the Geldart powder classification scheme.

Chapter 2 describes, in detail, the experimental equipment used in this research project. Details on the plenum chamber and distributor design appear in this chapter. The operating conditions, under which the experiments were carried out, are also covered in this chapter.

Chapter 3 describes the pressure fluctuation measurements in detail. Some correlation calculations used for this study are also included in this chapter, such as the autocorrelation and power spectral density. Pressure fluctuation frequencies are compared with correlations proposed in the literature. This chapter ends with a discussion of the results.

Chapter 4 introduces the hot-wire anemometry measurement technique and its use in the gas-solid fluidized bed. Then the detailed design of the hot-wire sensor and its circuit are described. This is followed by a discussion of measurement techniques and some difficulties in using this sensor. A discussion of the results is included at the end of this chapter.

Chapter 5 begins with a brief review of previous experimental and theoretical studies on bubble formation in a single orifice in gas-liquid and gas-solid systems. Then, details of a model suggested for this study are described, followed by model predictions.

Finally, the main conclusions drawn from this work are presented in Chapter 6, together with some recommendations for future studies. Several computer programs prepared for this work are provided in the appendices at the end of this thesis.

Chapter 2: Experimental Set-up

2.1 Apparatus

2.1.1 Column Design

The experiments in this study were carried out in a transparent fully cylindrical column constructed of Plexiglas with a specially designed plenum chamber. Two types of distributor were designed to determine their effects on fluidized-bed hydrodynamics.

The cylindrical section has an inside diameter of 127 mm (5 inches) and an overall height of 1646 mm as shown in Figure 2.1. Sampling ports of different spacing and size were installed along the height of the column in order to measure pressure at different levels inside the fluidized bed. One set of ports consisted of five holes, 19.1 mm in diameter, drilled into the wall of the column. The spacing between adjacent holes is 152.4 mm, with the lowest one 38.1 mm above the bottom of the cylinder. Plexiglas sleeves of 50.8 mm outer diameter with 19.1 mm (3/4 inch) NPT taps drilled into them were glued over the holes for support. Another set of ports was positioned along the bed height, at 90° in orientation to the first set of ports. In this case, these consisted of three holes, 12.7 mm in diameter drilled into the wall of cylinder. Plexiglas sleeves with the same dimensions as for the first set of ports were installed over the holes for support. The first two ports were installed at 101.6 mm intervals, with the lowest one 38.1 mm above the bottom of the cylinder. The last port was 203.2 mm above the second port.

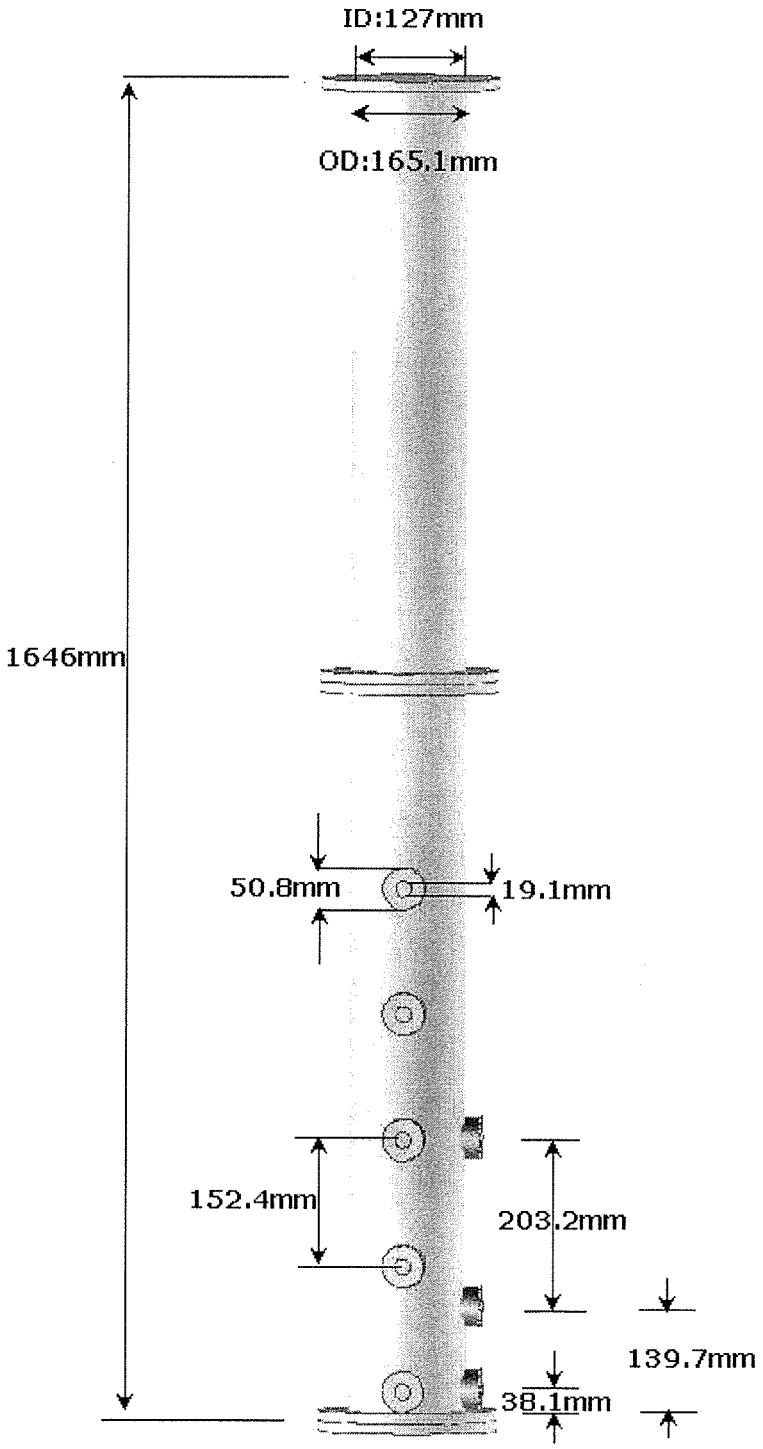

Figure 2.1. Schematic diagram of fluidization experimental column (All dimensions in mm).

2.1.2 Plenum Chamber (Windbox) Design

Unlike most plenum chambers reported in the open literature, which have asymmetric geometry of the air supply system and plenum chamber, the windbox was designed to be axially symmetric in order to have minimal influence of geometry. It was designed carefully to consist of two sections; the first one is a shallow cone with a short column to provide the minimum possible plenum volume, whereas the second section consists of two fully cylindrical columns of different diameters.

The top part of the first section is a flange identical to the flange installed at the bottom of fluidized bed in order to connect them simply as shown in Figure 2.2. The short column in this section has an inside diameter of 127 mm and a height of 38.1 mm. One hole, 12.7 mm in diameter, is drilled into this short cylinder 19.05 mm below the bottom of the flange. A Plexiglas sleeve of 25.4 mm outer diameter with a 12.7 mm (1/2 inch) NPT tap drilled into it was glued over this hole to hold a pressure probe. The bottom part of the first section is a shallow cone of height 19.05 mm and inside upper and lower diameters of 127 mm and 343 mm respectively as shown in Figure 2.2. One hole, 12.7 mm in diameter, was drilled into the cone in order to connect the plenum to a water-filled manometer, which also acts as a pressure relief valve.

The second section of the plenum chamber consists of two cylindrical columns of the same height, 572 mm, but different inside diameters. The inner column, (column A) has an inside diameter of 139.7 mm, whereas the outer one (Column B) has an inside diameter of 342.9 mm. The volume contained between these two columns forms part of the plenum chamber. The configuration is shown in Figure 2.3. A circular plate was glued to the bottom of these two columns, with its outer diameter the same as column B and an axisymmetric hole of the same diameter as column A. In order to change the effective volume of the plenum chamber, water could be added or removed by means of two holes of 19.05 mm diameter drilled in the outer annular part of this circular plate, one for water input and one for drainage, as shown in Figure 2.3. Small PVC tubes of outer diameter 19.05 mm were connected to both these ports.

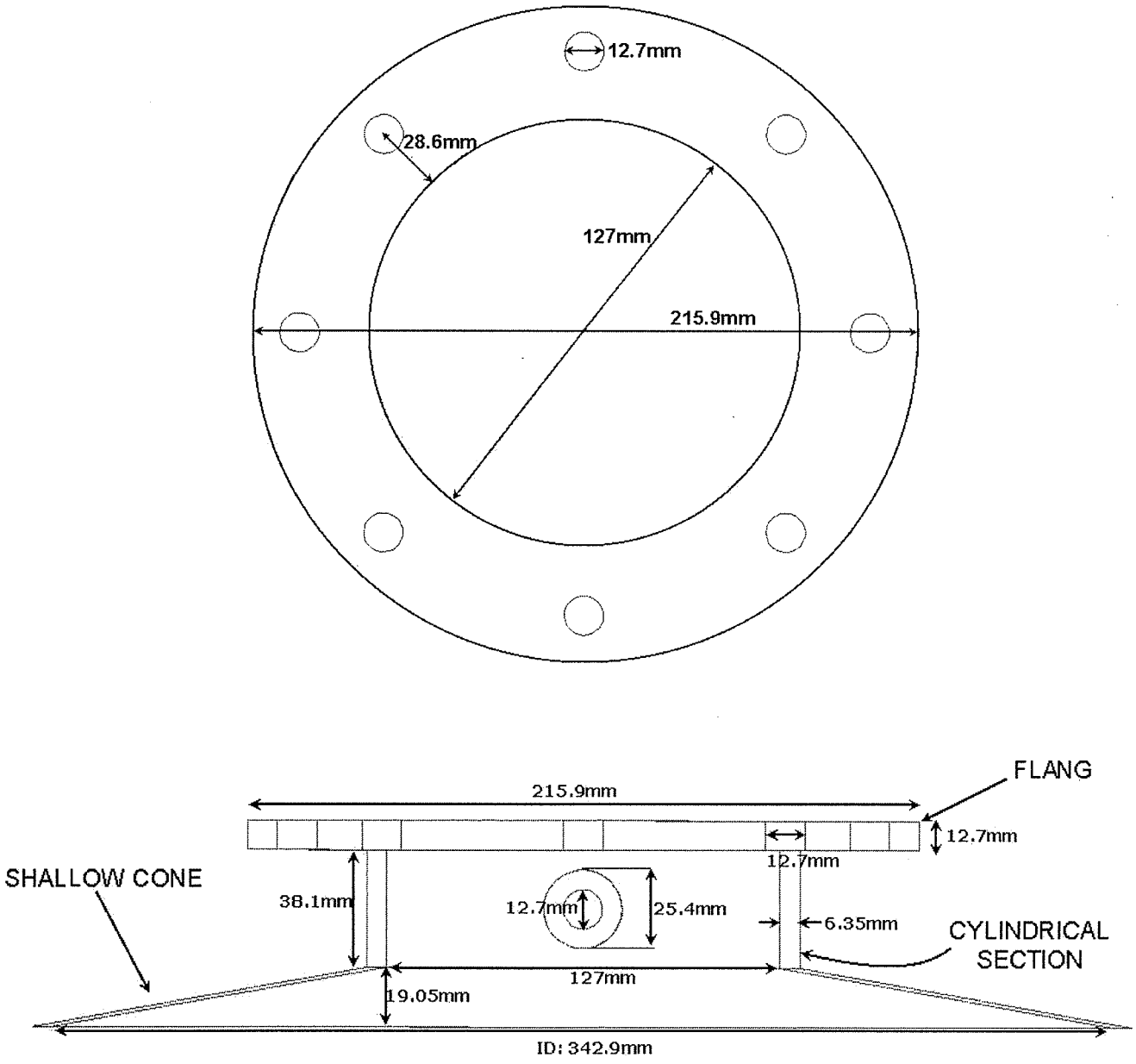

Figure 2.2. Details of flange and top section of plenum chamber.

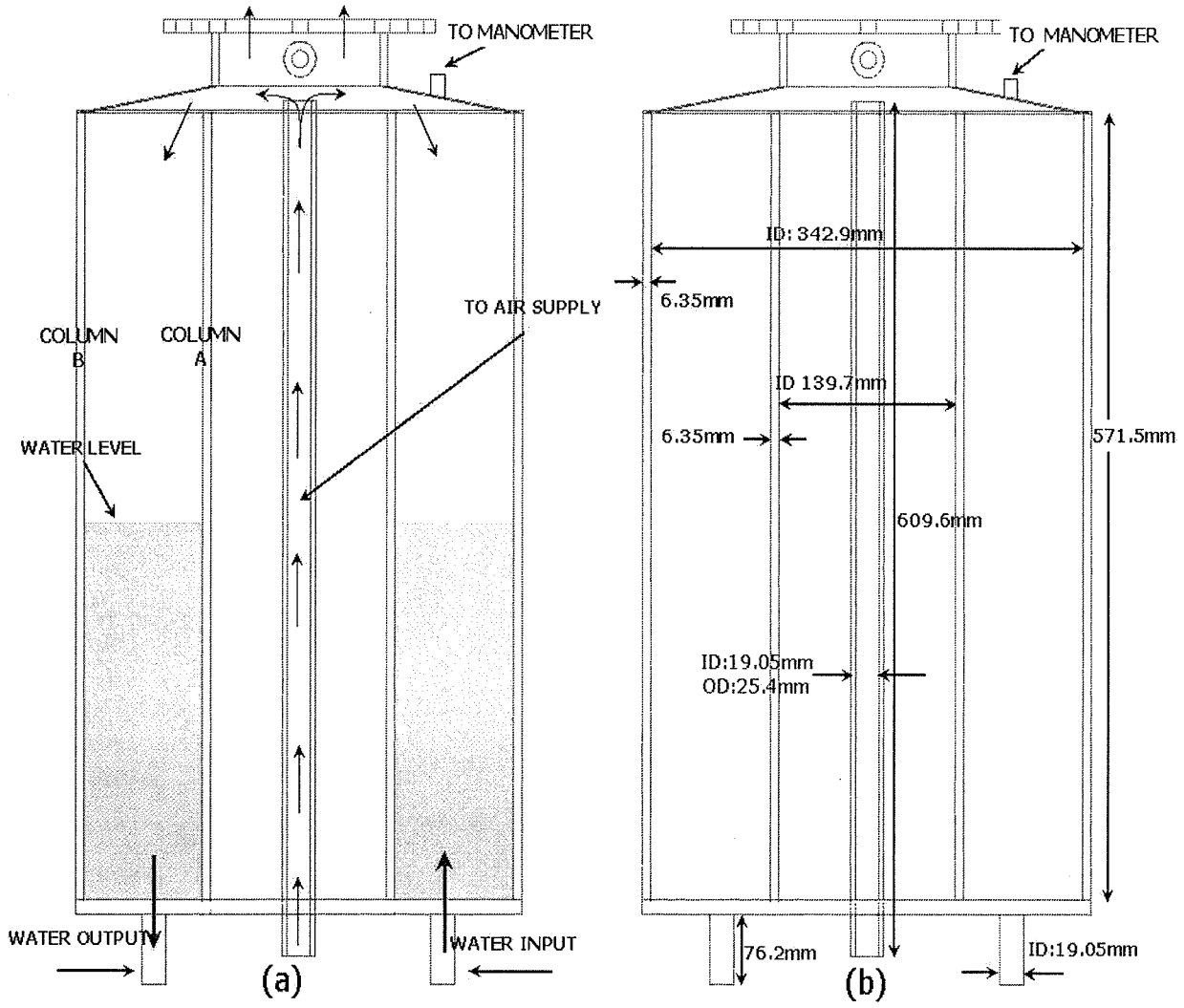

Figure 2.3. Schematic diagrams of plenum chamber showing: (a) paths of air and water; (b) dimensions. (All dimensions in mm.)

The air is supplied to the plenum by a Plexiglas tube of inner diameter 19.05 mm and height 609.6 mm. One end is connected to the main building compressor, and the other end was cut to make 4 small legs of height 12.7 mm and width 6.35 mm as shown in Figure 2.4. A circular plate 30 mm in diameter was glued on top of these legs. Therefore the outlet of supply tube acts as a pre-distributor to prevent gas from passing preferentially through the middle of the distributor as suggested by Karri and Werther (2003). Some researchers have used different pre-distributors such as a Chinese Hat (Nelson et al., 1993), and vertical pipe (Kage et al., 1993), but the simple four-leg pre-distributor was geometrically more suitable in this study.

One hole of 25.4 mm diameter was drilled in a circular Plexiglas plate of diameter 152.4 mm and glued to the bases of those four legs as shown in Figure 2.4. The end of that circular plate was glued to the top of the column A in order to seal the volume required for windbox.

2.1.3 Distributor Design

As the effect of plenum chamber on fluidization bed was the main focus of this study, careful design was needed for the distributor. As mentioned by Svensson et al. (1996) when the distributor has a high pressure drop (e.g. ratio of distributor pressure drop to bed pressure drop > 0.3), the windbox does not influence the fluidized bed hydrodynamics significantly, because high-pressure-drop distributors act like filters, so the plenum chamber and fluidized bed are effectively decoupled (Svensson et al., 1996). Geldart and Kelsey (1968) varied ΔP_{dist} by adding one or more sheets of porous material beneath the distributor. They found that if $\Delta P_{dist}/\Delta P_b < 0.1$ the bubble size increased with decreasing ΔP_{dist} , whereas for $\Delta P_{dist}/\Delta P_b > 0.1$ the bubble size was not affected by ΔP_{dist}. It seems that for low gas velocity (U-$U_{mf} < 0.25$ m/s) the bubble size is influenced by the pressure drop across the distributor, whereas the number of holes and the size of the holes are of less importance (Svensson et al., 1996).

Other researchers have proposed different criteria for distributor design. For instance Sathiyamoorthy and Sridhar Rao (1981) suggested $\Delta P_{dist}/\Delta P_b$ as a function of U_{mf} , and based on experiments they recommended a rule of thumb for distributor design: $\Delta P_{dist}/\Delta P_b > 0.12$ for fine particles and $\Delta P_{dist}/\Delta P_b > 0.24$ for coarse particles to give even distribution of gas through the fluidized bed.

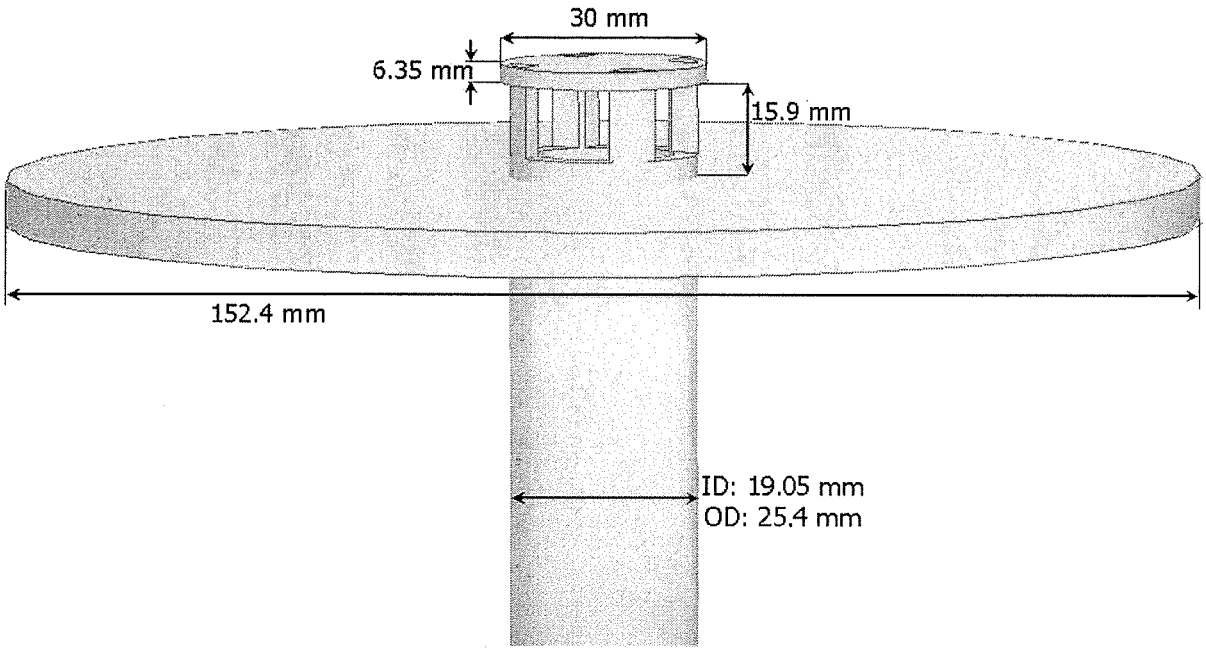

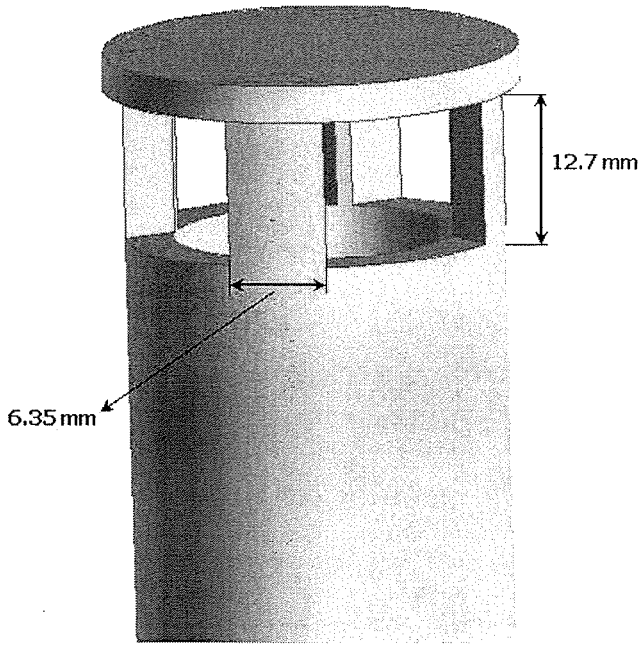

CLOSE-UP VIEW OF
PRE-DISTRIBUTOR

Figure 2.4. Details of pre-distributor in the windbox. (All dimensions in mm.)

In the experiments described in this thesis, the criterion recommended by Agarwal et al. (1962) and Geldart and Baeyens (1985) for low pressure drop distributor was used together with the design equations suggested by Karri and Werther (2003). A gas-superficial velocity of 0.20 m/s and a static bed height of 0.20 m of FCC particles (ρ_p=1600 kg/m^3) were considered for distributor design because for lower gas-superficial velocities and higher static bed height, $\Delta P_{dist}/\Delta P_b$ decreases. With ΔP_{dist} estimated as 10% of ΔP_b the velocity of gas through the grid hole was determined from;

$$U_h = \xi_d \sqrt{\frac{2\Delta P_{\text{dist}}}{\rho_{\text{g,h}}}} \tag{2.1}$$

Here ξ_d is the orifice discharge coefficient which depends on the grid plate thickness and hole pitch. It was estimated as ~0.7 based on the literature (Karri and Werther, 2003). The volumetric flow rate of gas was calculated based on the above gas-superficial velocity and then the hole diameter (d_h) can be estimated from;

$$G = N\frac{\pi d_h^2}{4}U_h \tag{2.2}$$

Since the effect of a single orifice on a fluidized bed was also important in this study, two distributors were used. At first N (the number of orifices) was chosen as one, giving a d_h of 12 mm. The area of this hole was divided by 33 (number of holes) in order to calculate the area of each hole in the second multi-orifice distributor.

Two circular Plexiglas plates of 216 mm diameter and 9.5 mm thickness were used for the two distributors. In the middle of one, a hole of diameter 12.0 mm was drilled to provide a single-orifice distributor; in the other, 33 holes of 2.1 mm diameter were drilled with an isosceles triangular geometry with a base of 20 mm and a height of 20 mm as shown in the Figure 2.5. Eight outer holes were also drilled in each plate in order to clamp each between the fluidized bed flange and the top of the plenum chamber. (See hole pattern in Figure 2.5)

Two other circular Plexiglas plate with the exact same geometry but larger holes (14.0 mm diameter in the case of the single-orifice distributor and 3.0 mm diameter in the case of multi-orifice distributor) were prepared, and a 38-μm stainless steel mesh was sandwiched between the two plates in each case to prevent particles from falling through the holes into the

plenum chamber. In order to seal the space between the two plates where the mesh was placed, an O-ring was mounted between the two plates, with a diameter of 50.8 mm in the case of the single orifice distributor and 152.4 mm for the multi-orifice distributor.

2.1.4 Flow Rate Measurement

Gas flow rates were set by a rotameter calibrated by the supplier, Cole Parmer. It had a maximum capacity of 300 LPM (0.005 m^3/s) at 21°C and 1 atm (101.3 kPa) (Cole Parmer, model# WZ-32121-00). The rotameter is connected to an air supply system by high pressure hose with appropriate fittings. The air is supplied by the main building compressor at pressures between 0 and 160 psig (1100 kPa). A pressure reducing valve and regulator were installed upstream to reduce the pressure fluctuations and maintain a relatively steady flow of clean air through the plenum chamber and fluidized bed. A schematic diagram of the overall apparatus is shown in Figure 2.6. For determination of the minimum fluidization velocity, the rotameter was replaced by two high-resolution rotameters. The first one (Cole Parmer, model# RK-03217-00), with maximum capacity of 850 CCM ($1.42x10^{-5}$ m^3/s) at standard conditions, was used for FCC particles. The second one (Brooks Instrument Division, model# 1355XB1A1AAA) had a maximum capacity of 30 LPM ($5x10^{-4}$ m^3/s) at standard conditions. It was used for the glass beads experiments.

A pressure tap was installed in the plenum chamber 25.4 mm below the distributor and connected to a water-filled manometer to measure the time-mean pressure in the windbox. From the rotameter readings and rotameter pressure, the air flow rate through the plenum chamber could be calculated. Corrections could then be made to determine the flow rate through the bed at its operating temperature and pressure.

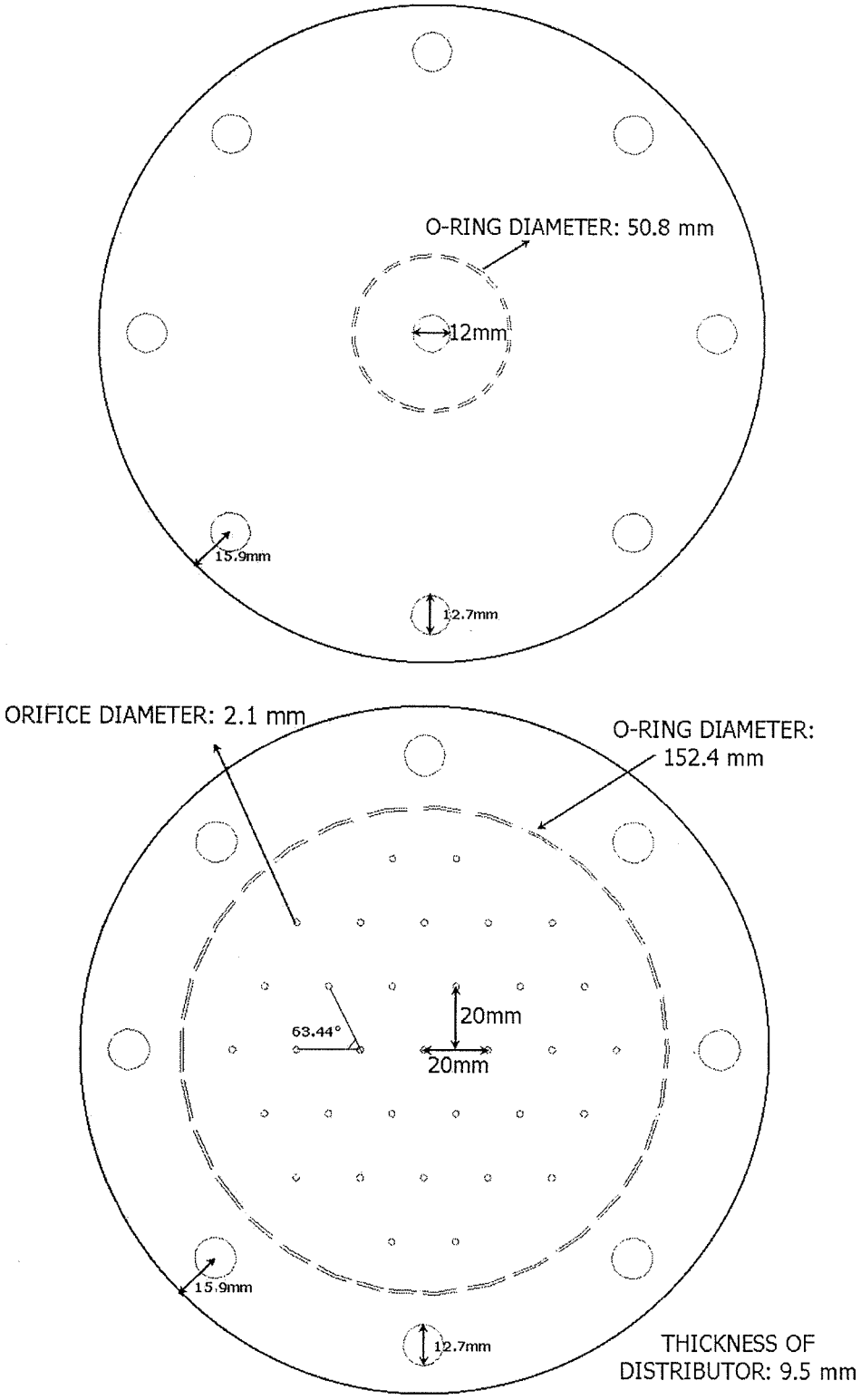

Figure 2.5. Details of single and multi-orifice distributor. (All dimensions in mm.)

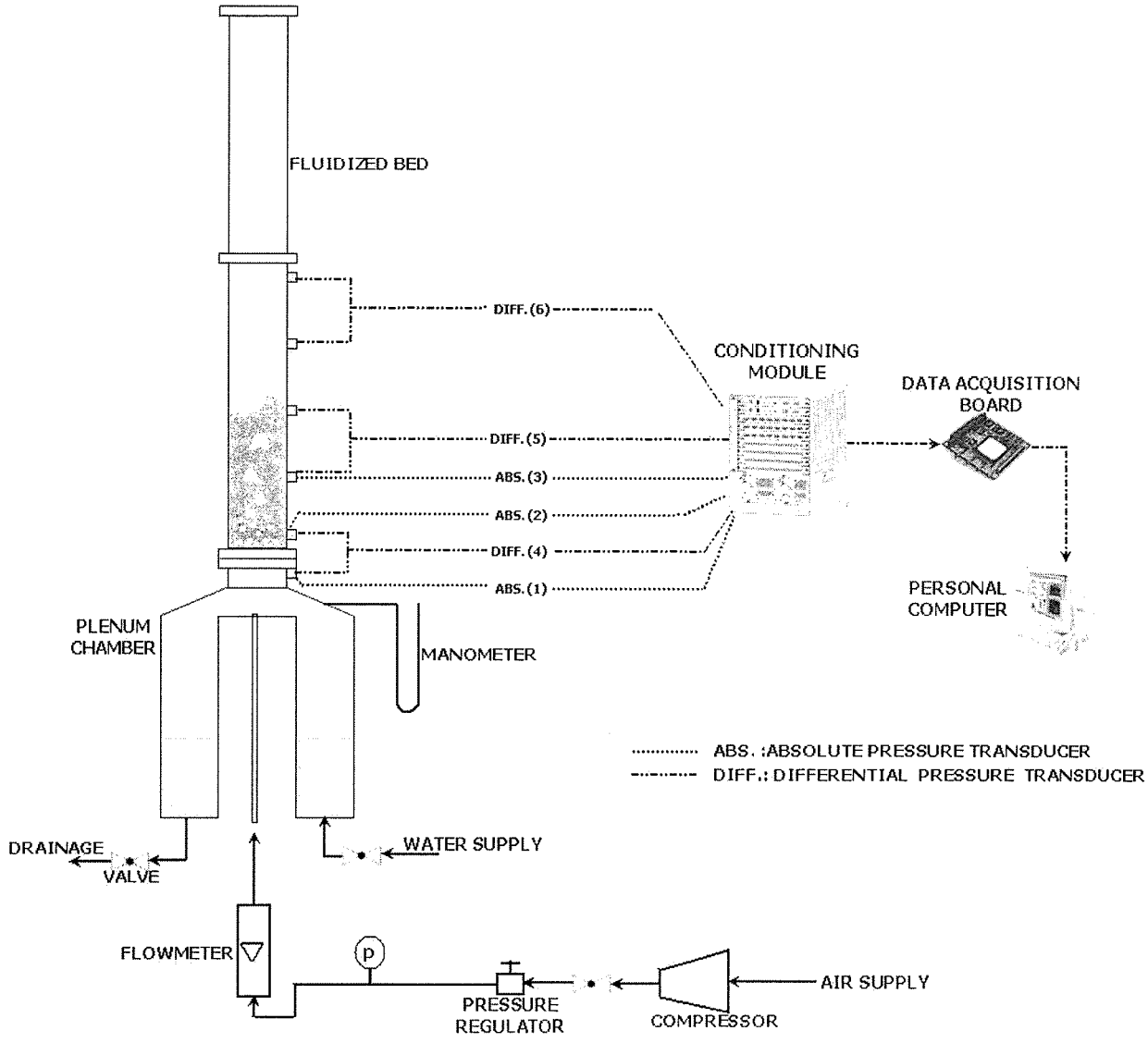

Figure 2.6. Schematic showing overall layout of experimental equipment.

2.1.5 Pressure Measurement

Eight 6.35 mm (1/4 inch) NPT male connectors from Swagelok were used to mount the pressure sensors. One of them with a thread size of 12.7 mm (1/2 inch) was used for the plenum chamber, and the rest with thread size of 19.05 mm (3/4 inch) were placed at the wall of the fluidization column, inside the above-mentioned ports. Xie and Geldart (1997) suggested that the optimum pressure probe diameter inside the fluidized bed is 4 mm. A stainless steel tube of inner diameter 4 mm and length 25.4 mm was soldered to the tip of each male connector working as a pressure probe. 38-μm stainless steel mesh was attached over the top of each tube to prevent particles from entering the pressure transducers. Polyethylene tubes of 6.35 mm diameter connected the pressure probes to pressure transducers. The length of each tube is less than 200 mm as recommended by Van Ommen et al. (1999). Three absolute (Omega 142PC series, maximum 5 psig (34473 Pa)) and five differential (Omega PX162 series, maximum 27.68 inches of water (6895 Pa)) pressure transducers were used for pressure measurement as shown in the Figure 2.6. (All differential pressure transducers are not shown in the figure; the rest are behind the column). All pressure transducers were calibrated by a water-filled manometer. The transducers have a nearly linear relationship between pressure (or pressure drop) and output voltage. Calibration constants were used in a software program as described in the next paragraph for acquiring data.

Signals from the pressure transducers were sent to an analog/digital converter data acquisition board (DAS08) and then to a personal computer via 32-channel expansion boards. Once steady state was achieved, data were recorded with a sampling frequency of 100 Hz using a custom-made program in LabVIEW 8.2 from National Instruments (Appendix A). Data from all probes were recorded simultaneously for 10 s; then, signals from the absolute pressure transducers (1) and (2) and the differential one (4) (Figure 2.6) were recorded separately for 60 s for better resolution and to prevent aliasing in Fast Fourier Transformation.

2.2 Particles

Spent fluid cracking catalyst (W.R. Grace & Co.-CONN, Maryland, USA) and spherical glass beads (Potter Industries, New Jersey, USA; P0070) were used in the experiments as bed

materials, representing groups A and B of the Geldart classification. The key properties of these materials are given in Table 2.1.

Table 2.1. Properties of particles used in experiments.

Particles	d_p^* (μm)	$\rho_p^\dagger$ (kg/m^3)	$\rho_b^\ddagger$ (kg/m^3)	$\varepsilon_o^\S$	U_{mf} (m/s)
FCC (A)	70	1600	877	0.451	0.0025
Glass Beads (B)	157	2500	1468	0.416	0.0279

* from sieve analysis ; † from supplier; ‡ measured from graduated cylinder; § from Equation 2.4

Sieve analysis was performed to obtain the mean particle diameter of FCC and glass beads particles from:

$$\overline{d_p} = \frac{1}{\sum \frac{x_i}{d_{pi}}} \tag{2.3}$$

Here x_i is the mass fraction of particles within an average screen aperture size of d_{pi}. Glass beads had a relatively narrow size distribution. The beads were nearly spherical in shape. FCC particles had a wider size distribution than glass beads as shown in Table 2.2.

Table 2.2. Size distribution of particles.

FCC particles		**Glass beads**	
Mesh size (μm)	Mass fraction (%)	Mesh size (μm)	Mass fraction (%)
125-150	5.1	250-300	1.3
90-125	39.2	212-250	4.1
61-90	28.5	180-212	20.6
53-61	16.4	150-180	46.2
45-53	4.9	125-150	13.6
38-45	2.4	106-125	8.7
0-38	3.5	90-106	5.4

The densities of particles were determined by liquid displacement where a known mass of particles (glass beads or FCC) was slowly added to a 1000 ml graduated cylinder containing a known quantity of water. The increase in the level of water was used to determine the volume of particles added. After several measurements the average densities were calculated (at a confidence level of 95%). For FCC particles the density was 1589 kg/m^3 (the value provided by company was 1600 kg/m^3) and for glass beads it was 2492 kg/m^3 (again close to the value provided by company, 2500 kg/m^3). Note that since the FCC particles are porous, this method assumes that no water enters the pores, an assumption that may not be completely valid.

To obtain the loose-packed bed voidage, the bulk density of the particles was determined. Particles were poured partially into a graduated cylinder with its top end covered. Then the cylinder was inverted and returned quickly to its upright position. The volume was measured and therefore bulk density was calculated. After several measurements the average was used to calculate the loose-packed voidage:

$$\varepsilon_o = 1 - \frac{\rho_b}{\rho_p} \tag{2.4}$$

During experiments with both FCC particles and glass beads, a crackling sound could be heard because of static electricity build-up inside the column. It was strong enough to cause electric discharge whenever a metal part was touched. At the beginning, it was assumed that passing the air over water inside the plenum chamber would eliminate the generation of static electricity, but this did not work efficiently. Adding some anti-static powder such as Larostat to the particles was considered. However, as mentioned by Pianarosa (1996), adding Larostat can cause significant effects on bed properties such as bed expansion. Therefore a simple procedure was adopted, which was to connect the probes and column via a piece of copper wire to the metallic frame to provide grounding.

2.3 Operating Conditions

To determine the effect of plenum chamber on fluidization, four different windbox volumes were investigated in this study. The minimum one was 0.0020 m^3, and the maximum one was 0.0425 m^3. The outer cylinder of the plenum chamber was graduated in order to add the right volume of water. During the operation, small waves could be seen at the water

surface. To check their effect on pressure fluctuations in plenum chamber video movies were recorded for 5 minutes and watched carefully. The amplitude of these high frequency waves was so small that they are believed to have been too small to have influenced the measurements in this study.

Since plenum chamber characteristics have not been reported at different bed depths in the literature, four different static bed heights were tested as listed in Table 2.3. Examining bed depths above 0.5 mm was difficult because of carry-over of fine particles from the top of the fluidized bed. The influence of the superficial gas velocity was also tested with five different flow rates, as listed in Table 2.3.

Table 2.3. Values of variables tested in the experiments

Tested variables	**Values of tested variables**
Gas superficial velocity, FCC (m/s)	0.040 , 0.080 , 0.120 , 0.160 , 0.200
Gas superficial velocity, glass beads (m/s)	0.065 , 0.106 , 0.145 , 0.185 , 0.225
U-U_{mf} (m/s)	0.037 , 0.077 , 0.117 , 0.157 , 0.197
Bed height (m)	0.10 , 0.20 , 0.35 , 0.50
Plenum chamber volume (m^3)	0.0425 , 0.0290 , 0.0155 , 0.0020

Chapter 3: Pressure Fluctuation Measurements

3.1 Introduction

Since pressure fluctuations provide information on the dynamics of gas-solid fluidized beds, they have been widely investigated by researchers. Moreover, this type of measurement is simply achieved by inexpensive pressure transducers with different ranges and accuracies depending on the operating conditions and positions of the probes. However, pressure fluctuations are difficult to interpret because they can originate from different sources in gas-solid fluidized beds such as bubble passage; self-exited oscillation of fluidized particles or gas in the plenum chamber, bubble formation, surface waves, and bubble coalescence. Moreover, the characteristics of pressure fluctuations depends on experimental conditions, such as static bed height, particle properties, gas velocity and even the position and properties of the pressure measurement system.

A number of researchers have focused on the decoupling of pressure fluctuation signals to extract useful information about different phenomena in gas-solid fluidized bed. Three main methods of analysis have been used by researchers: time analysis, frequency or correlation analysis, and chaos or state-space analysis.

In the case of time analysis, standard deviation of pressure signals has been used to detect fluidization flow regimes. However Johnsson et al. (2000) criticized this method because the amplitude of pressure fluctuations can change because of the redistribution of bed material from the riser to the cyclone side, while the fluidization regime remains the same.

Frequency domain analysis, mainly used in this study, has been applied in fluidization research by many researchers to transform pressure signals from the time domain to the frequency domain. Fast Fourier Transform (FFT) has been utilized as the mathematical tool in this kind of transformation. Dominant frequency and frequency spectrum can be determined using the power spectral density function. Moreover, by means of the autocorrelation function, the presence of a periodic phenomenon can be revealed. In the case of two signals, the cross-correlation function is commonly used to determine the relationship and time delay between two periodic signals, as well as to determine bubble velocity in fluidized beds.

From the governing equations (equation of motion and mass conservation for the gas and solid phases), two-phase flow in fluidized system is governed by non-linear relationships. Several researchers (e.g. Johnsson et al., 2000, Hay et al., 1995) have reported that time series from pressure measurements exhibit the characteristic of low-dimensional deterministic chaos. Chaos analysis is still a subject of research, and different algorithms have been proposed. Most methods are based on the principle of reconstruction of the data into an attractor in state-space (Johnsson et al., 2000).

In this study the first two types of analysis, i.e. time and frequency analysis; have been applied to pressure signals. In the case of frequency analysis, Welch's method was used for Fast Fourier computations. This is believed to be the most common method in frequency analysis for pressure fluctuations in fluidized beds. In this method the variance is reduced by estimating power spectra as an average of several sub-spectra (Sasic et al., 2007). To prevent leakage in the frequency spectrum, Bendat and Piersol (2000) suggested applying an appropriate window (a Hamming window was used in this study). Details about the spectral and statistical analysis methods are presented below.

3.2 Statistical Analysis of Pressure Fluctuation Signals

One of the basic tools in statistical analysis is the probability density function, $p(x)$, of a random variable $x(t)$, defined by

$$p(x) = \lim_{\Delta x \to 0}\left(\frac{prob[x < x(t) \le x + \Delta x]}{\Delta x}\right) \tag{3.1}$$

For a sample record, $x(t)$, which may take on values in the range of $-\infty$ to $+\infty$, the expected or the mean value of $x(t)$, μ_x, is obtained by

$$E[x(t)] = \int_{-\infty}^{+\infty} x.p(x)dx = \mu_x \tag{3.2}$$

where $p(x)$ is the probability density function associated with $x(t)$. Similarly, the expected value of any real single-variable continuous function, $g(x)$ of random variable $x(t)$ is given by

$$E[g(x(t))] = \int_{-\infty}^{+\infty} g(x).p(x)dx \tag{3.3}$$

For $g(x) = x^2(t)$, the mean square value of $x(t)$ is given by

$$E\left[x^2(t)\right] = \int_{-\infty}^{+\infty} x^2 . p(x)dx = \mu_x^2 \tag{3.4}$$

The variance of *x(k)* is defined by the mean square value of *x(k)* about its mean. Therefore $g(x)=(x-\mu_x)^2$, and

$$E\left[(x(t)-\mu_x)^2\right] = \int_{-\infty}^{+\infty} (x-\mu_x)^2 . p(x)dx = \Psi_x^2 - \mu_x^2 = \sigma_x^2 \tag{3.5}$$

By definition, the standard deviation of *x(t)*, denoted by σ_x, is the square root of the variance. In the case of a finite number of experimental data, the mean value and variance of *x(k)* based on *N* independent observation, can be calculated from:

$$\bar{x} = \mu_x = \frac{1}{N}\sum_{i=1}^{N} x_i \tag{3.6}$$

$$S_b^2 = \sigma_x^2 = \frac{1}{N}\sum_{i=1}^{N} (x_i - \bar{x})^2 \tag{3.7}$$

where S_b^2 is the biased sample variance. An unbiased sample variance is estimated by

$$S^2 = \sigma_x^2 = \frac{1}{N-1}\sum_{i=1}^{N} (x_i - \bar{x})^2 \tag{3.8}$$

The standard deviation of pressure fluctuations is calculated using this equation.

3.3 Spectral Analysis of Pressure Fluctuation Signals

3.3.1 Correlation Function

It is difficult to determine whether a set of data contains a periodic component by observing its time history because noise may be present. Moreover, several frequencies may be superimposed. Correlation functions are used frequently to characterize periodic signals. A correlation function is described by considering two signals as a function of time (e.g. pressure as a function of time). Assuming two functions *x(t)* and *y(t)* which are sampled such that x_k and y_k occur simultaneously from *k=0* to *k=N* (total number of data points), the discrete correlation function is:

$$Rxy_k = \frac{\sum_k x_k y_k}{N} \tag{3.9}$$

This value represents the correlation at the discrete point *k*. It is evident that for two zero-mean signals, the correlation will be the greatest if the signals are identical. For two dissimilar signals, the sum of the products will be smaller since some products are positive and some negative.

In a similar manner, correlation can also be applied to a single signal, titled autocorrelation. Autocorrelation determines the periodicity of a signal by correlating the value of a function at *y(t)* to that at a subsequent time, y(t + τ). The autocorrelation function, $R_{yy}(\tau)$, can be calculated form the average product of the original signal value and its time-shifted value. For a continuous system it is defined as:

$$R_{yy} = \lim_{T\to\infty} \frac{1}{T} \int_{-T/2}^{T/2} y(t).y(t+\tau)dt \tag{3.10}$$

where *T* is the total length of the time record. For a signal containing a periodic component, the autocorrelation function results in a sharp peak after time zero. The time corresponding to this time is the period of that periodic component. Purely random or white noise signals will yield an autocorrelation function with a sharp peak only at zero, since there is no correlation at any other point.

3.3.2 Spectral Density Function

One method to directly determine the frequency or frequencies associated with a system is to calculate the power spectral density (PSD). The PSD is defined as the Fourier transform of the autocorrelation function, which represents the amount of power in given frequency interval contained in the data set. Considering a time series function, *x(t),* the spectral density function is given by:

$$S_{xx}(f,T,k) = \frac{1}{T} X_k^*(f,T).X_k(f,T) \tag{3.11}$$

where

$$X_k(f,T) = \int_0^T x_k(t)e^{-j2\pi ft}dt \tag{3.12}$$

is the finite Fourier transform of $x_k(t)$, and $X_k^*(f,T)$ is the complex conjugate of $X_k(f,T)$. From the power spectral density, one can find the dominant frequency and intensity of pressure

fluctuation signals. Welch (1967) introduced a simple procedure, described in Appendix B, for direct computation of the power spectral density using Fast Fourier Transform (FFT) with suitable resolution and confidence.

Brown and Brue (2001) suggested using a logarithmic scale of PSD to characterize gas-solid fluidized beds because the frequency of over-damped peaks is impossible to determine accurately from the linear scale. Moreover, the order of the system can be determined more easily from the logarithmic scale of PSD.

3.4 Results and Discussion

3.4.1 Time-Domain Analysis

To characterize the pressure fluctuation signals, the simplest, but not the most efficient way, is to perform time-domain analysis. (In the time domain many signals may be superimposed, so that it is difficult to understand the dynamics of the system). Pressure signals from absolute pressure transducers inside the plenum chamber were used in this project for this analysis, with a sampling frequency of 100 Hz. Only 10 s of the data were used for time-domain analysis to determine the structure of the pressure-time signals, although the recording time was 60 s.

For a shallow bed (e.g. 0.10 m depth) it is difficult to discern a different trend between the pressure fluctuations from the minimum and maximum plenum volumes, as shown in Figure 3.1. However the structure of the pressures fluctuation signals differ, with the amplitude of pressure fluctuations higher when the minimum plenum volume was used. This is reasonable because the fluidized bed dynamics can affect a small plenum chamber more easily than a large plenum chamber, with the latter tending to dampen fluctuations received from the bed.

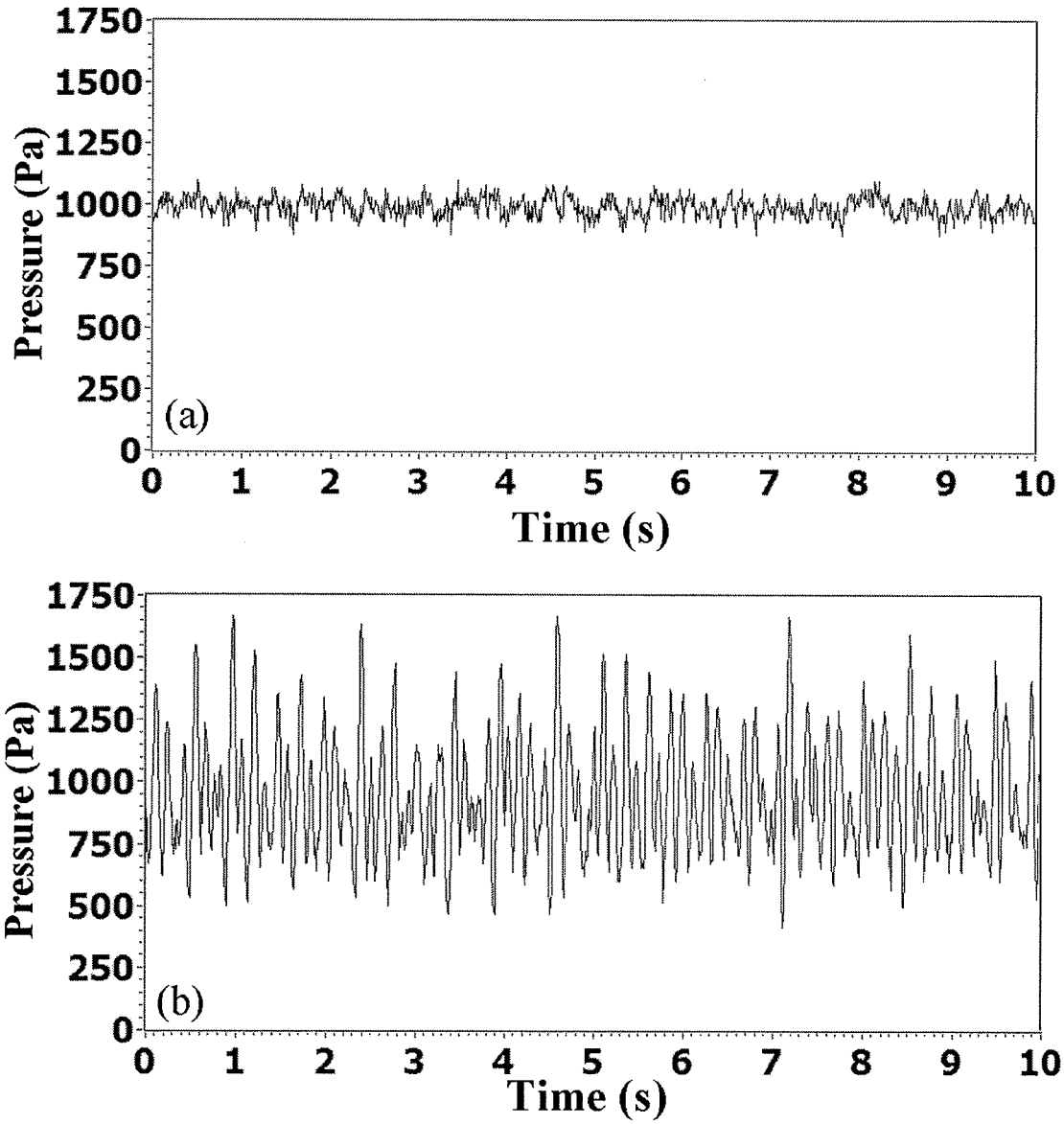

Figure 3.1. Pressure gauge fluctuations of the plenum chamber with single-orifice distributor for FCC particles, H_o=0.10 m, U=0.04 m/s. (a) Maximum plenum chamber volume, 0.0425 m^3 (b) Minimum plenum chamber volume, 0.0020 m^3.

For a higher static bed height (e.g. 0.50 m), the amplitude of pressure fluctuations measured from the maximum plenum volume became more regular as shown in Figure 3.2. This is in agreement with Baird and Klein (1973) who observed that for large plenum volume (0.019 m^3), both the period and the amplitude of pressure fluctuations became regular. (They did not report the distributor characteristics in their experiments).

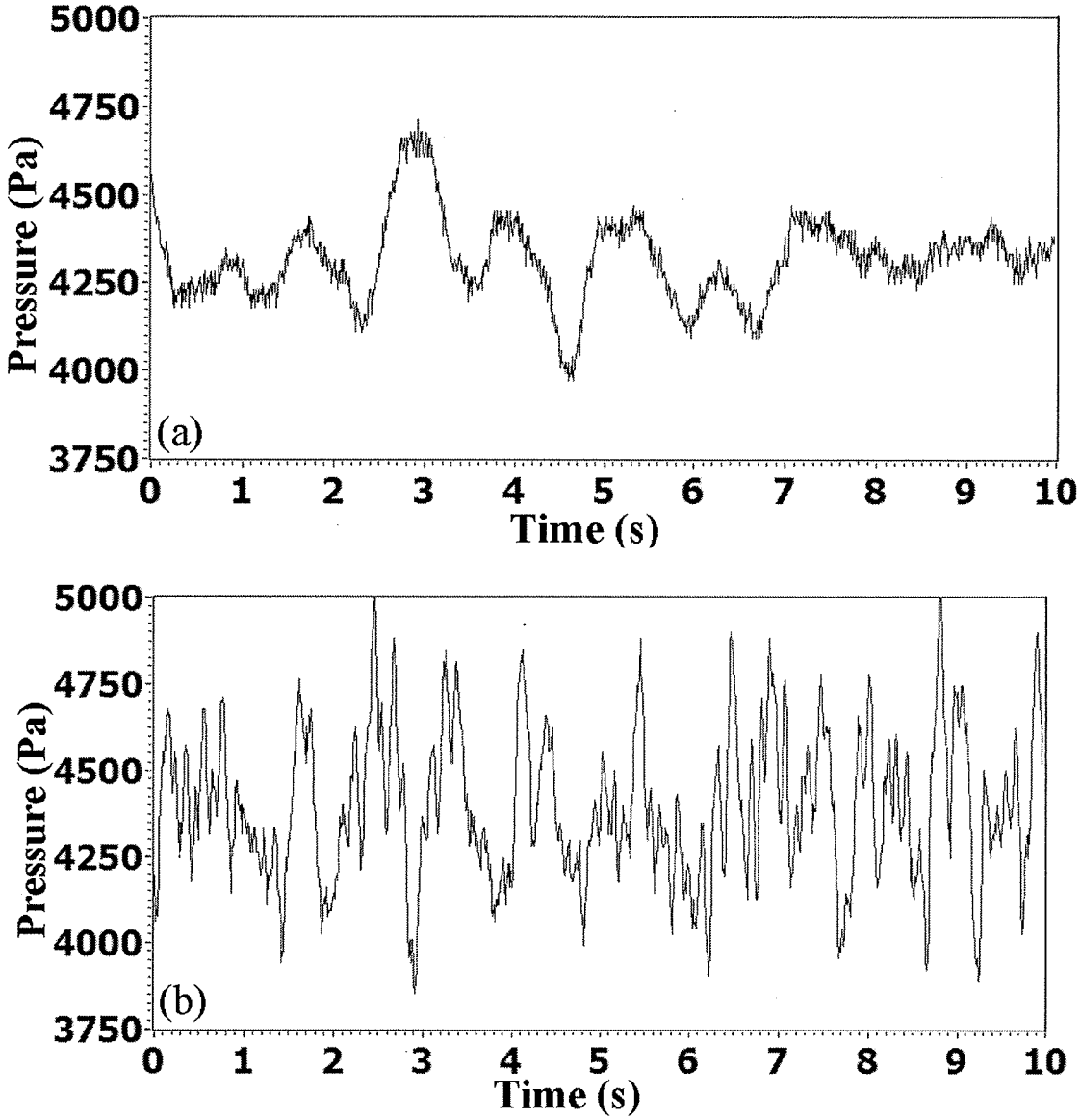

Figure 3.2. Pressure gauge fluctuations of the plenum chamber with single-orifice distributor for FCC particles, H_o=0.50 m, U=0.04 m/s. (a) Maximum plenum chamber volume, 0.0425 m^3 (b) Minimum plenum chamber volume, 0.0020 m^3.

Figure 3.2(a) shows some low-amplitude, high-frequency fluctuations; however, the frequencies cannot be determined, even from the frequency spectrum, because the sampling frequency for pressure recording was 100 Hz, so that based on the Nyquist rule only up to 50 Hz can be characterized in the frequency spectrum.

Standard deviation of pressure fluctuations is usually performed in the time-domain to determine the statistical characteristics of the system. Pressure fluctuation signals from two absolute pressure transducers, one in the plenum chamber and the other in the bed, 38.1 mm above the distributor, were used for standard deviation calculations. In general, the standard deviation of pressure fluctuations in the plenum chamber decreased with increasing plenum volume as shown in Figure 3.3.

In the case of single-orifice distributor, one large bubble is released at a time, whereas many small bubbles form randomly at a multi-orifice distributor. Forming one large bubble causes higher amplitude pressure fluctuations in the plenum chamber than forming many small bubbles out of phase with each other. This can be confirmed by comparing Figures 3.3 and 3.4.

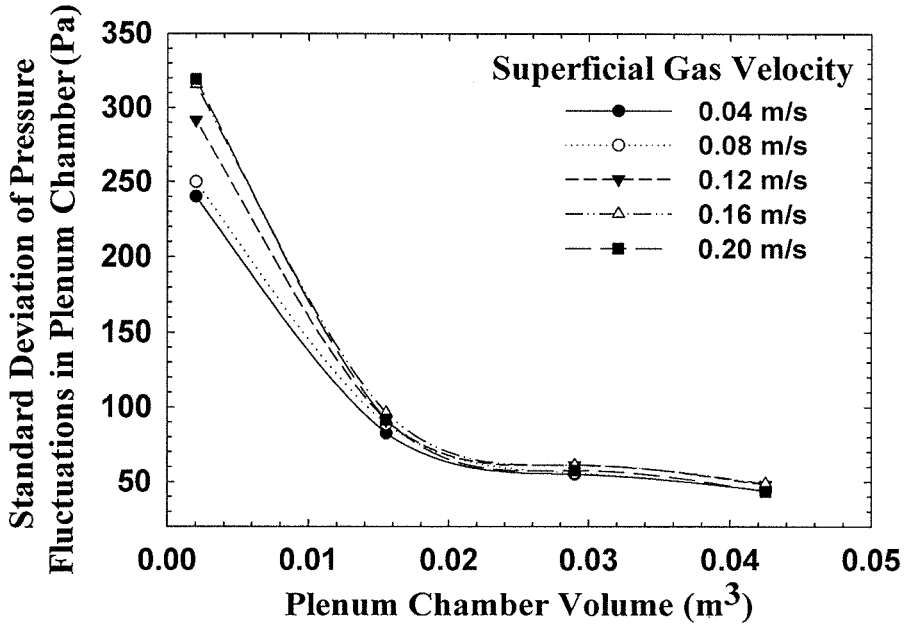

Figure 3.3. Standard deviation of pressure fluctuations in the plenum chamber (FCC particles, Single-orifice distributor, and static bed height of 0.10 m).

Note that the effect of plenum volume is more pronounced for a higher static bed height. As shown in Figure 3.4 for a 0.10 m static bed height, the standard deviation becomes almost constant when the plenum volume is increased for the same superficial velocities, but for a higher static bed height (0.50 m); the decrease of the standard deviation with increasing plenum volume is more evident at high superficial gas velocities, as shown in Figure 3.5.

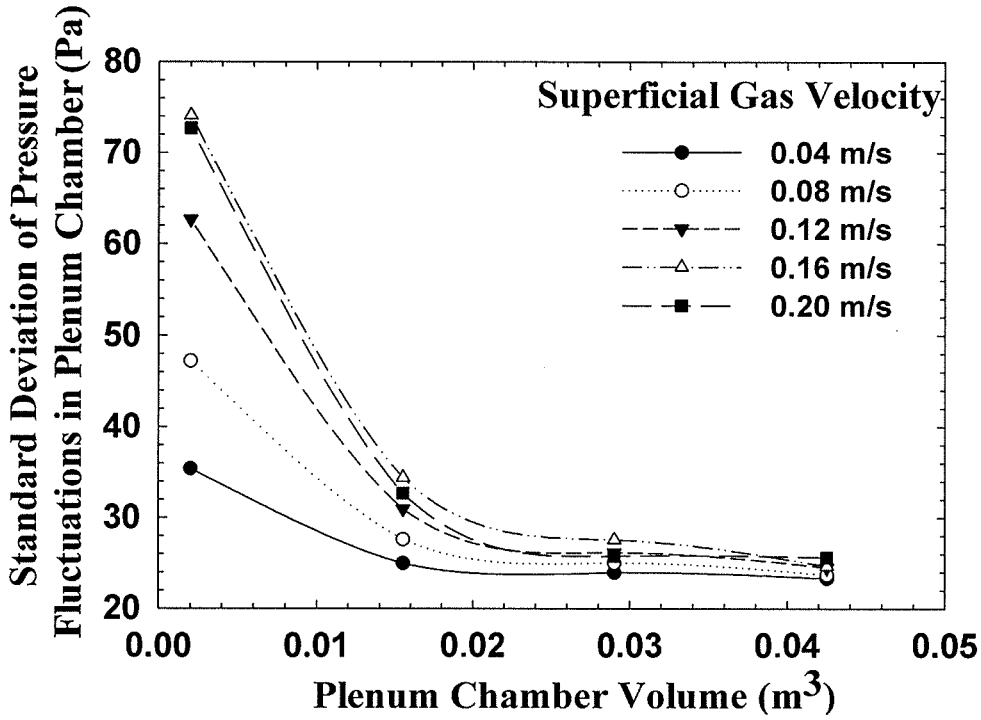

Figure 3.4. Standard deviation of pressure fluctuations in the plenum chamber (FCC particles, multi-orifice distributor, and static bed height of 0.10 m).

Glass beads showed a similar trend as portrayed in Figure 3.6. Since fluidization of Geldart group B particles results in larger bubbles than for group A particles, the standard deviation of pressure fluctuations in the plenum chamber is higher for glass beads at the same operating conditions. Baeyens and Geldart (1974) also tested the effect of particle size and density on plenum pressure fluctuations in a slugging fluidized bed and concluded that coarse materials result in higher windbox pressure fluctuations than finer materials and that this may be due to the higher terminal velocity of coarse materials, resulting in higher kinetic energy when slug burst through the surface of the bed and powder falls back.

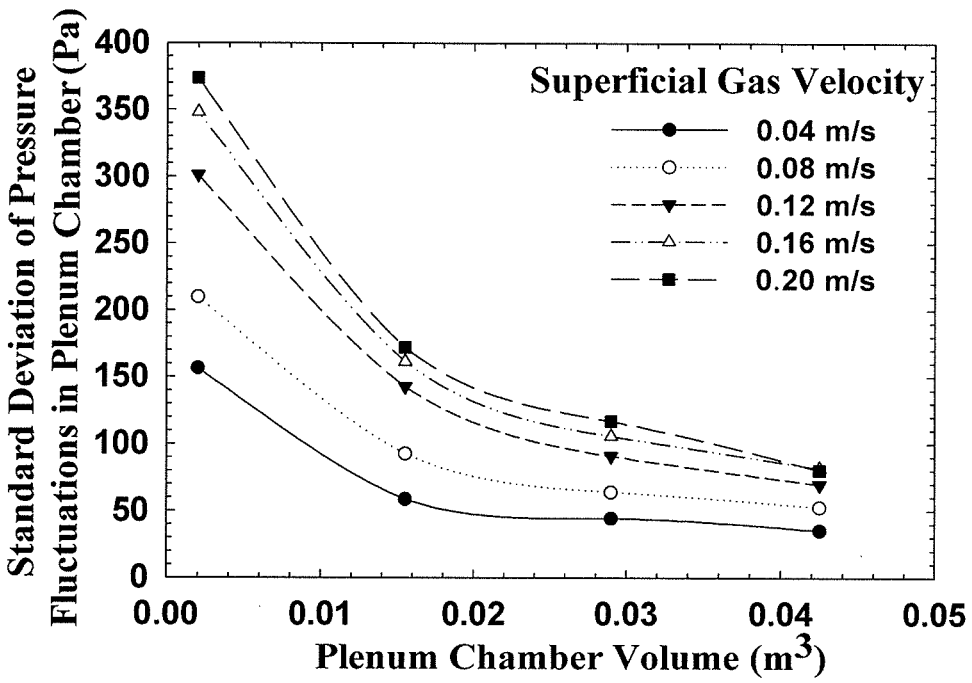

Figure 3.5. Standard deviation of pressure fluctuations in the plenum chamber for FCC particles, (multi-orifice distributor, and static bed height of 0.50 m).

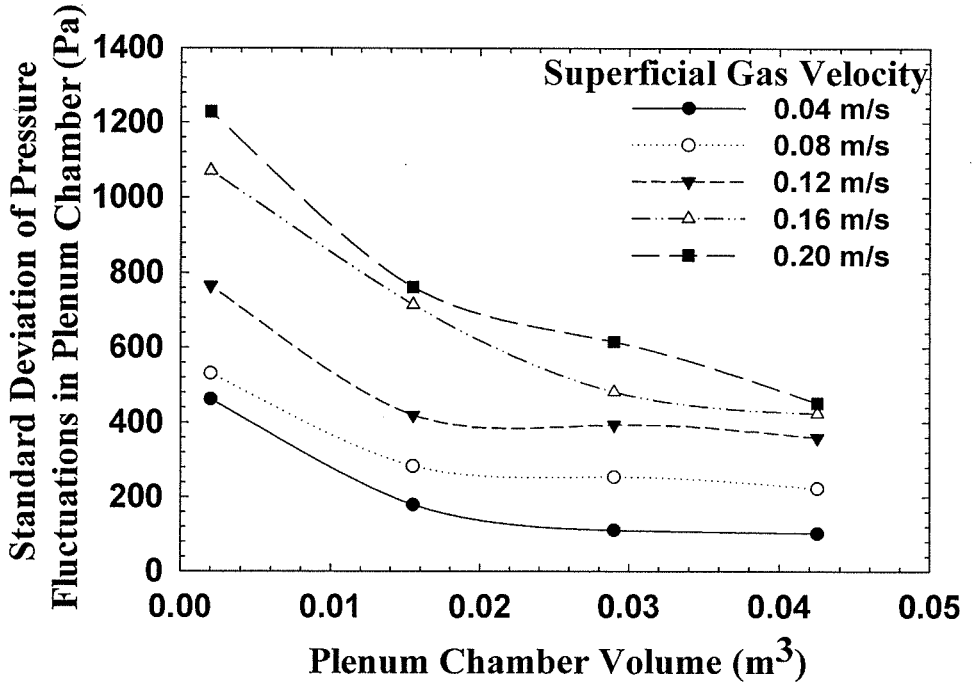

Figure 3.6. Standard deviation of pressure fluctuations in the plenum chamber for glass beads, (multi-orifice distributor, and static bed height of 0.50 m).

Figure 3.7 shows that the standard deviation of pressure fluctuations from an absolute pressure transducer inside the bed (38.1 mm above the distributor) decreases slightly with increasing plenum chamber volume.

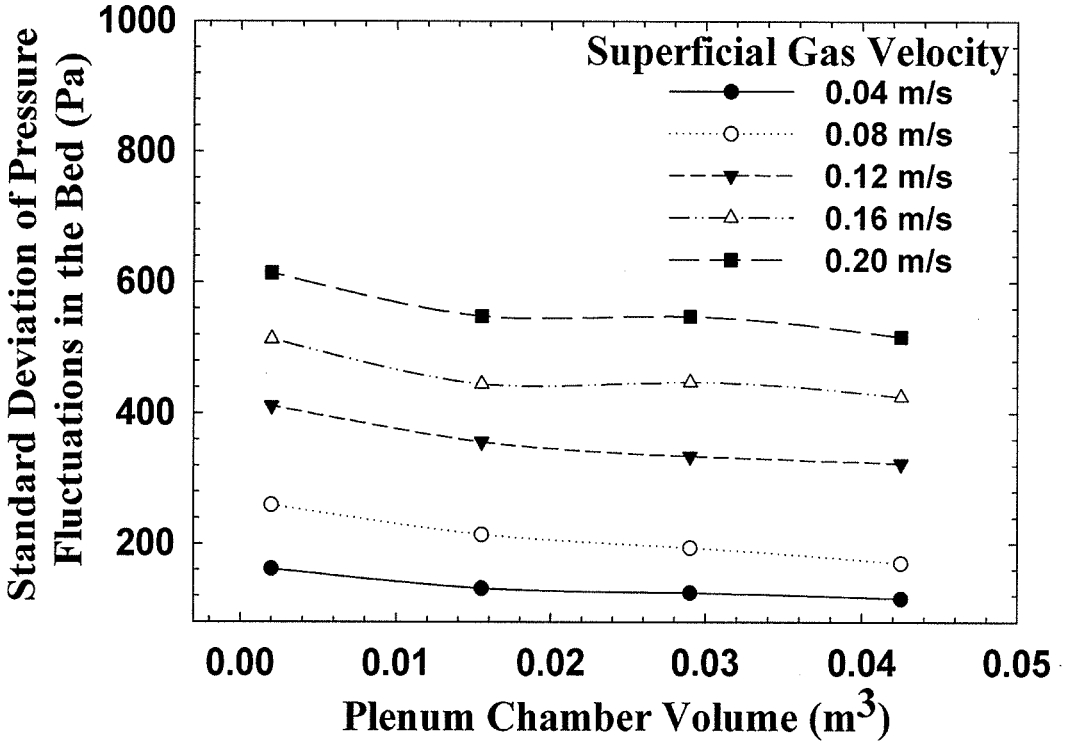

Figure 3.7. Standard deviation of pressure fluctuations in the fluidized bed (FCC particles, single-orifice distributor, and static bed height of 0.50 m).

Time-domain analysis is probably the easiest way to treat pressure fluctuations data, but in order to understand the dynamics of the fluidized bed, other types of analysis such as frequency and chaos analysis are preferred.

3.4.2 Frequency-Domain Analysis

CPSD (Cross Power Spectral Density), PSD (Power Spectral Density), and correlation functions were determined for the frequency-domain analysis. CPSD was used to estimate bubble size for various plenum volumes, whereas PSD was applied to the pressure-time signals to determine dominant frequencies by decoupling of pressure fluctuations, and autocorrelation was performed to determine the periodicity of the pressure signals in the plenum chamber and fluidized bed.

Pressure waves caused by different source of pressure fluctuations travel upwards and downwards in the bed from the point of origin. Because of their high propagation velocity, the pressure waves can be measured simultaneously throughout the entire bed. Van der Schaaf et al. (1998) showed experimentally that the amplitude of pressure fluctuations does not decrease appreciably in the downward direction. Thus pressure waves generated at the upper bed surface can also be measured in the plenum chamber and will be coherent with in-bed positions. In addition to fast-traveling waves, gas bubbles and turbulence generate local pressure fluctuations rather than a traveling pressure wave through the fluidized bed. Therefore, these phenomena are not measured in the plenum. Based on this assumption Van der Schaaf et al. (2002) performed spectral analysis and proposed a new approach to separate single-point pressure signals into two components, coherent and incoherent. They concluded that the incoherent part is related to gas bubbles and local turbulence and proposed a procedure to estimate the size of bubbles based on spectral analysis. At first the coherence factor is calculated as:

$$\gamma_{xy}^2(f) = \frac{S_{xy}(f)S_{xy}^*(f)}{S_{xx}(f)S_{yy}(f)} \tag{3.13}$$

where S_{xx} is the power spectral density of a pressure time series measured at position x (calculated from Equation 3.11), and S_{xy} is the cross power spectral density of pressure time series at position x and y, defined as:

$$S_{xy}(f,T,k) = \frac{1}{T} X_k^*(f,T).Y_k(f,T) \tag{3.14}$$

$X_k(f,T)$ and $Y_k(f,T)$ is the Fast Fourier Transform of the pressure time series, and $X_k^*(f,T)$ is the complex conjugate of $X_k(f,T)$. The pressure time series measured at position y in the fluidized bed, which contains parts which are coherent and incoherent with the pressure time series measured in the plenum chamber (x), can be expressed in terms of the coherent part (COP_{xy}) and incoherent part (IOP_{xy}) respectively by:

$$COP_{xy}(f) = \gamma_{xy}^2 S_{yy} \tag{3.15}$$

$$IOP_{xy}(f) = (1-\gamma_{xy}^2) S_{yy} \tag{3.16}$$

According to Parseval's theorem, the standard deviations of the incoherent and coherent pressure fluctuations can be calculated by:

$$\sigma^2_{xy,c} = \int_0^\infty COP_{xy}(f)df\,, \qquad \sigma^2_{xy,i} = \int_0^\infty IOP_{xy}(f)df \tag{3.17}$$

Van der Schaaf et al. (2002) compared their approach with the Darton et al. (1977) bubble coalescence model and suggested a measurement level in the fluidized bed not higher than 0.19 m above the distributor because the increase of the incoherent standard deviation with height up to 0.19 m can be understood with the bubble growth model of Darton et al. (1977). They concluded the bubble size could be estimated by:

$$D_b \approx \sigma_{xy,i} / \left(\rho_p g\left(1-\varepsilon_{mf}\right)\right) \tag{3.18}$$

Pressure time series from absolute pressure transducers in the plenum chamber and 38.1 mm above the distributor were applied to determine the effect of the plenum chamber and superficial gas velocity on the bubble size estimated in this manner. A custom-made LabVIEW program was written to apply this bubble size estimation procedure (Appendix C). It should be noted that the estimation of bubble size by this procedure may not be very accurate. However, the effect of the plenum volume on the bubble size based on the Van der Schaaf et al. (2002) approach should be suitable for relative comparison.

Figure 3.8 shows that, as expected, the bubble volume, derived in this manner, increases with increasing superficial gas velocity for FCC particles using the single-orifice distributor. This is in agreement with experiments from Harrison and Leung (1961) for formation of bubbles at a single orifice in a fluidized bed. Davidson and Schuler (1960) and McCann and Prince (1969) also experimentally found larger bubbles when superficial gas velocity was increased for bubble formation in a low-viscosity liquid.

Figures 3.8 and 3.9 both demonstrate that large bubbles formed for minimum plenum volume (0.0020 m^3) than for maximum plenum volume (0.0425 m^3), for both single- and multi-orifice distributor. The effect of plenum chamber on the bubble size for moderate plenum volumes (i.e. 0.0290 and 0.0155 m^3) is barely perceptible, but Figures 3.8 and 3.9 show distinct difference in bubble formation between the minimum and maximum plenum volumes. With glass beads as the bed material, the same trend was found as shown in Figure 3.10.

Bubbles formed at the single-orifice distributor were larger than those formed by the multi-orifice distributor because of larger orifice surface area and greater flow through the orifice in the case of the single orifice distributor. This can be inferred by comparing Figures 3.8 and 3.9. For glass beads, Geldart group B particles led to larger bubbles than FCC particles. This can also be concluded from a comparison of Figures 3.8 and 3.10 for the single-orifice distributor.

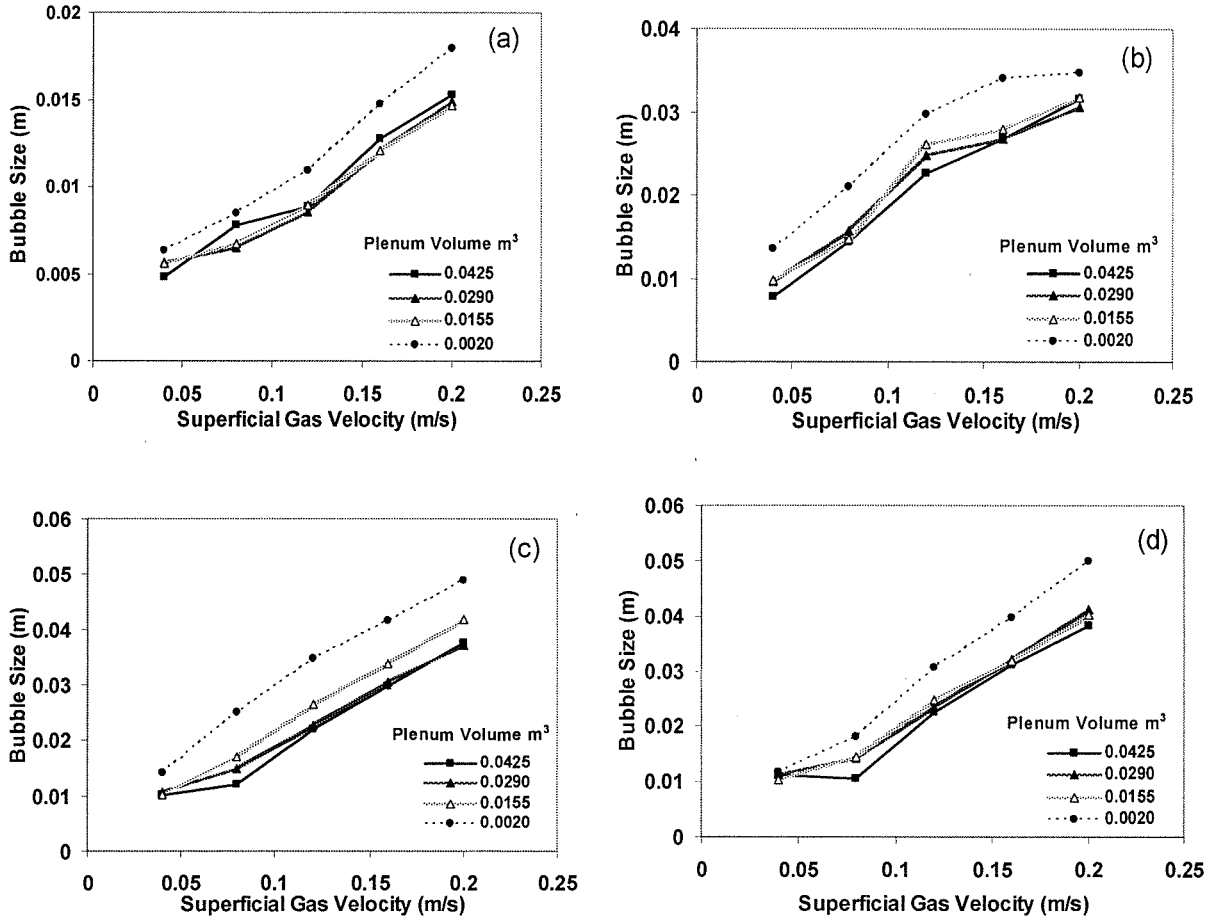

Figure 3.8. Effect of superficial gas velocity and plenum volume on the bubble size derived from the incoherent pressure fluctuations for single-orifice distributor and FCC particles. Note that the ordinate scales differ; static bed height: (a) 0.10 m; (b) 0.20 m; (c) 0.35 m; (d) 0.50 m.

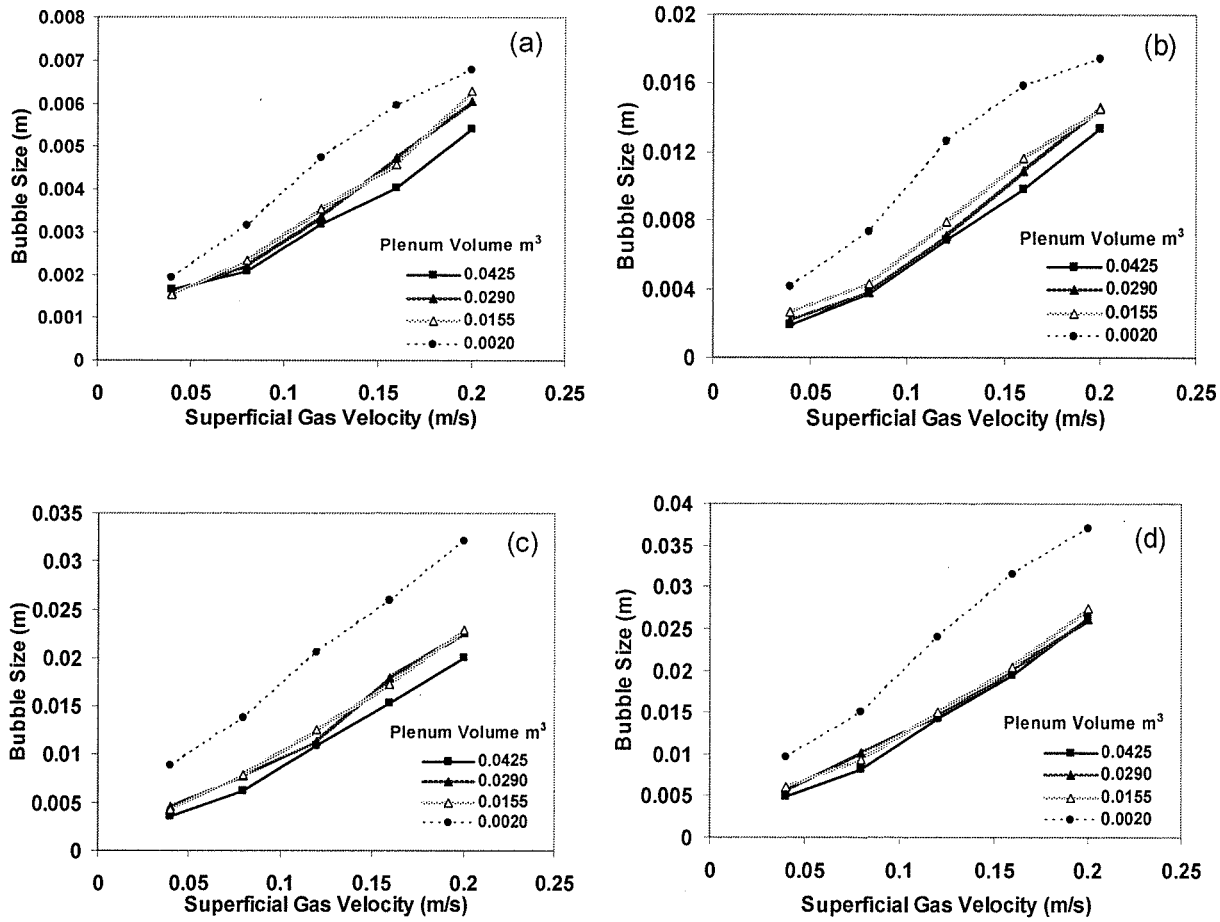

Figure 3.9. Effect of superficial gas velocity and plenum volume on the bubble size derived from the incoherent pressure fluctuations for (a) 0.10 m (b) 0.20 m (c) 0.35 m and (d) 0.50 m of the bed height using multi-orifice distributor for FCC particles. Note that the ordinate scales differ.

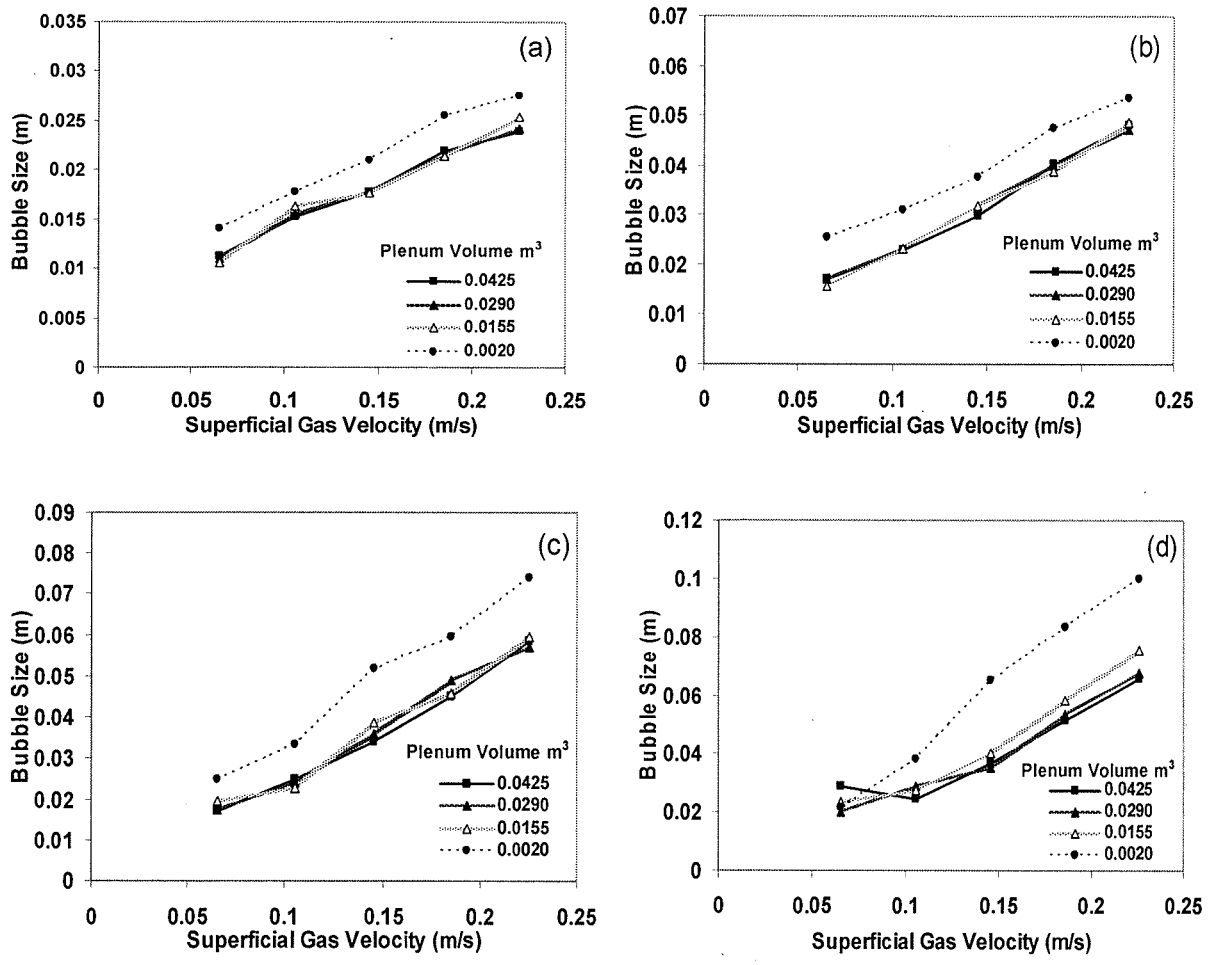

Figure 3.10. Effect of superficial gas velocity and plenum volume on the bubble size derived from the incoherent pressure fluctuations for (a) 0.10 m (b) 0.20 m (c) 0.35 m and (d) 0.50 m of the bed height using single-orifice distributor for glass beads. Note that the ordinate scales differ.

Based on the Welch's method, a custom-made program (Appendix D) was developed in MATLAB and then linked to LabVIEW program to plot the PSD and autocorrelation functions in order to determine the dominant frequency and the effects of plenum volume, superficial gas velocity, and bed height on the system dynamics. In the case of the single-orifice distributor, the frequency spectrum from the distributor pressure drop fluctuations (differential pressure transducer over the distributor) shows multiple peaks as reported by Kage et al. (2000). The sharpest peak is believed to represent the bubbling frequency (bubble formation frequency) as shown in Figure 3.11. Recorded video movies confirm this frequency to be the bubbling

frequency; moreover the autocorrelation function proves its strong periodicity (Figure 3.11). For FCC particles this frequency was between 5.9 and 7.5 Hz, whereas for glass beads it was between 7.1 and 8.8 Hz. The second sharp is believed to represents the bubble eruption at the surface. Frequency spectra from pressure fluctuations determined by absolute pressure transducers in the plenum chamber and fluidized bed also show this frequency. Note that the two peaks in Figure 3.11 are not harmonics, since the smaller one moves considerably to lower frequencies with increasing bed depth, while the bubbling frequency peak is almost unchanged. It was observed that most of the bed was being fluidized when the single-orifice distributor was operating. However, a dead zone was observed at the bottom, far from the orifice.

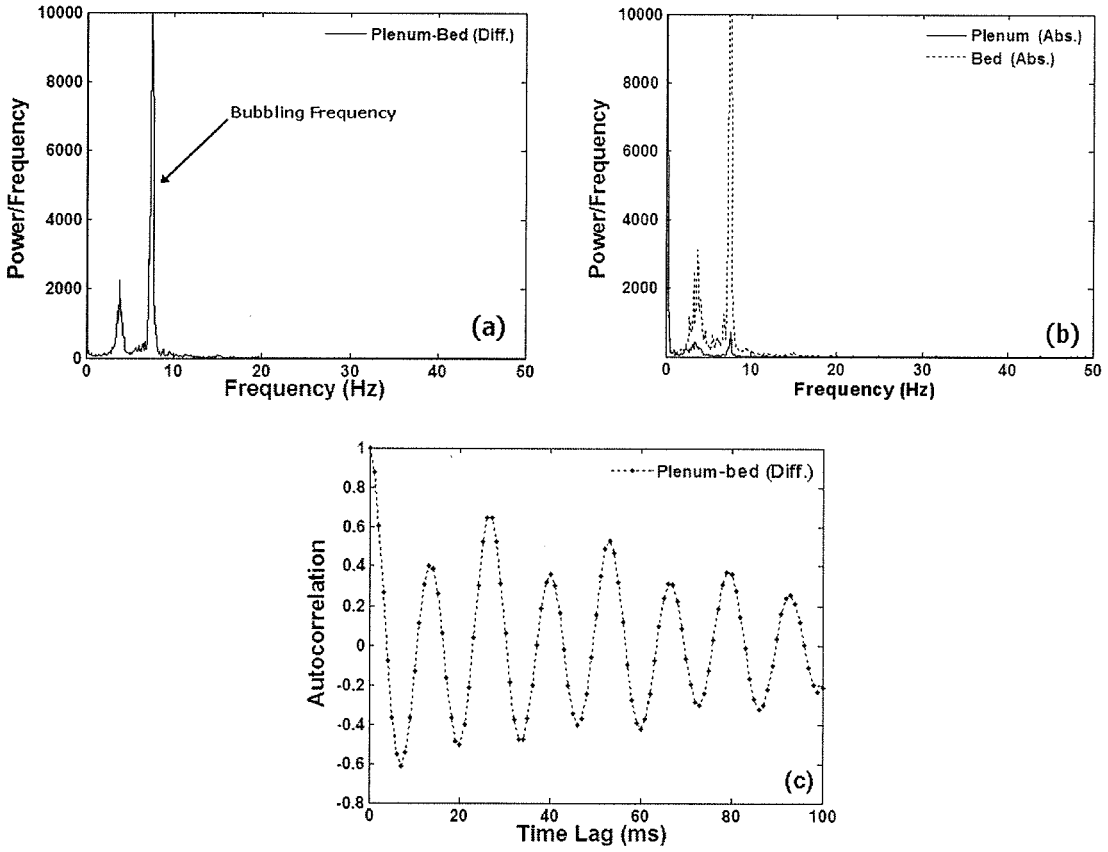

Figure 3.11. Frequency spectra of (a) differential and (b) absolute pressure transducers, with (c) autocorrelation of differential pressure using single-orifice distributor for FCC particles (H_o=0.10 m, V_p=0.0425 m^3, U=0.06).

Increasing superficial gas velocity caused a broadening of the sharp peak of bubbling frequency indicating that at high orifice gas flow rates, bubbling did not occur at a single

frequency, but was spread as shown in Figure 3.12. This might be due to multiple bubble formation at the same time in the orifice. For a gas-liquid system McCann and Prince (1969) reported that at high gas flows, pairs of bubbles coalesced close to the orifice. The two merged bubbles rose only a small distance above the orifice before shattering into many small bubbles of varying sizes, leading to irregular bubbles. They also recorded video movies confirming pairing bubble formation in gas-liquid systems for high orifice flow rates.

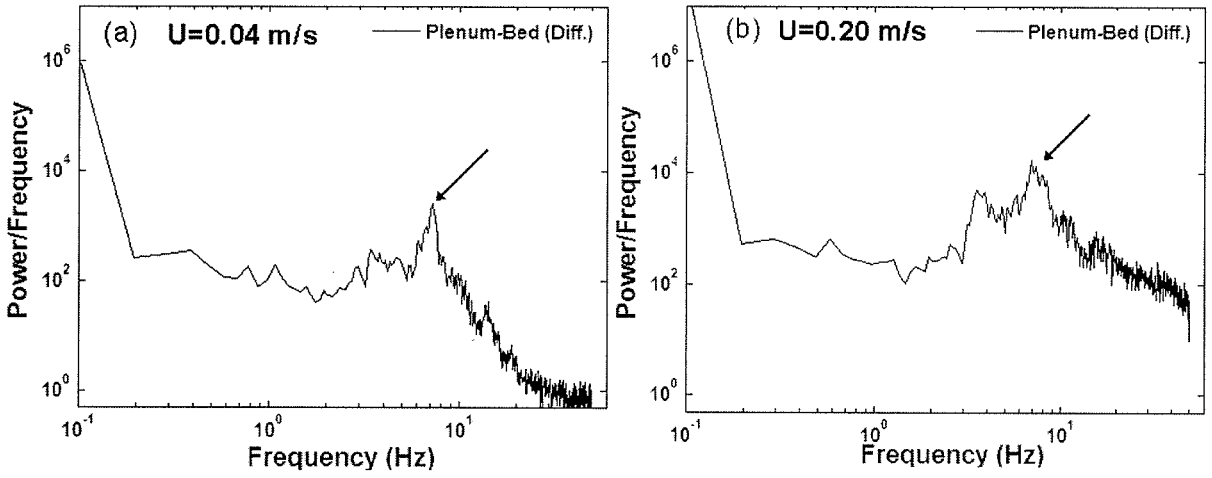

Figure 3.12. Effect of superficial gas velocity on broadening the frequency of the difference in pressure between the plenum chamber and a point inside the bed 38.1 mm above the distributor using single-orifice distributor for FCC particles. Arrows indicate bubbling frequency. (H_o=0.10 m, V_p=0.0425 m^3, (a) U=0.04 m/s, (b) U=0.2 m/s).

McCann and Prince (1969) proposed a model for bubble formation in an inviscid liquid considering the plenum volume. They showed experimentally and theoretically that the bubbling frequency increases with increasing orifice gas velocity in an inviscid liquid, leveling off beyond a certain value. Nguyen and Leung (1972) studied bubble formation at an orifice in a two-dimensional fluidized bed and, after taking into account gas flow through the bubble, showed that the bubbling frequency decreases with orifice gas flow rate. In this study the bubbling frequency was almost constant when the superficial gas velocity was varied for glass beads and FCC particles; however, a slightly decrease in bubbling frequency with increasing orifice flow rate was sometimes observed, as shown in Figure 3.13.

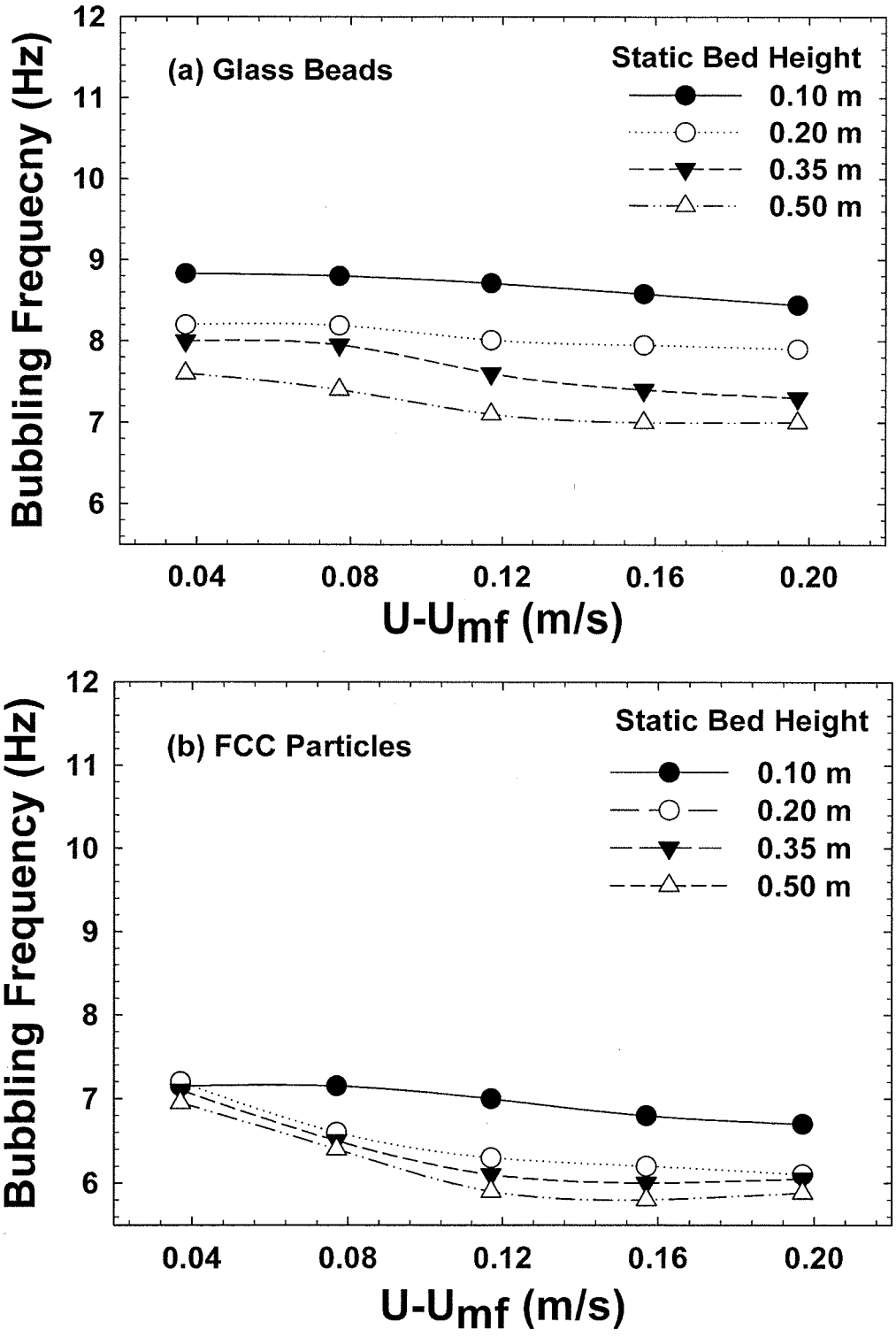

Figure 3.13. Effect of superficial gas velocity and static bed height on bubbling frequency for (a) glass beads; (b) FCC particles using single-orifice distributor (V_p=0.0425 m^3).

In these experiments, increasing bed height resulted in a lowering of the bubble frequency. This might be due to the fact that increasing the bed height results in more compression at the orifice, causing the air to enter the bed at a lower velocity for constant U, determined at the bed surface.

For single-orifice distributor, the bubbling frequency increased slightly with decreasing plenum volume as shown in Figure 3.14. This is in agreement with McCann and Prince (1969, 1971) in a study of bubble formation at a submerged orifice in a low-viscosity liquid. They also proposed a model for bubble formation in an inviscid fluid considering the effect of plenum volume and showed a decrease in bubbling frequency with increasing plenum volume. More details on the modeling are given in Chapter 5. Kage et al. (2000) also showed that the measured bubbling frequency increased as the plenum volume decreased. The effect of plenum volume on bubbling frequency was more noticeable for FCC particles than for glass beads.

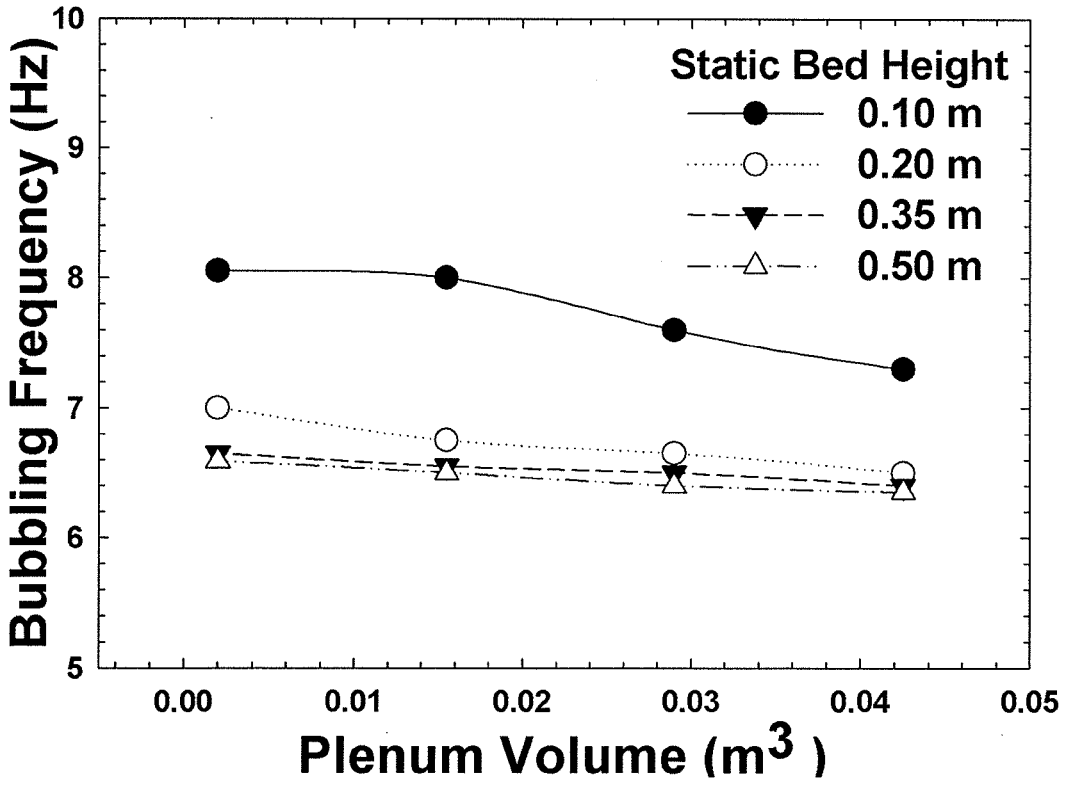

Figure 3.14. Effect of plenum volume on bubbling frequency for single-orifice distributor and FCC particles (U-U_{mf} = 0.077 m/s).

As mentioned above, decreasing the chamber volume caused the bubbling frequency to increase. Eventually a state was reached where the wake of one bubble affected the next one, deforming it and resulting in irregular bubble formation (McCann and Prince, 1969). They also pointed out that decreasing the plenum volume caused multiple bubble formation. Figure 3.15 shows that in the case of minimum plenum volume, instead of a sharp peak for bubbling frequency, there is some spreading in the frequency spectrum, possibly related to bubble pairing and irregular multiple bubble formation. Accordingly, bubble formation for a large plenum chamber is more regular than for a small plenum chamber.

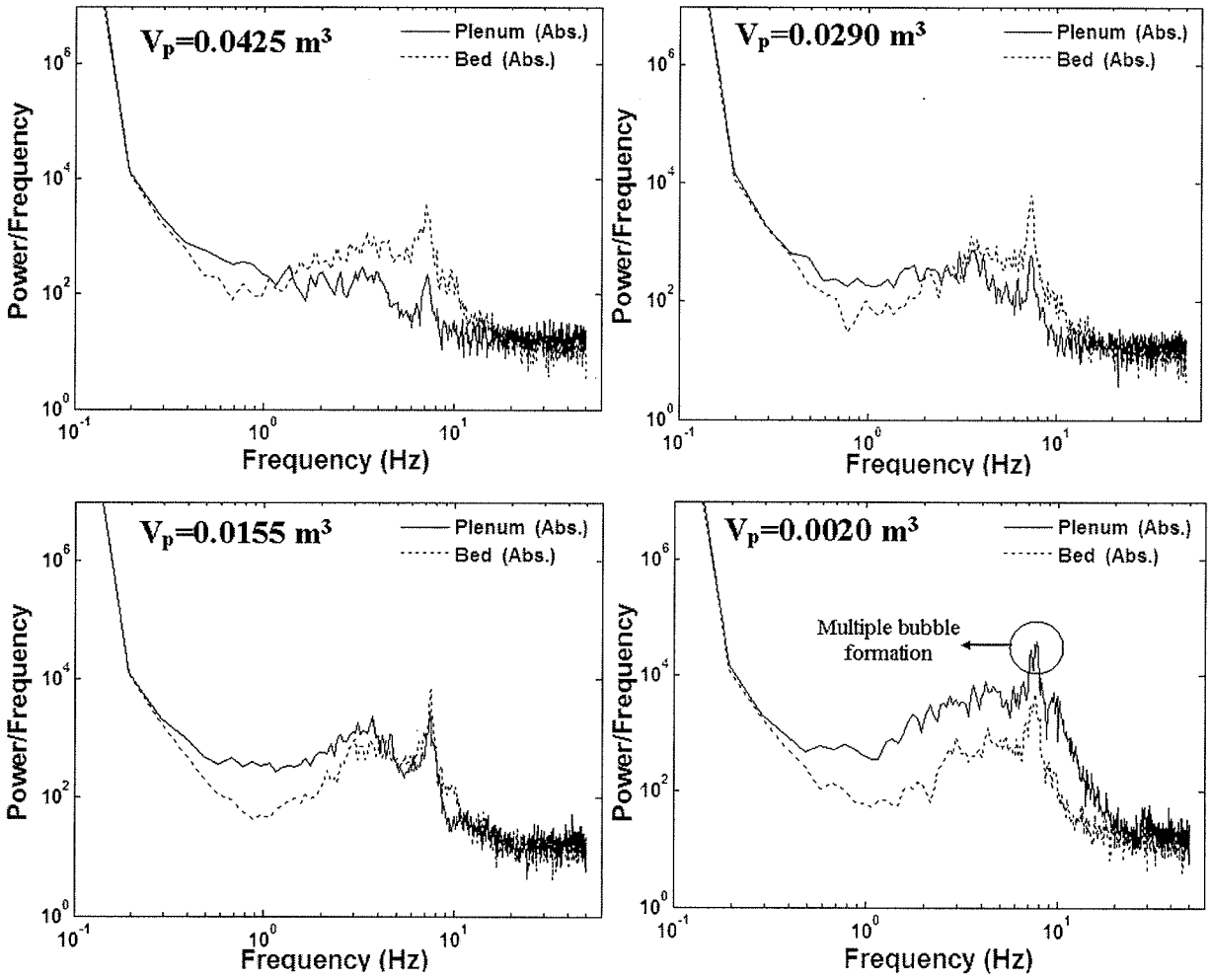

Figure 3.15. Effect of plenum volume on frequency spectrum for single-orifice distributor and FCC particles, H_o=0.10 m, U-U_{mf}= 0.037 m/s.

To determine the periodicity of pressure-time signals, autocorrelation was performed on the pressure fluctuations from the plenum chamber, bed, and differential pressure transducer across the distributor. Figure 3.16 shows strong periodicity for the distributor pressure drop, related to the bubbling frequency.

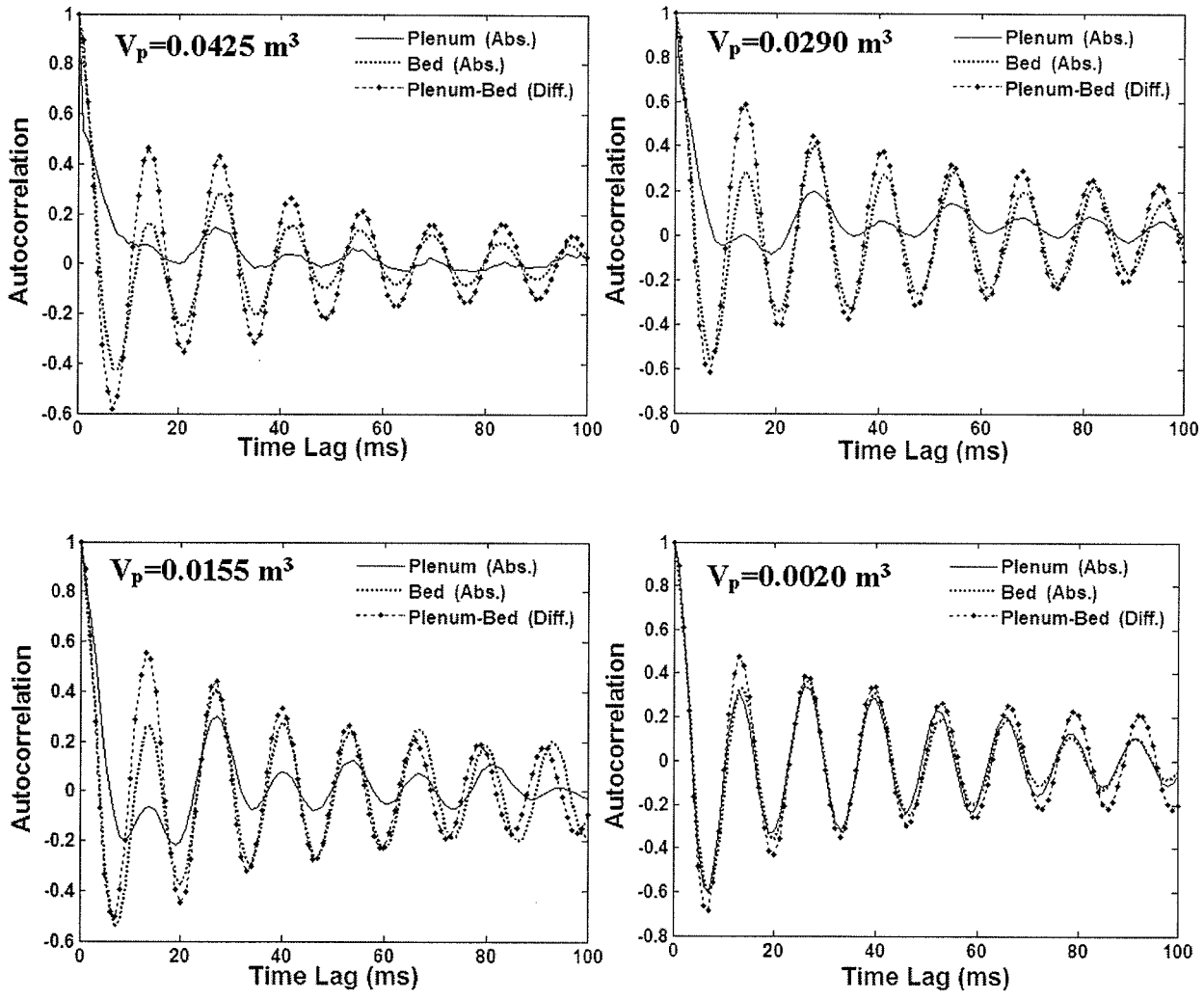

Figure 3.16. Effect of plenum volume on periodicity of pressure fluctuations for single-orifice distributor and FCC particles, H_o=0.10 m, U-U_{mf}= 0.037 m/s.

With decreasing plenum volume, the autocorrelation reveals more periodic fluctuations in the plenum chamber. Moreover, it can be inferred from Figure 3.16 that by reducing the plenum volume, pressure signals from the plenum chamber reflect the pressure fluctuations of the distributor pressure drop and at the bottom of the bed. This can be explained by relating

pressure fluctuations of the plenum chamber and bed. As suggested by Sierra and Tadrist (2000), the instantaneous distributor pressure drop can be determined from:

$$P_p(t) - P_b(t) = \xi_d(t).\frac{1}{2}\rho_g U^2(t) \tag{3.19}$$

where ξ_d is the discharge coefficient. Pressure in the plenum, pressure at the bottom of the bed, and the inlet velocity can be split into stationary and fluctuating parts:

$$P_b(t) = \overline{P}_b + \tilde{P}_b(t) \tag{3.20}$$

$$P_p(t) = \overline{P}_p + \tilde{P}_p(t) \tag{3.21}$$

$$U(t) = \overline{U} + \tilde{U}(t) \tag{3.22}$$

Combining equations (3.19) to (3.22) with the assumptions of small amplitude of the fluctuating velocity component ($\tilde{U}^2 \approx 0$) and $\xi_d(t) = \overline{\xi}_d$ results in:

$$\tilde{P}_p(t) - \tilde{P}_b(t) = \rho_g \overline{\xi}_d \tilde{U}\overline{U} \tag{3.23}$$

to relate superficial gas velocity fluctuations to the pressure fluctuations inside the plenum, it should be assumed that the pressure fluctuations in the plenum chamber are reversible and adiabatic. Therefore these fluctuations can be related to the air density by:

$$\frac{\delta\rho_g}{\rho_g} = \frac{\delta m_g}{m_g} = \frac{-\int \rho_g \tilde{U} A dt}{\rho_g V_p} = \frac{-A}{V_p}\int \tilde{U} dt \tag{3.24}$$

$$\frac{\tilde{P}_p}{\overline{P}_p} = \gamma \frac{\delta\rho_g}{\rho_g} \tag{3.25}$$

$$\tilde{U} = -\frac{V_p}{\gamma A \overline{P}_p}\frac{d\tilde{P}_p}{dt} \tag{3.26}$$

Combining of Equations 3.26 and 3.23 leads to:

$$\frac{d\tilde{P}_p}{dt} + \left(\frac{\gamma A \overline{P}_p}{\rho_g \overline{\xi}_d V_p \overline{U}}\right)\tilde{P}_p = \left(\frac{\gamma A \overline{P}_p}{\rho_g \overline{\xi}_d V_p \overline{U}}\right)\tilde{P}_b \tag{3.27}$$

Equation 3.27 relates pressure fluctuations in the plenum chamber to bed pressure fluctuations. In Equation 3.28, if the plenum volume goes to infinity (large plenum volume), $d\tilde{P}_p/dt$ approaches zero. Therefore $\tilde{P}_p$ is constant and there will be no periodic fluctuation of pressure inside the plenum. On the other hand, for a small plenum volume with finite $d\tilde{P}_p/dt$,

pressure fluctuations in the plenum match those inside the bed. This can also be inferred from frequency spectra, as shown in Figure 3.17(d).

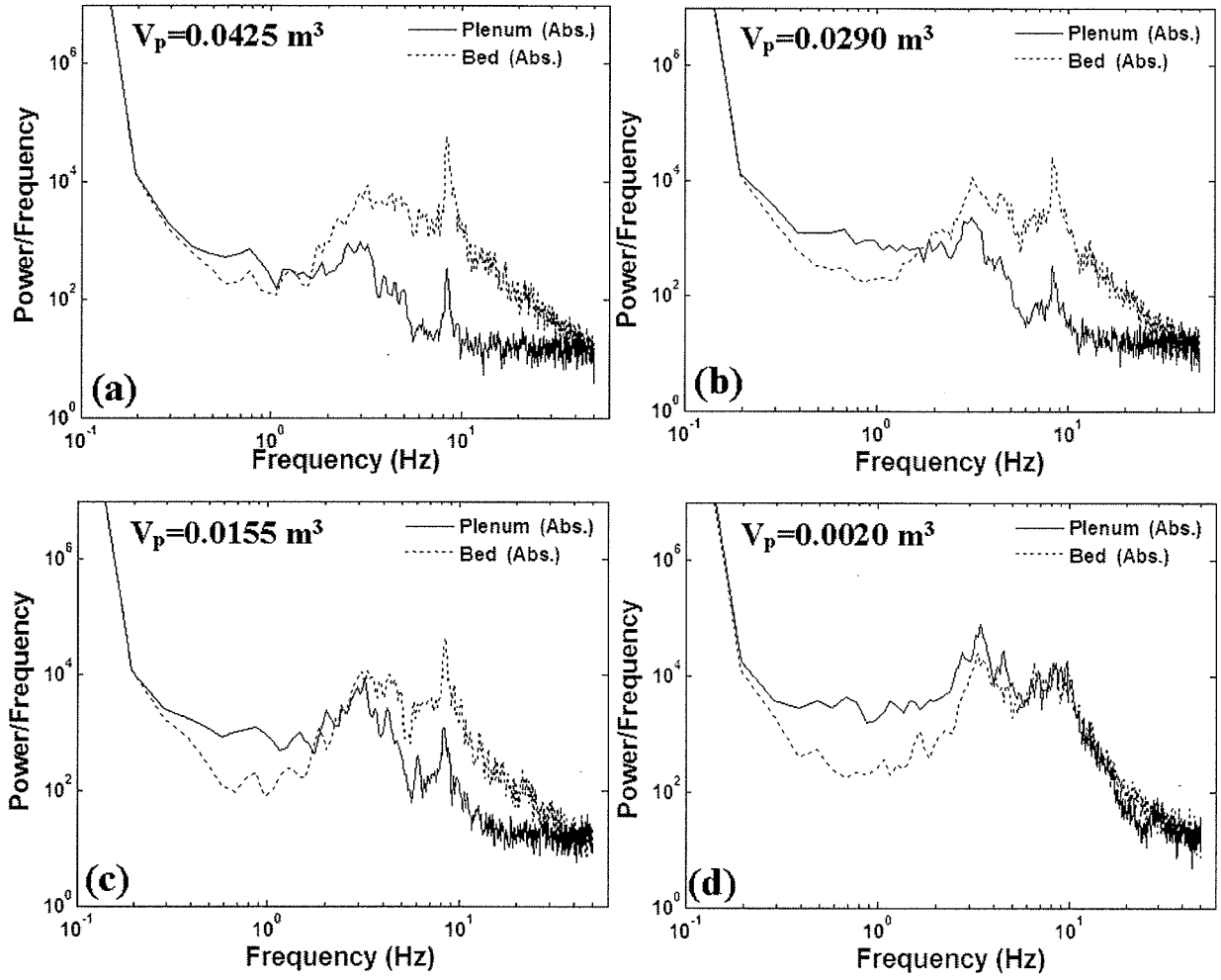

Figure 3.17. Influence of plenum volume on pressure fluctuations in plenum chamber and bed for single-orifice distributor, glass beads, H_o=0.10 m, U-U_{mf}= 0.037 m/s.

In addition to the bubbling frequency, a second sharp peak of lower frequency is noticeable in the frequency spectrum from the single-orifice distributor experiments (e.g. see Figures 3.11(a) and (b)). This frequency did not change significantly with varying plenum volume, especially for a low static bed height. Therefore, for the single-orifice distributor, this is not the natural frequency calculated by the Davidson (1968) or Moritomi (1980) models

because these models take into account the volume beneath the fluidized bed to estimate the natural frequency.

In this study, increasing the bed height caused the second frequency to decrease; moreover, it seems that this frequency was independent of the superficial gas velocity. Therefore, bursting bubbles on the surface of the fluidized bed could be the source of these fluctuations. Figure 3.18 shows acceptable agreement between experimental results for this frequency and predictions from the model of Baskakov et al. (1986), who showed that the pressure drops simultaneously in both the upper and lower sections of the bed at the instant when bubbles emerge at the surface. The bursting bubble forms a crater on the surface, and the bed height is therefore diminished in this regime. As a result, the resistance to the flow of gas decreases too, leading to a simultaneous decrease in pressure along the entire bed height and even in the plenum chamber. Baskakov et al. (1986) simplified bubble eruption on the surface of the fluidized bed by the oscillation of an ideal liquid in a U-shape of constant cross-sectional area as shown in Figure 3.19. Accordingly, they proposed that the pressure oscillation frequency is:

$$f = \frac{1}{\pi}\sqrt{\frac{g}{H_{mf}}} \tag{3.28}$$

Video movies taken from the bed surface confirmed that bubbles bursting at the bed surface were the source of this peak in the frequency spectrum. Bi (2007) reviewed the literature for pressure fluctuations in gas-solid fluidized bed and concluded that the dominant frequency from absolute pressure fluctuations generally corresponds to the bubble eruption frequency detected at the bed surface.

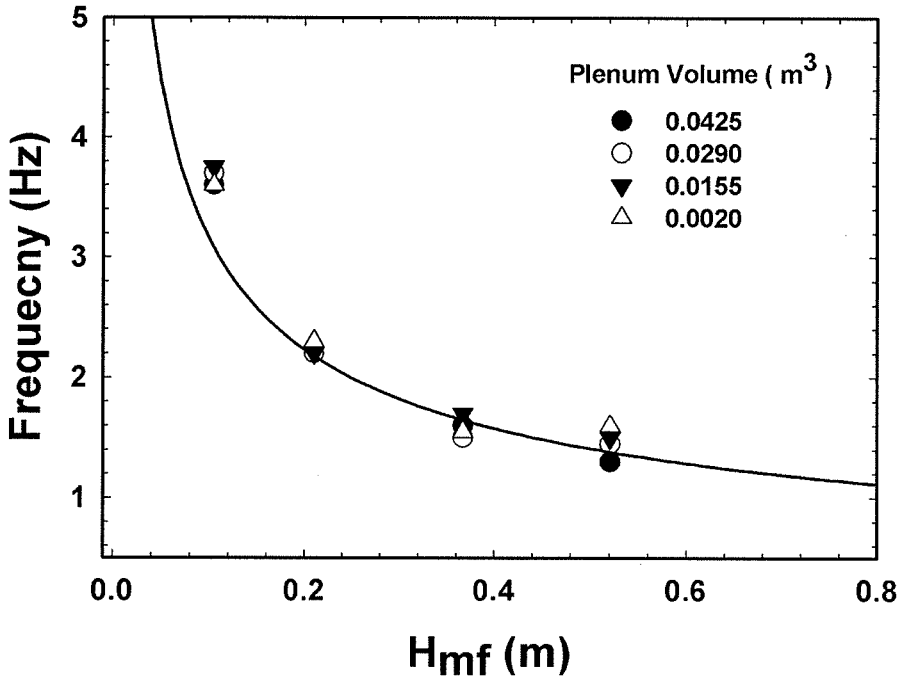

Figure 3.18. Effect of bed height on bubble eruption frequency for FCC particles, single-orifice distributor, $U\text{-}U_{mf}$ = 0.077 m/s. Line is from the model of Baskakov et al. (1986). Points are from the second (lower) peak from frequency spectra, as in Figure 3.11.

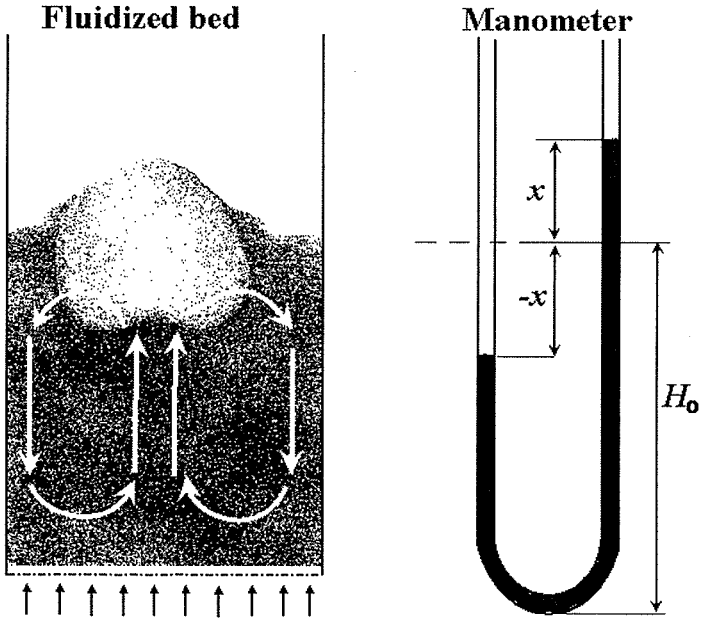

Figure 3.19. Circulatory motion in a fluidized bed caused by a rising bubble and its similarity to manometer oscillation.

For low static bed heights, the volume-dependent equations for natural frequency proposed by Davidson (1968) and Moritomi (1980) do not match the above-mentioned peaks from the frequency spectra. Only for a relatively high static bed height (0.50 m), another peak appears in the frequency spectrum, dependent on the plenum volume. Figure 3.20 shows that this peak moves towards higher frequencies (from 0.8 Hz to 3 Hz) with decreasing plenum volume. A higher static bed height has more ability to compress the air in the plenum chamber; therefore the effect of plenum volume is more noticeable for a deeper static bed.

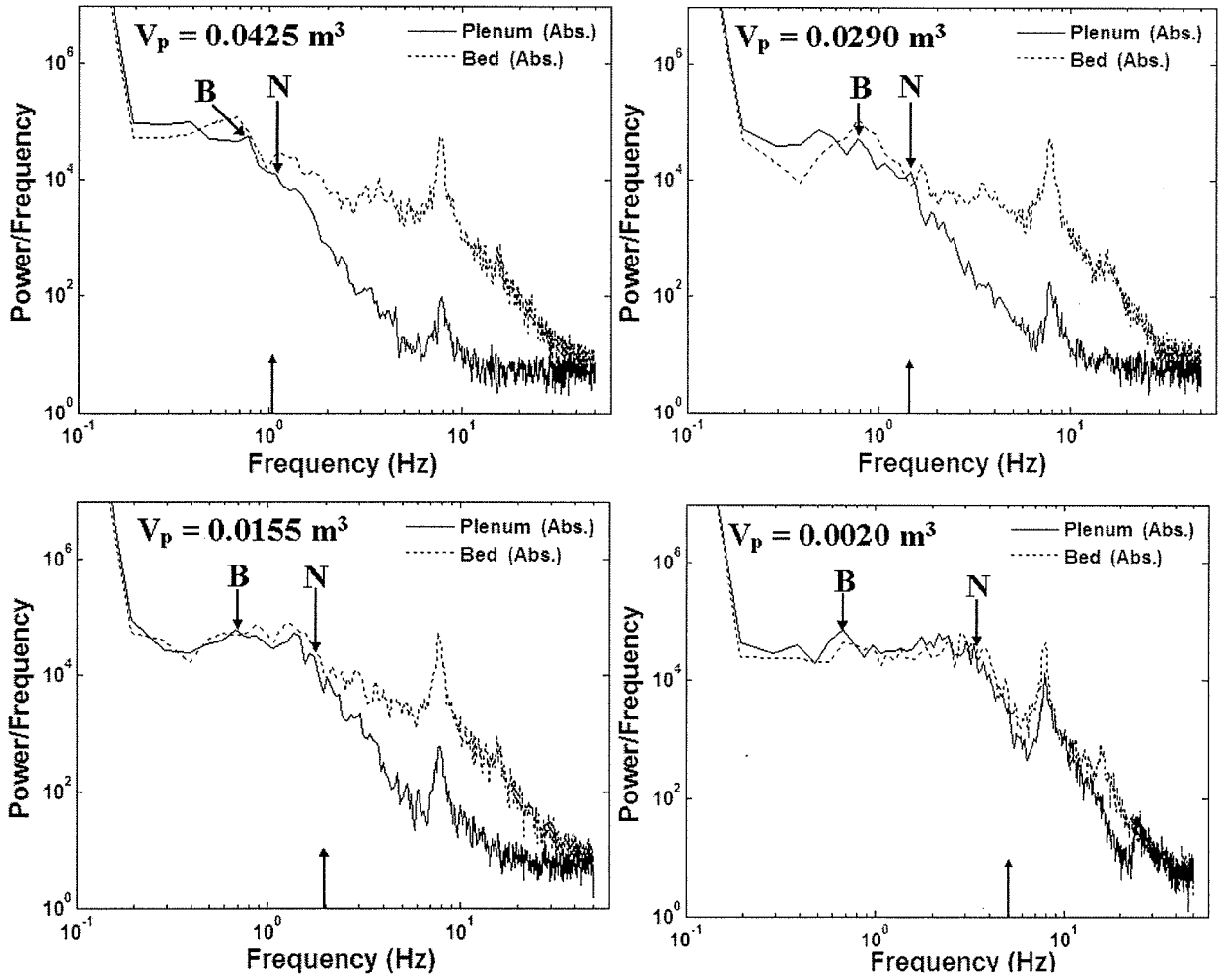

Figure 3.20. Effect of plenum volume on the natural frequency for a single-orifice distributor and glass beads. H_o=0.50 m, U-U_{mf}= 0.037 m/s. The upward-pointing arrows show the natural frequencies predicted by the Davidson (1968) model. "B" Represents bubble eruption frequency and "N" represents natural frequency.

Frequency spectra for the multi-orifice distributor show that by decreasing the plenum volume the dominant frequency moved to higher frequencies. This is even noticeable for a low static bed height, unlike the finding for a single-orifice distributor. The reason might be related to the single-orifice distributor having a higher pressure drop (Figure 3.21 b) than the multi-orifice distributor (Figure 3.21 a), even though the total open area for both distributors was equal. As suggested by Davidson (1986), the ability of the fluidized particles to compress the air in the plenum chamber is higher for multi-orifice distributor. In the Davidson (1986) model, the ability to compress the air in the plenum chamber is the basis of the natural frequency in the gas-solid fluidized bed. Figure 3.21 shows the distributor pressure drop for various operating conditions.

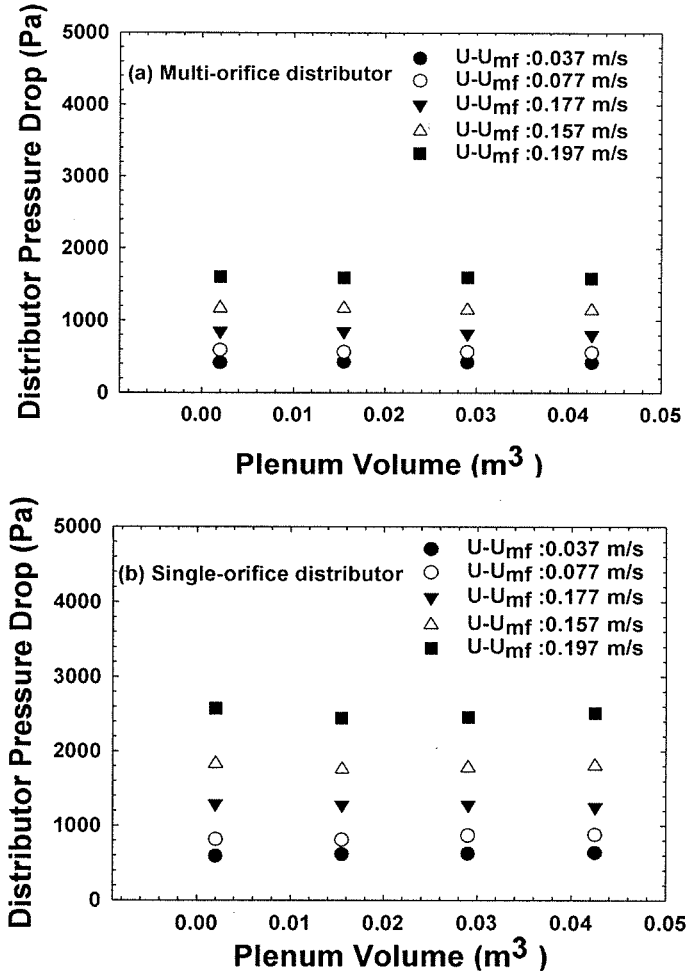

Figure 3.21. Distributor pressure drop for single and multi-orifice distributors with FCC particles and H_o= 0.02 m.

A multi-orifice distributor causes the release of many small bubbles from a discrete number of sites, which may occur in or out of phase. As a result, the multi-orifice distributor shows a broader frequency spectrum than the single-orifice distributor. Moreover, single bubbles released from a single-orifice are much larger than those from the multi-orifice distributor. Hence the related bubbling frequency has more power than from the multi-orifice distributor as shown in Figure 3.22. Unlike frequency spectra from the single-orifice distributor, it is difficult to locate a specific frequency for bubbling or natural oscillation from the multi-orifice spectra.

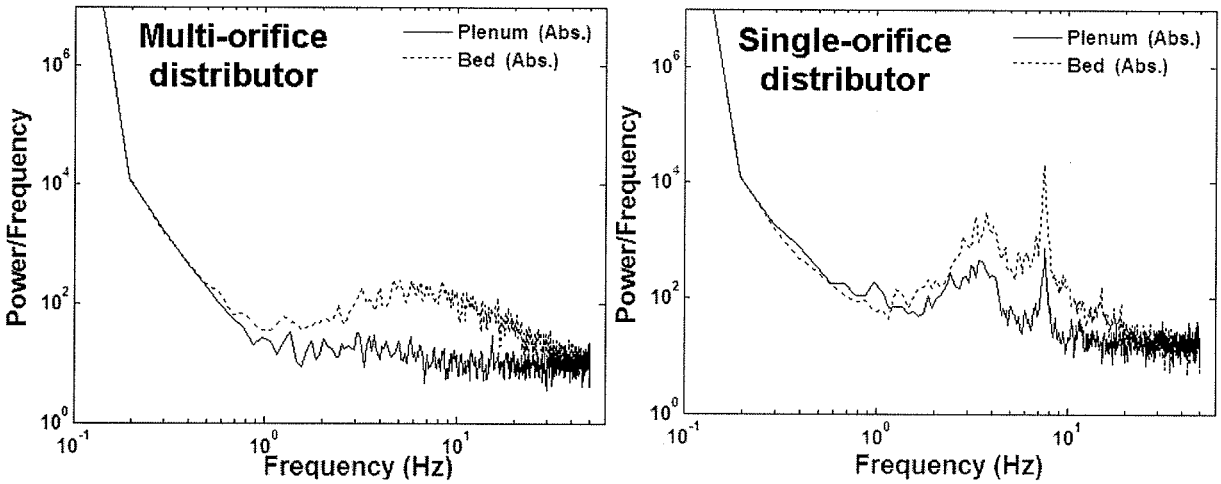

Figure 3.22. Influence of distributor plate on the frequency spectrum for FCC particles, H_o=0.10 m, U-U_{mf}= 0.077 m/s, V_p=0.0425 m^3.

Decreasing plenum volume caused the broad frequency spectrum of the plenum pressure fluctuations to move slightly towards higher frequencies, as shown in Figure 3.23. This may be related to the natural frequency of self-excited oscillation of gas in the plenum chamber. However for a minimum plenum volume, the frequency does not match the Davidson (1986) model very well. Wong and Baird (1971) also reported that for a small plenum volume the Davidson model overestimated the measured natural frequencies. As mentioned above, with decreasing plenum volume, pressure fluctuations in the plenum chamber match those in the bed (Equation 3.27). It is also shown in Figure 3.23 that at the minimum plenum volume, frequency spectra for both the plenum and bed overlap.

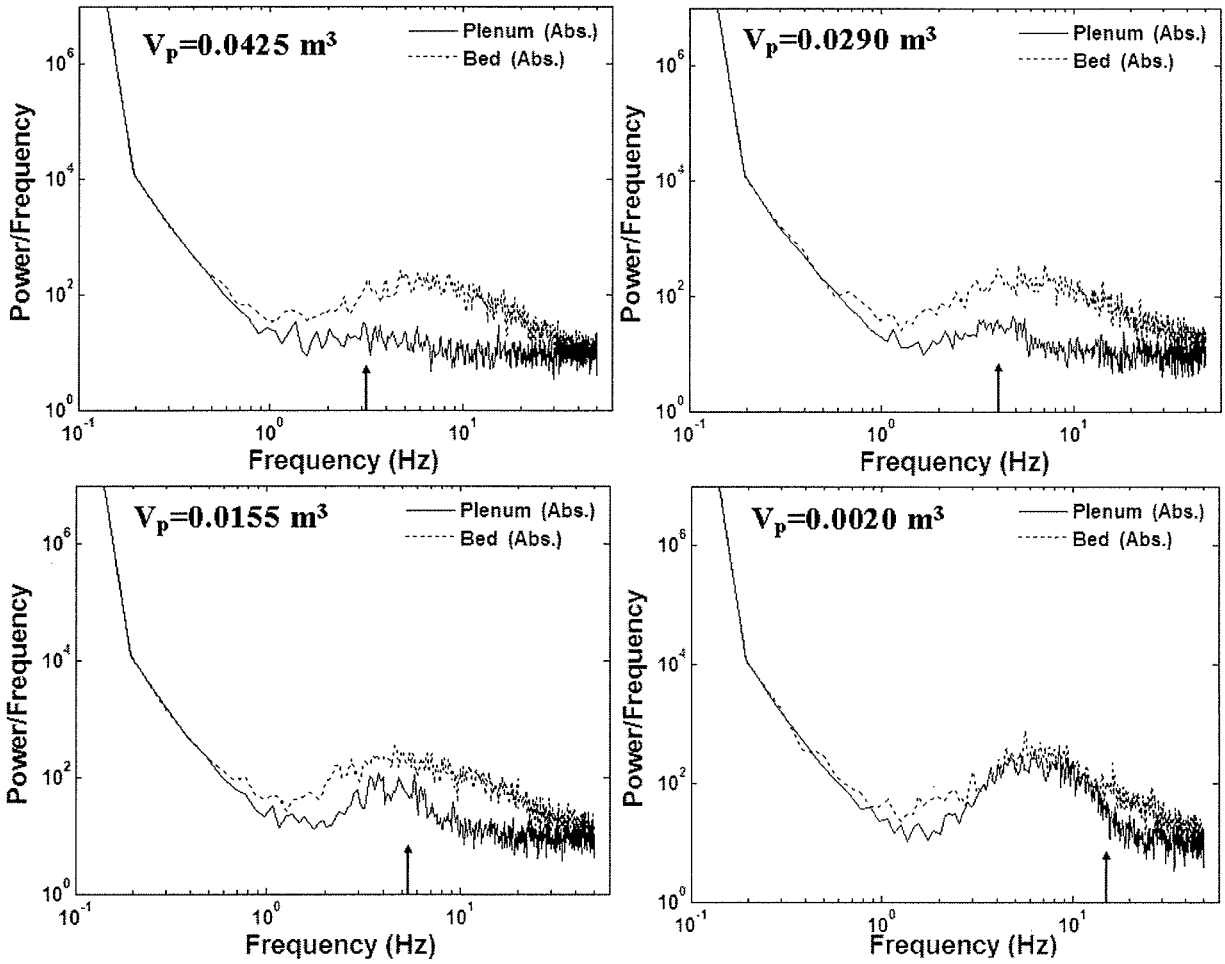

Figure 3.23. Effect of plenum volume on natural frequency for FCC particles, multi-orifice distributor, H_o=0.10 m, U-U_{mf}= 0.077 m/s. The arrows show the natural frequency predicted by the Davidson (1986) model.

Another effect of the plenum volume was that the frequency spectrum narrowed to a specific frequency with decreasing plenum volume for both glass beads and FCC particles. This effect is more pronounced for deeper static beds (i.e. H_o= 0.35 or 0.50 m). Figure 3.24 shows that at the minimum plenum volume, the frequency spectrum has a relatively sharp frequency at 4.6 Hz, which was not observable in the frequency spectrum for the maximum plenum volume. This indicates that for small plenum chambers, relatively coordinated or coherent bubbling occurs compared with multiple bubbling, the latter leading to a broader and flatter frequency spectrum. This might be due to the fact that for small plenum volume, the whole volume of plenum can be easily subjected to pressure variation causing bubbles to form in

phase, whereas for large plenum volume, the pressure inside the plenum chamber is almost constant and random bubbling is more probable.

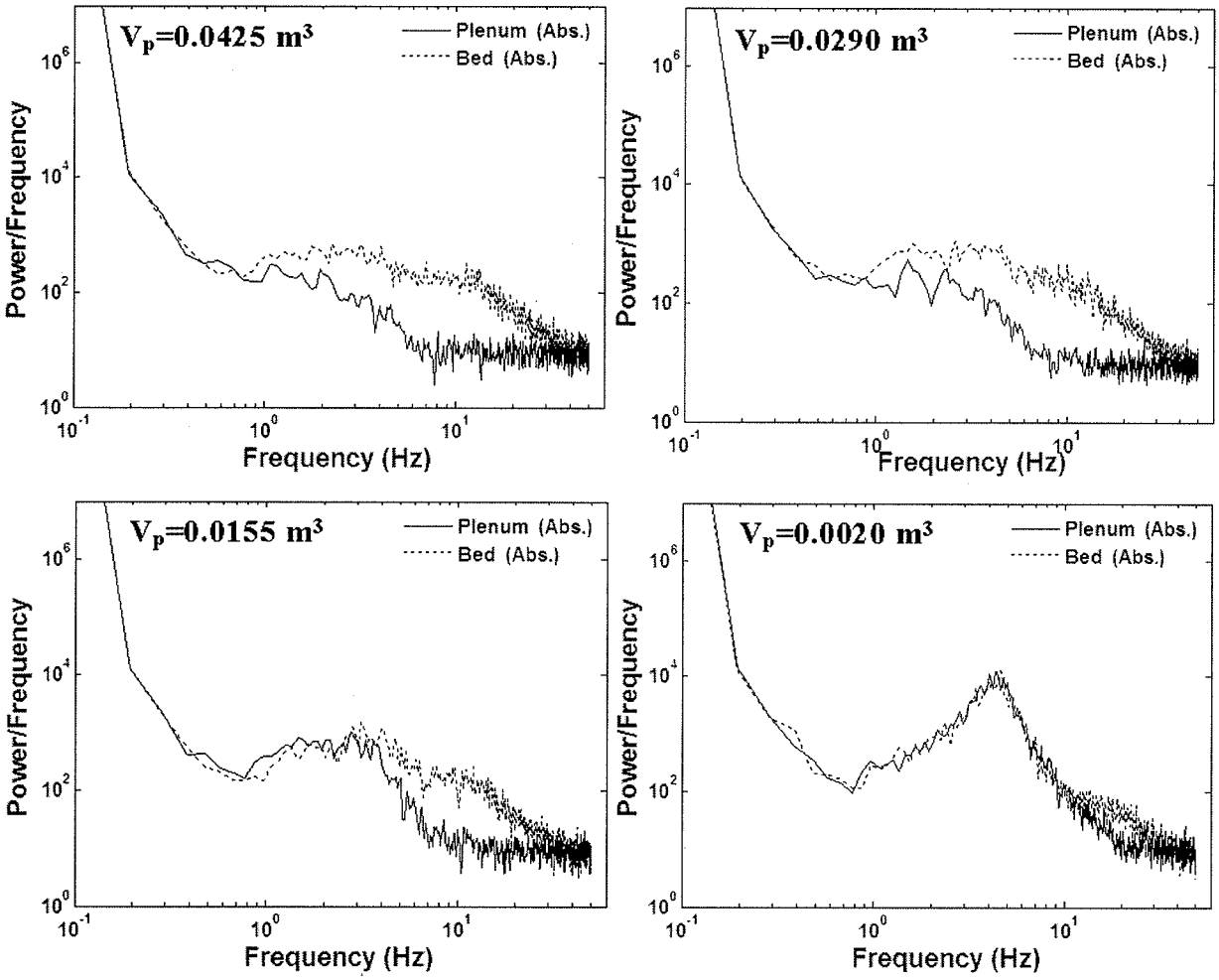

Figure 3.24. Effect of plenum chamber on frequency spectrum for FCC particles and a multi-orifice distributor, H_o=0.35 m, U-U_{mf}= 0.037 m/s.

As mentioned above for the single-orifice distributor measurements, bed height has a similar effect for the multi-orifice distributor. Increasing the static bed height causes the dominant frequency to decrease. Figure 3.25 shows that in the case of minimum plenum volume (for which it is easier to locate the dominant frequency), by increasing bed height, the dominant frequency shifted from 7.0 to 4.0 Hz. However, this frequency change cannot be estimated very well by the Baskakov (1986) equation (eq. 3.28 above), not surprising as in that study it was assumed that only one bubble erupted at a time.

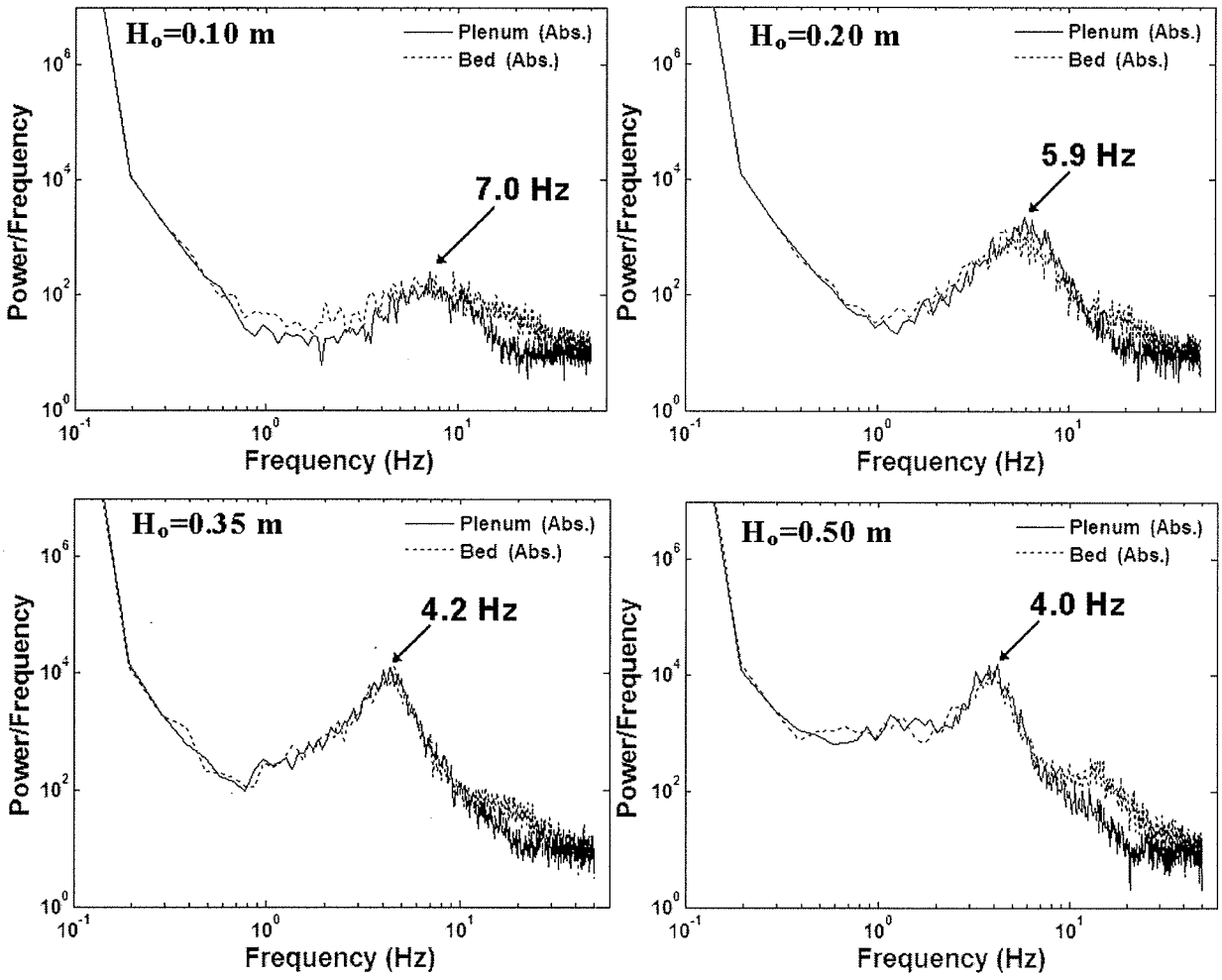

Figure 3.25. Effect of static bed height on frequency spectrum for FCC particles and a multi-orifice distributor, V_p= 0.0020 m^3, U-U_{mf}= 0.037 m/s.

In this study, the dominant frequency was found to decrease with increasing superficial gas velocity for the multi-orifice distributor. Figure 3.26 shows that the dominant frequency shifted from 4.2 to 2.9 Hz for fluidization of FCC particles with H_o=0.35 m and the minimum plenum volume. This is in agreement with Nguyen and Leung (1972) who studied bubble formation at an orifice in a gas-solid fluidized bed. Decreasing the bubbling frequency with increasing the gas orifice velocity implies that the bubble size should increase with increasing superficial gas velocity. This was previously shown in Figures 3.8 to 3.10.

Another effect of superficial gas velocity on the fluidization by multi-orifice distributor is that the frequency spectrum became broader with increasing superficial gas velocity as inferred from Figure 3.26. This might be due to the fact that an increase in superficial gas velocity causes an increase in distributor pressure drop, thus isolating the plenum chamber more from the fluidized bed. The higher distributor pressure drop therefore causes a more even distribution of multiple bubbles, resulting in the corresponding frequency spectrum becoming broader.

It is noteworthy that in the case of multi-orifice measurements, the dominant frequency for glass beads was lower than for the FCC particles. This is related to the fact that fluidization by glass beads (Geldart group B) resulted in larger bubbles than fluidization with FCC particles (Geldart group A). Thus the dominant frequency for glass beads was lower than for the FCC particles. This is shown in Figure 3.27 for different static bed heights while fluidizing with minimum plenum volume.

Based on the above-mentioned results from pressure measurements for different plenum volume, it seems that the van der Schaaf et al. (2002) approach for bubble size estimation by incoherent part of pressure fluctuations has some defects while using small plenum volume (i.e. less than 0.002 m^3). This can be justified in several ways. The first one can be explained by bubbling frequency. As shown in Figure 3.14, bubbling frequency decreased with increasing plenum volume, so for the same superficial gas velocity larger bubbles occurred for large plenum volume, whereas the van der Schaaf et al. (2002) approach predicted larger bubbles for small plenum volume (e.g. 0.002 m^3). The other reason is tied to Equation 3.27, which relates the fluctuating parts of plenum pressure to the bed pressure. As mentioned above for small plenum chambers, the plenum pressure fluctuations match the bed pressure fluctuations, so they are more coherent for small plenum chambers. This has also been confirmed with experimental results shown in Figures 3.16 and 3.17. But the van der Schaaf et al. (2002) approach predicts higher values for the incoherent part of pressure fluctuations for small plenum chambers which results in predicting higher values for bubble size. Moreover, the mechanistic model developed for bubble formation in Chapter 5 below also predicts decreasing bubble volume with decreasing plenum volume.

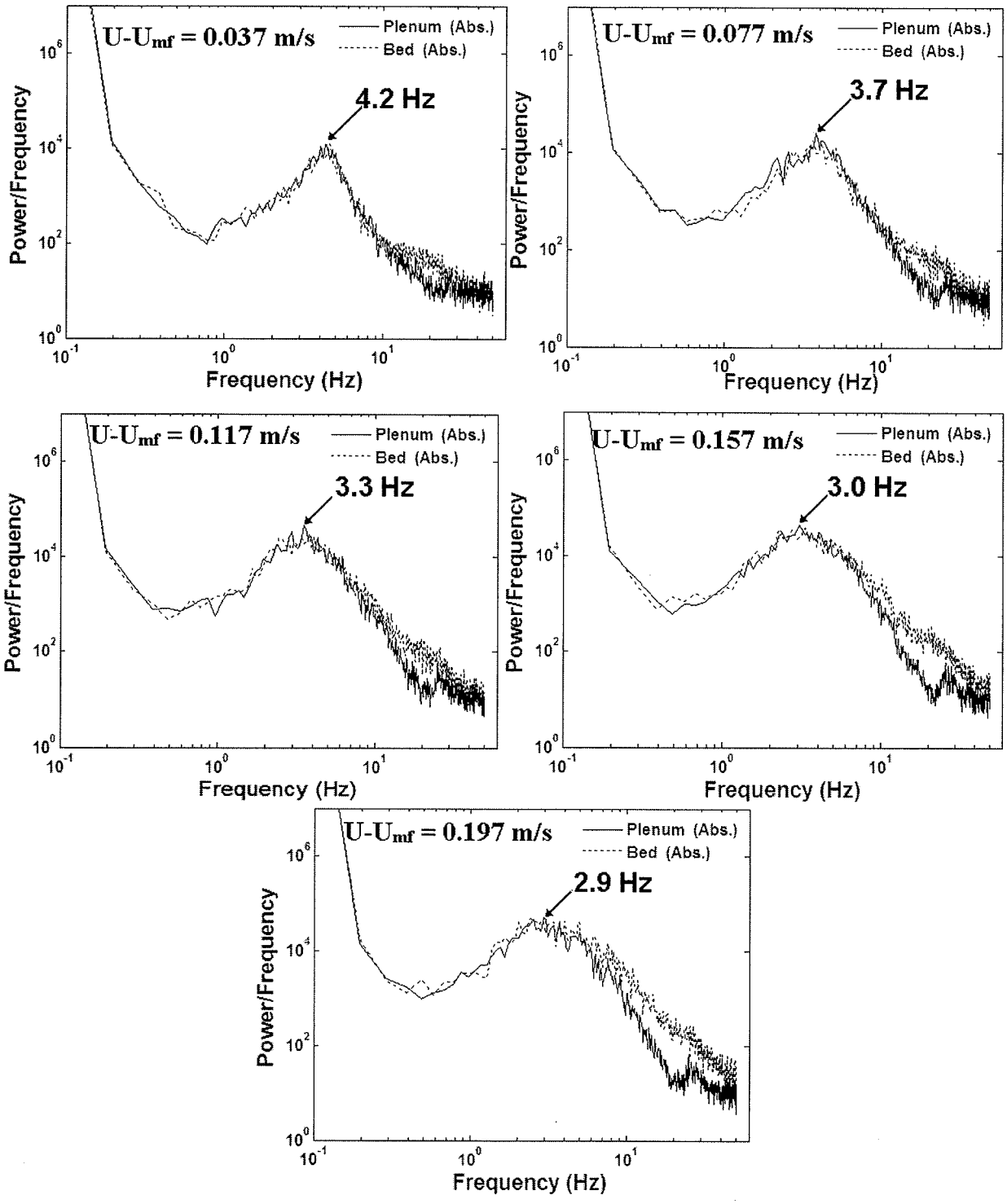

Figure 3.26. Effect of superficial gas velocity on frequency spectrum for FCC particles with multi-orifice distributor, V_p= 0.0020 m^3, H_o=0.35 m.

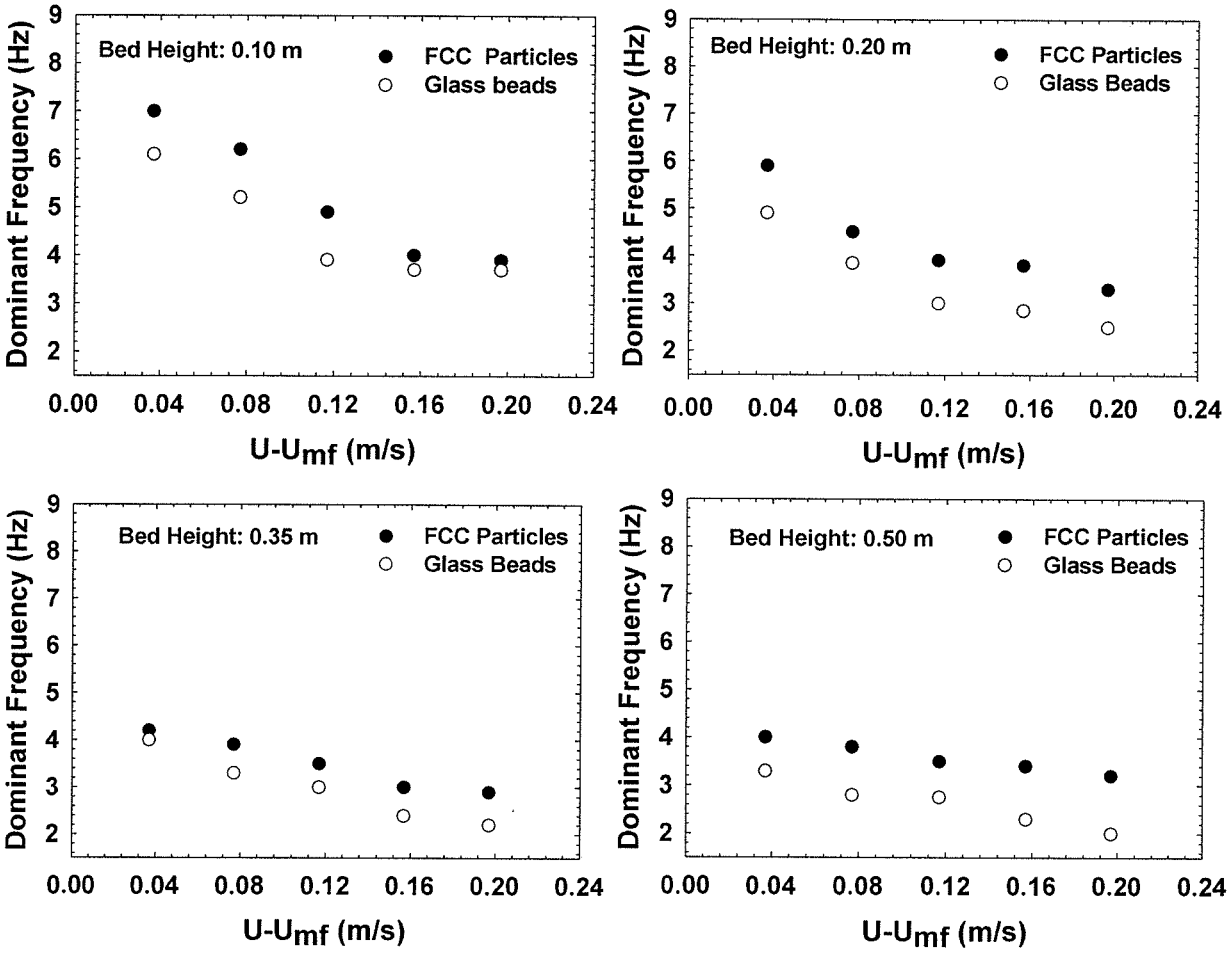

Figure 3.27. Effect of particle type on dominant frequency for multi-orifice distributor with V_p= 0.0020 m^3.

It should be mentioned that comparing results from single and multi-orifice distributor is difficult, since measurements from multi-orifice distributor result in broad frequency spectra. Therefore, there is no prominent peak in the frequency spectrum, except when using the minimum plenum chamber volume where more coherent bubbling occurs.

3.5 Summary

To elucidate the dynamics of the gas-solid fluidized bed, the most common type of measurement, pressure fluctuations, was applied. By means of frequency analysis, dominant, natural, and bubbling frequencies were extracted from the frequency spectra. The effects of plenum volume and operating conditions were studied.

In the case of the single-orifice distributor, two main peaks were usually present in the frequency spectrum. The higher one, representing the bubbling frequency, slightly decreased with increasing plenum volume and superficial gas velocity. The other peak is related to bubble eruption at the surface of the fluidized bed and is in agreement with the Baskakov (1986) equation. Unlike the single-orifice distributor, the multi-orifice distributor measurement had a broad frequency spectrum. In addition to bed height and superficial gas velocity, plenum volume can influence the dominant frequency for a multi-orifice distributor.

Chapter 4: Velocity Fluctuations Measurement

4.1 Introduction

Accurate measurement of fluid velocity and flowrate is required in many applications. Based on hydrodynamic and physical principles, measurement tools have been developed to measure fluid velocity and its fluctuations. For incompressible flow of low-viscosity gases and liquids, the principle of continuity and the Bernoulli equation are useful in determining average flow properties along a streamline, with time-averaged velocity measurements made by Pitot-static tubes. However, to measure velocity fluctuations and unsteady flows, Pitot-static tubes are not appropriate because they measure time-averaged velocity. Hot-wire anemometry is often suitable for accurate measurement of instantaneous gas velocity. In this study, while fluidizing with the single-orifice distributor, a hot-wire anemometer was used to measure velocity fluctuations at the orifice.

4.2 Hot-Film and Hot-Wire Anemometry

Hot-wire anemometers have been used since the late 1800s when experimentalists in fluid mechanics built their own rudimentary anemometers. The principle of operation of a hot-wire or a hot-film sensor is very simple: if an electrically-heated fine wire is placed normal to, or at some angle to, a flow stream, the wire will be cooled by the flowing fluid due to heat transferred from the wire to the fluid. The amount of heat transferred is related to the magnitude of the velocity, increasing with increasing velocity. Since the resistance of the wire is a function of temperature, the voltage/current is a function of gas velocity.

Every hot-wire anemometer, regardless of type, contains the same basic parts: a probe with its cable, and an electronics package. A typical hot-wire probe is illustrated in Figure 4.1. The sensor of the typical hot-wire probe is a wire, usually made of tungsten or platinum, typically 1 mm long and 5 μm in diameter. The sensor is attached between the tips of two support needles by arc welding or soldering, and it is then electrically heated. A hot-wire type sensor must have two characteristics to make it useful: a high temperature coefficient of resistance, and an electrical resistance such that it can be easily heated with an electrical current at practical voltage and current levels (Lomas, 1986).

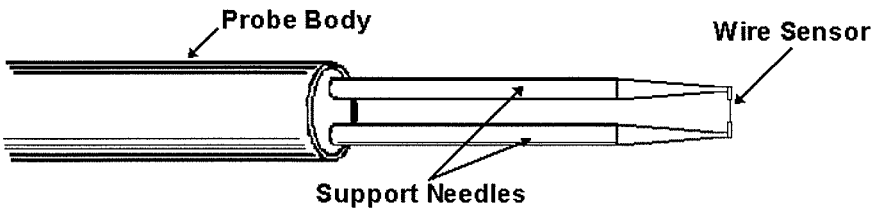

Figure 4.1. Typical hot-wire probe.

Hot-film probes have also been used for special applications. A hot film anemometer is usually made of nickel or platinum deposited in a thin layer onto a backing material, such as quartz, and connected to the electronics package by leads attached to the ends of the film. This kind of sensor has some advantageous compared with hot-wire probes such as better frequency response, more flexibility in sensor configuration, and less susceptibility to fouling. A typical hot film anemometer is shown in Figure 4.2 (Perry, 1982). Since both hot-wire and hot-film anemometers contain thin sensor, special care is needed when using them. Moreover, they may affected by fluid fouling, sensor burnout, and sensor aging.

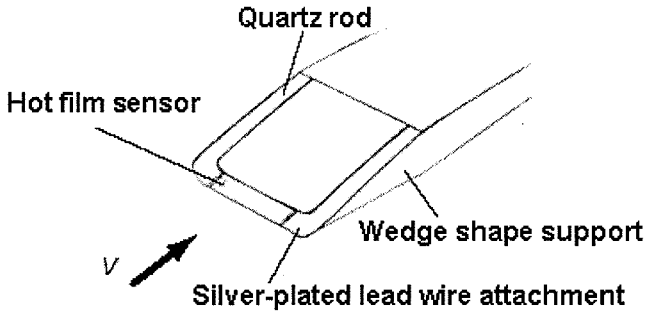

Figure 4.2. Typical hot film probe.

Two types of electronic packages are used, each controlling the sensor heating current in a different way. The most common one is the constant temperature anemometer, which supplies a sensor heating current that varies with fluid velocity to maintain constant resistance and, thus, constant sensor temperature. The electronic circuit for a constant temperature anemometer contains a Wheatstone bridge with the sensor as one arm of the bridge, two fixed

resistors and one adjustable resistor as shown in Figure 4.3 (Morris and Foss, 2003). A differential feedback amplifier senses the bridge unbalance and adds current to hold the sensor temperature constant. Before operating the system, the adjustable resistor is set to a value larger than required to balance the bridge. When power is applied, the feedback amplifier increases the sensor heating current, causing the sensor temperature to rise and increase the sensor resistance until the bridge becomes balanced. Passing the fluid over the sensor cools the sensor and unbalances the bridge. This makes the feedback amplifier increase the sensor heating current, bringing the bridge back into balance. The sensor temperature remains virtually constant as the velocity changes because the feedback amplifier responds rapidly. Thus, the voltage difference across the bridge depends on to the fluid velocity.

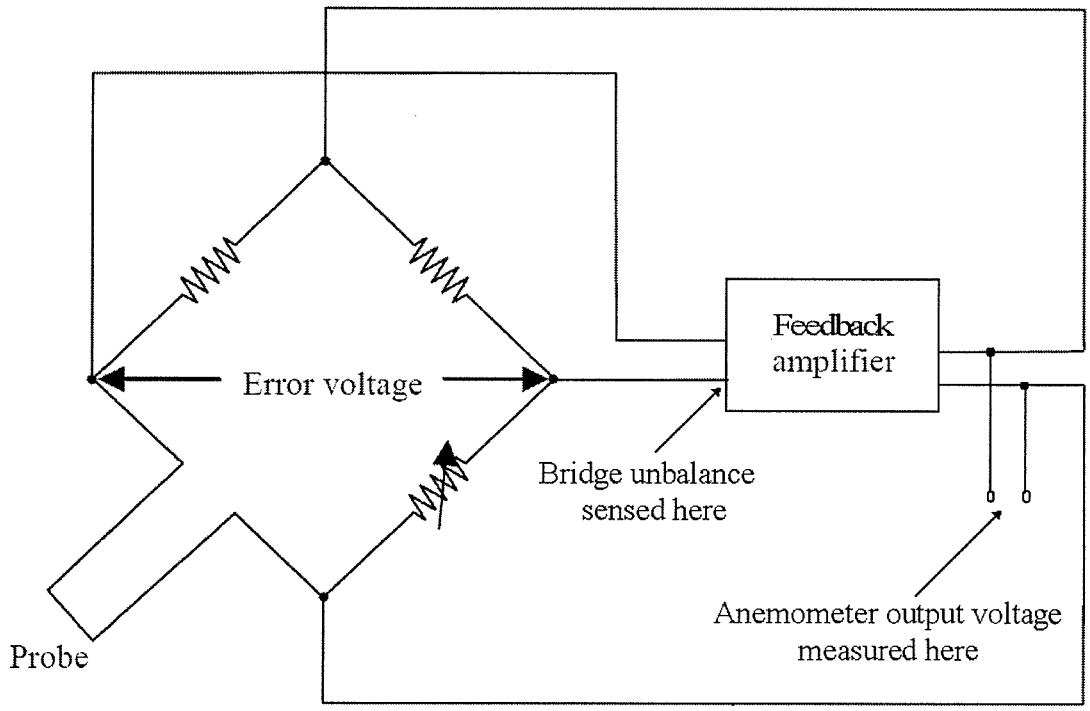

Figure 4.3. Electronic circuit of a constant-temperature anemometer.

Another type of circuit for hot-wire sensors is the constant-current anemometer, which is less used in the literature. In this method, instead of feedback technique, the bridge current is

provided by a constant current power supply, as shown in Figure 4.4. The Wheatstone bridge is balanced at only one velocity and becomes unbalanced as the velocity changes. The voltage across the Wheatstone bridge depends on the velocity. To improve the frequency response, this voltage is modified by a shaping network and amplifier.

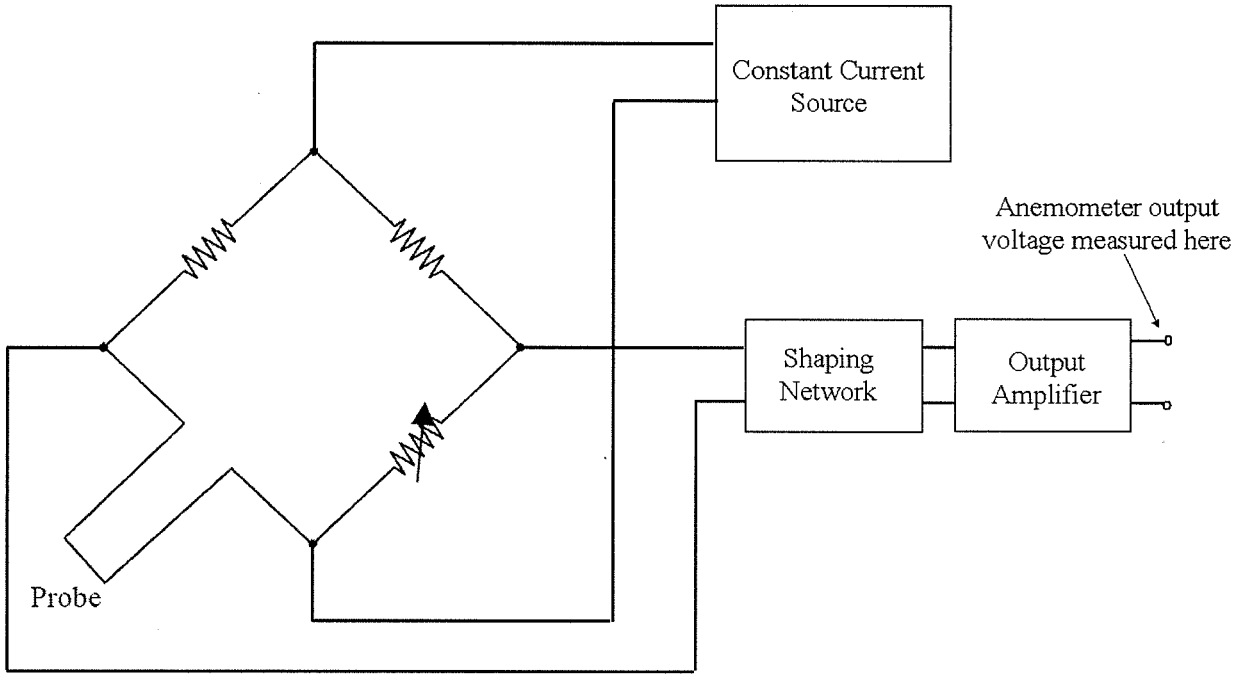

Figure 4.4. Electronic circuit of a constant-current anemometer.

To find the equation for temperature profile of the sensor, as well as the average temperature and frequency response characteristics of the sensor, an energy balance for the hot-wire sensor is needed. As shown in Figure 4.5 a differential element of hot-wire sensor with length of dx and cross-sectional area of A_s is chosen for the energy balance resulting in:

$$A_s \frac{\partial}{\partial x}\left(k_s \frac{\partial T_s}{\partial x}\right) + \frac{I^2 \rho_r}{A_s} - \rho_s c_s A_s \frac{\partial T_s}{\partial t} - \pi d_s h(T_s - T_f) - \pi d_s \sigma \varepsilon^{\circ}(T_s^4 - T_f^4) = 0 \qquad (4.1)$$

The first term is related to heat conduction in the element; the second term shows the amount of heat generated due to passing electrical current through the wire; the third one is the accumulation term, and the last two terms represent heat lost due to the convection and radiation respectively. This is the general hot-wire equation. For circular cylinders of infinite length, Karmer (1946) suggested the following correlation for $0.1 < \mathrm{Re} < 10000$ (Lomas, 1986):

$$Nu = 0.42\,\mathrm{Pr}^{0.20} + 0.57\,\mathrm{Pr}^{0.33}\,\mathrm{Re}^{0.50} \tag{4.2}$$

where *Nu Pr,* and *Re* represent Nusselt, Prandtl, and Reynolds numbers respectively, defined as:

$$Nu = h.d_s/k_s \tag{4.3}$$

$$Pr = \mu_g.c_s/k_s \tag{4.4}$$

$$Re = \rho_g.U_f.d_s/\mu_g \tag{4.5}$$

when all fluctuating quantities are expressed as the sum of a mean component and a fluctuating component, Equations 4.1 and 4.2 result in a first-order linear ordinary differential equation with response frequency of a few hundred Hertz (response time less than 0.005 s) (Lomas, 1986). This response frequency is acceptable for measuring the bubbling frequency in a gas-solid fluidized bed with a single-orifice distributor.

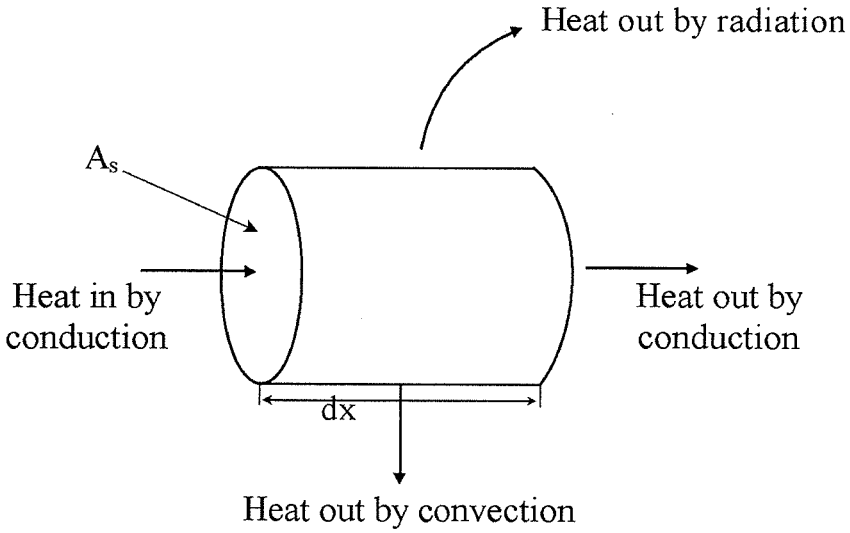

Figure 4.5. Heat transfer contribution for a differential element of a hot-wire sensor.

4.3 Instrumentation

In this study hot-wire anemometry was used to measure the velocity fluctuations and corresponding bubbling frequency for a single-orifice distributor. In order to obtain accurate measurements and readings for single-orifice distributor, the length of wire should be the same as the orifice diameter (12 mm). This should allow global velocity measurements for the orifice as a whole within the orifice rather than local ones. Since most commercial hot-wire anemometers are of shorter wire length, they measure local velocity fluctuations and were not appropriate for this experiment. Therefore, a custom-made hot-wire sensor and corresponding electronic circuit were designed and built.

Hauptmann (1968) proposed a simple way to build a low-cost hot-wire sensor. He used a small flashlight bulb with the glass envelope removed and made the hot-wire sensor with a lamp filament. He showed that with appropriate selection of the miniature lamp, acceptable compatibility could be achieved. However, he did not provide the electronic circuit specifications in his study. Williams (1984) suggested a constant-temperature electronic circuit for a hot-wire anemometer. This circuit, shown in Figure 4.6, was used in this study. As suggested by Williams (1984) a type 328 lamp was used to make the probe. First, the lamp's glass envelope was removed carefully, and then the two outlet wires of the lamp were soldered to two relatively thick wires to make the probe. The probe was placed in a Wheatstone bridge, monitored by A1's output (A1 to A4 are operational amplifiers). The current was amplified by Q1 and fed back to drive the bridge. The capacitors and 220 Ω resistor ensure stability. The 2k resistor enables start-up. When power is applied, the lamp is at a low resistance and Q1's emitter tries to come on full. As current flows through the lamp, its temperature quickly rises, forcing its resistance to increase. This increases A1's negative potential. Q1's emitter voltage decreases and the circuit finds a stable operating point. To keep the bridge balanced, A1 acts to force the lamp's resistance, so that its temperature remains constant. Air flow past the wire filament lamp cools it, and A1 increases Q1's output to maintain the filament's temperature constant. The voltage at Q1's emitter varies non-linearly, but predictably, related to the air flow. The non-linear behaviour of the hot-wire sensor can be explained by the law of King (1914), describing heat transfer from a cylinder of infinite length. It is expressed as:

$$\frac{I^2 R_s}{T_s - T_f} = A_o + B_o \sqrt{\mathrm{Re}} \tag{4.6}$$

where A_o and B_o are constants. For a hot-wire anemometer, King's law is usually written as:

$$E^2 = A + BU_f^{0.5} \tag{4.7}$$

where E is the anemometer output voltage across the Wheatstone bridge in the electronics package, U is the fluid velocity, and A and B are constants. This equation can be used for calibration. In order to have linearized output voltage versos fluid velocity, A2, A3 and the array transistors form a circuit which modifies and amplifies Q1's emitter voltage to give a linear calibrated output voltage versus air flow rate with sampling frequency of 100 Hz (Williams, 1984).

After building the hot-wire anemometer sensor and corresponding electronics package for measuring gas velocity, the probe was attached to the single-orifice distributor. In order to obtain accurate measurements, the sensor wire was placed inside the orifice in such a way that the wire length exactly matched the orifice diameter. To calibrate the probe, the orifice plate with attached hot-wire sensor was placed in a wind tunnel with the same diameter as the orifice plate. Then known flow rates of air were passed through the tunnel. The air velocity through the orifice was then plotted versus the output voltage from the circuit to provide the calibration curve, as shown in Figure 4.7. A linear fit has been utilized in view of the electronic circuit that is supposed to provide linearization, even though a non-linear equation would clearly give a better fit. Since we are only interested in frequencies of the fluctuations, this is not expected to be problematic.

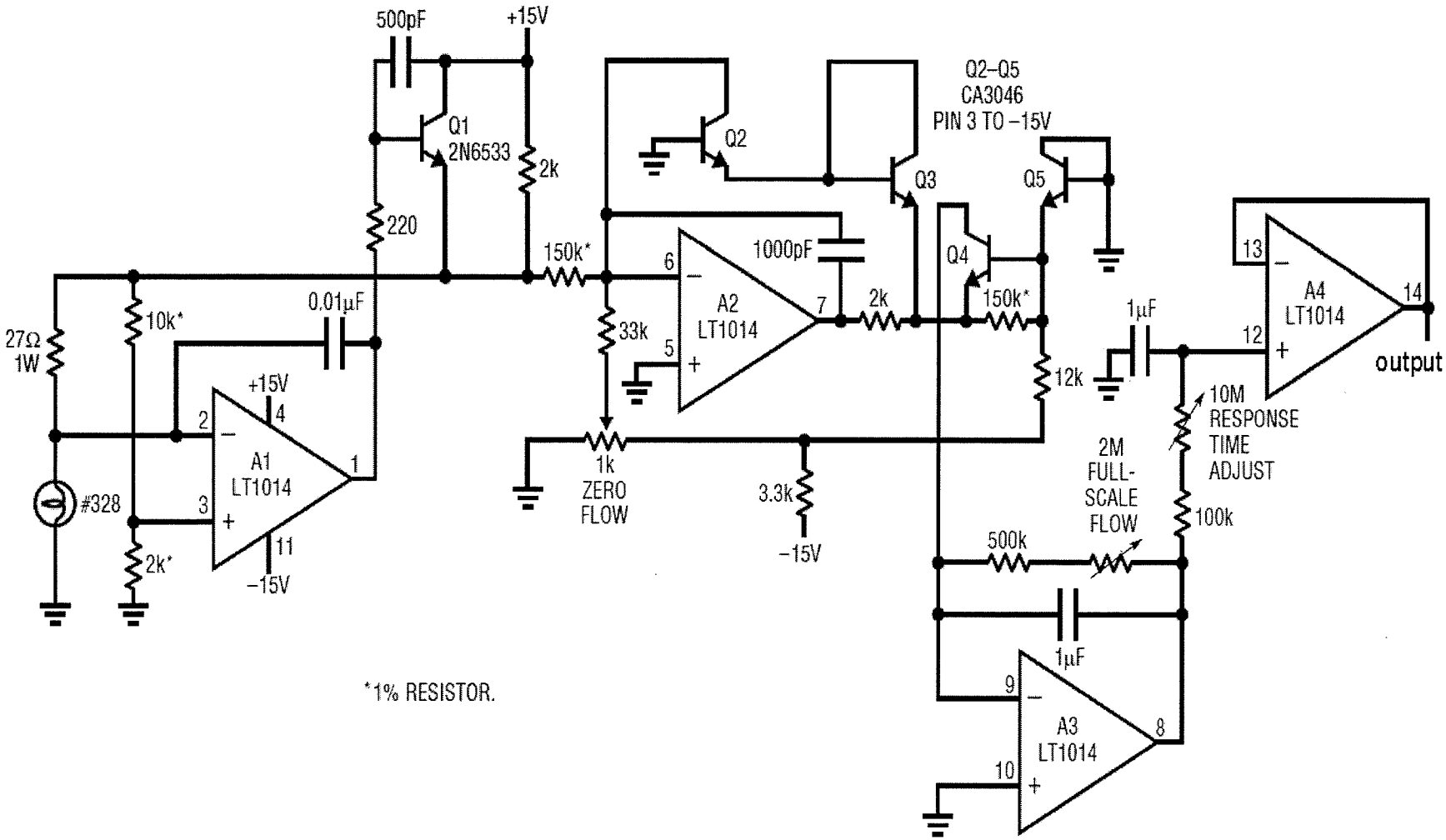

Figure 4.6: Electronic circuit used for hot-wire anemometer (Williams 1984)

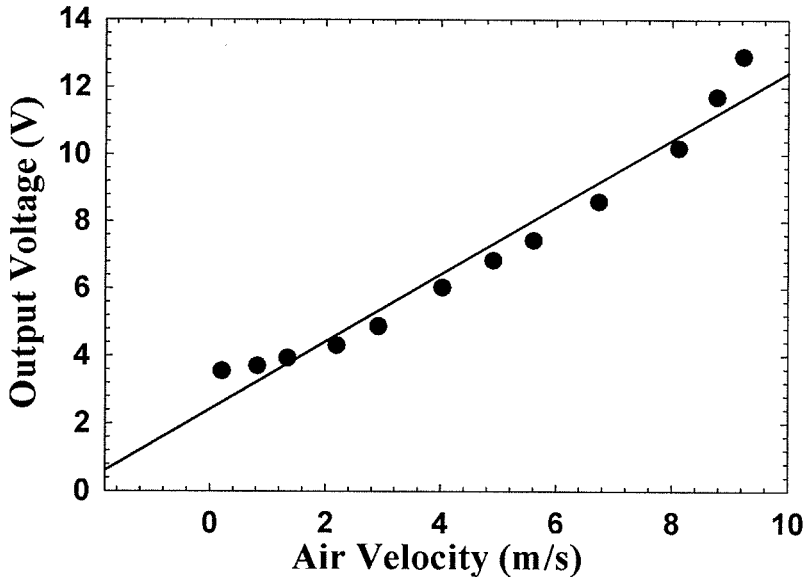

Figure 4.7. Calibration curve for custom-made hot-wire anemometer.

Note that the length of this custom-made hot-wire is longer than that of commercial ones. Moreover the filament coil is usually helical which is unfavorable for perfect heat transfer and therefore precise work. These defects may cause some noise in readings comparing with commercial hot-wire anemometries, but should not interfere with the purpose of finding bubbling frequency and demonstrating time-variation of flow through the orifice in this study.

During the experiments at superficial gas velocities larger than 0.01 m/s, the early hot-wire probes placed in the orifice broke. In addition, there were electronic circuit limitations for measuring gas velocities lower than 15 m/s. Hence velocity fluctuations were measured only for two superficial gas velocities corresponding to $U\text{-}U_{mf}$ = 0.037 and 0.077 m/s.

4.4 Results and Discussion

Similar to pressure fluctuation measurements, time-domain analysis was performed on the velocity fluctuations to determine the structure of velocity-time signals. Figure 4.8 shows velocity-time signals for various plenum volumes using glass beads and a 0.10 m static bed height. The amplitude of the velocity fluctuations decreased with decreasing plenum volume as

shown in Figure 4.8. This can be explained by relating superficial gas velocity fluctuations to the bed pressure fluctuations.

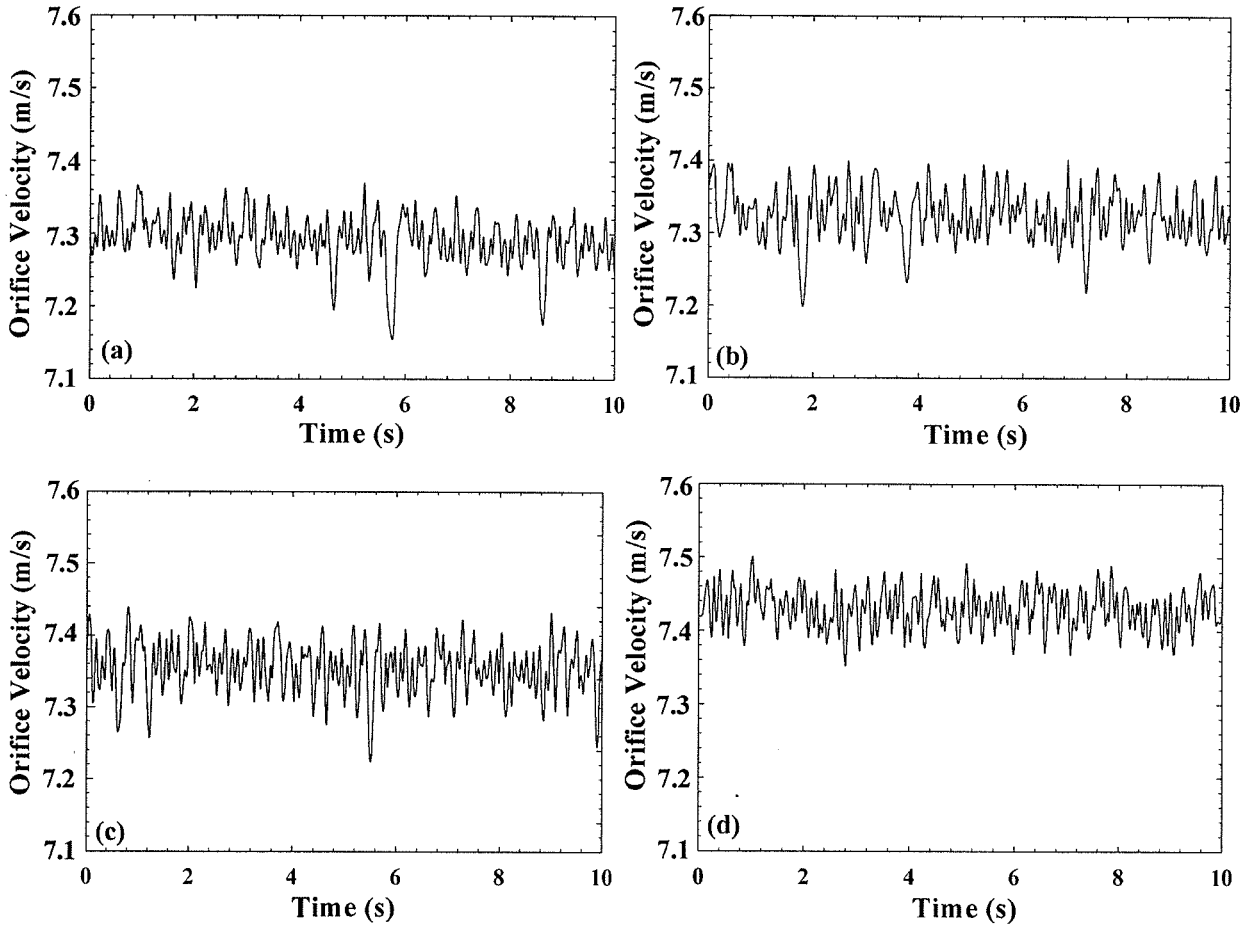

Figure 4.8. Orifice velocity fluctuations for single orifice-distributor with glass beads at different plenum volumes; (a) V_p=0.0425 m^3 (b) V_p=0.0290 m^3 (c) V_p=0.0155 m^3 (c) V_p=0.0020 m^3 (H_o= 0.10 m, U-U_{mf}= 0.037 m/s, mean orifice velocity = 7.32 m/s).

Taking the derivative of Equation 3.23 with respect to time and substituting $d\tilde{P}_p/dt$ from Equation 3.26 leads to:

$$\frac{d\tilde{U}}{dt}+\left(\frac{\gamma A\bar{P}_p}{\rho_g\bar{\xi}_d V_p\bar{U}}\right)\tilde{U}=\left(\frac{-1}{\rho_g\bar{\xi}_d\bar{U}}\right)\frac{d\tilde{P}_b}{dt} \tag{4.8}$$

From this Equation it is seen that the inlet boundary condition of the flow is not independent of time unlike the assumption which is usually made in CFD simulations. Moreover, this equation shows that for small plenum volume with finite $d\tilde{P}_b/dt$, $\tilde{U}$, the fluctuating part of superficial gas velocity, approaches zero. Therefore it can be concluded that the amplitude of orifice velocity fluctuations should decrease with decreasing plenum volume. On the other hand, for a large plenum volume, the variation of $\tilde{U}$ is directly proportional to the variation of pressure inside the bed. The same trend was observed for higher static bed height (0.20 m) with glass beads. Increasing the static bed height was found to cause velocity fluctuations to have lower frequency and higher amplitude as shown in Figure 4.9 for glass beads with static bed height of 0.20 m. It can also be inferred from Figure 4.9(d) that by decreasing the plenum volume, the velocity fluctuations become more frequent and to have lower amplitude, as expected from Equation 4.8.

Frequency-domain analysis was also used to determine frequencies associated with the velocity-time signals. Fast Fourier transformation (FFT) was performed on velocity-time signals collected with a sampling frequency of 100 Hz to determine the frequencies. The Hamming window module from OriginLab software was used to prevent leakage from the frequency spectrum. In general, the frequency spectrum of the velocity fluctuations featured two noticeable peaks, as shown in Figure 4.10. The one with higher frequency represents the bubbling frequency which matched the corresponding frequency from the pressure fluctuation measurements. The other peak in the frequency spectrum is again related to the bubble eruption at the surface of the fluidized bed since it changes with bed depth, as predicted by Baskakov et al. (1986). The reason for detecting this frequency by the hot-wire anemometer can be explained from the orifice equation (eq. 3.19), which relates the instantaneous pressure drop across the distributor to the instantaneous orifice velocity. When a bubble bursts at the bed surface, it forms a crater on the surface and the bed height is therefore diminished in that area. As a result, the bed pressure drop decreases and, accordingly, more gas flows into the bed, and the instantaneous orifice velocity increases, as detected by the hot-wire anemometer.

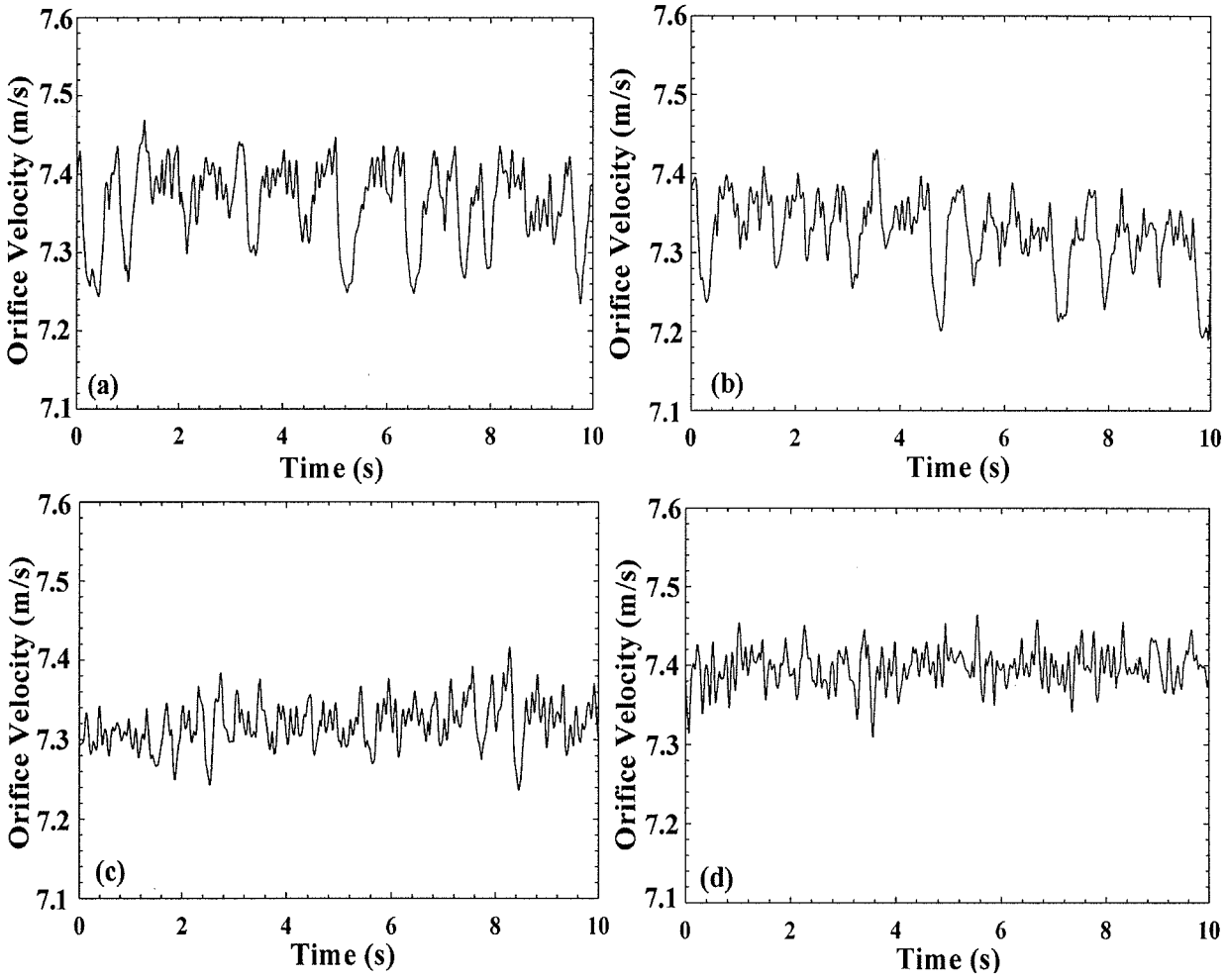

Figure 4.9. Orifice velocity fluctuations using single orifice-distributor for glass beads with different plenum volumes: (a) V_p=0.0425 m^3 (b) V_p=0.0290 m^3 (c) V_p=0.0155 m^3 (c) V_p=0.0020 m^3 (H_o= 0.20 m, U-U_{mf}= 0.037 m/s, mean orifice velocity = 7.32 m/s).

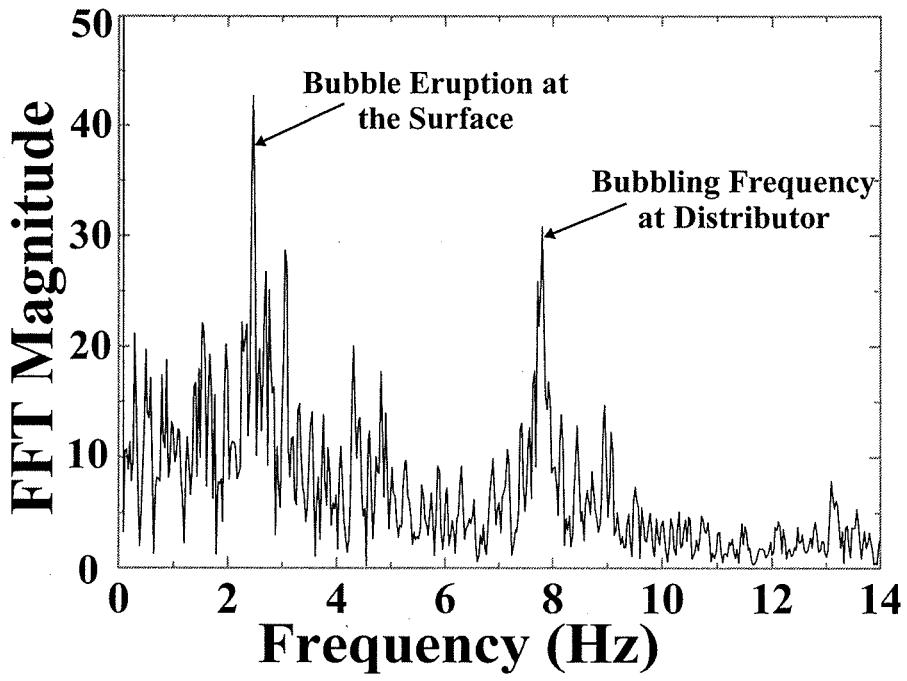

Figure 4.10. Frequency spectrum of orifice velocity fluctuations for glass beads, (H_o= 0.10 m, U-U_{mf}= 0.037 m/s, V_p=0.0425 m^3).

McCann and Prince (1969, 1971) studied bubble formation at a single orifice submerged in a low-viscosity liquid and showed that the bubbling frequency decreased with increasing plenum volume. This is in agreement with findings regarding bubbling frequency from velocity fluctuation measurements as shown in Figure 4.11. As shown in Chapter 3, pressure fluctuation measurements demonstrate the same trend. However, measurements from pressure fluctuations show slightly higher frequencies than the velocity fluctuation measurements. As mentioned in Chapter 3 when discussing the effect of static bed height, bubbling frequency slightly decreased with increasing static bed height, probably because a greater mass of particles above the distributor caused more compression resulting in a lower gas flow through the orifice, and correspondingly a lower bubbling frequency.

The second peak (of a lower frequency) in the frequency spectrum of orifice velocity fluctuations moves towards lower frequencies with increasing static bed height from 0.10 m to 0.20 m, but it is almost independent of plenum volume. Therefore it again appears that this peak represents bubbles bursting at the surface of the bed. Figure 4.12 shows that increasing the

static bed height from 0.10 m to 0.20 m caused the bubble eruption frequency to decrease from 3.4 to 1.9 Hz. This is in reasonable agreement with the Baskakov et al. (1986) model which predicts 3.1 Hz and 2.2 Hz for static bed heights of 0.10 m and 0.20, respectively.

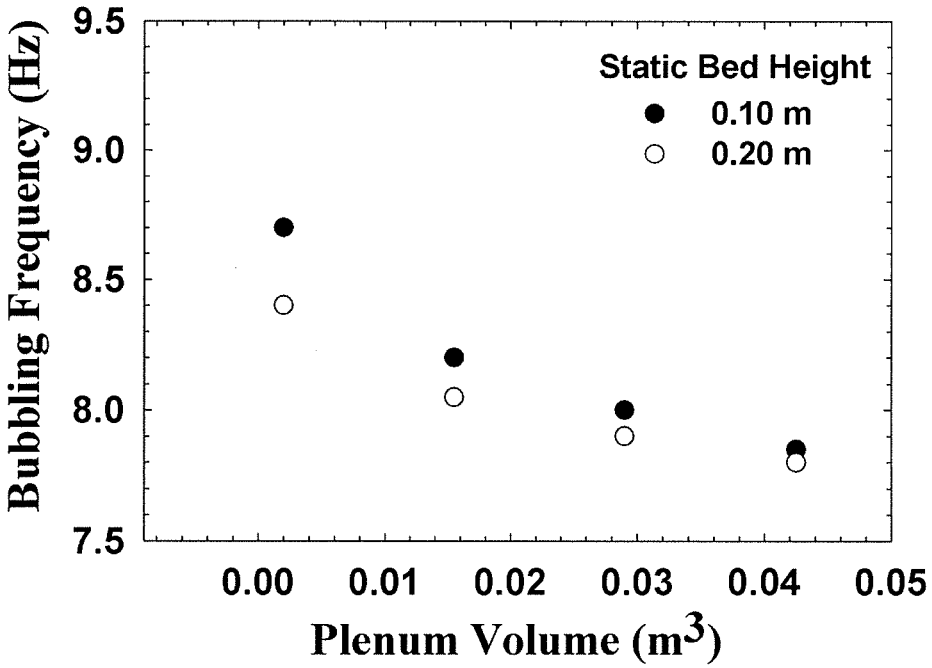

Figure 4.11. Effect of plenum volume on bubbling frequency measured from orifice velocity fluctuations (Glass beads, $U\text{-}U_{mf}$ = 0.037 m/s).

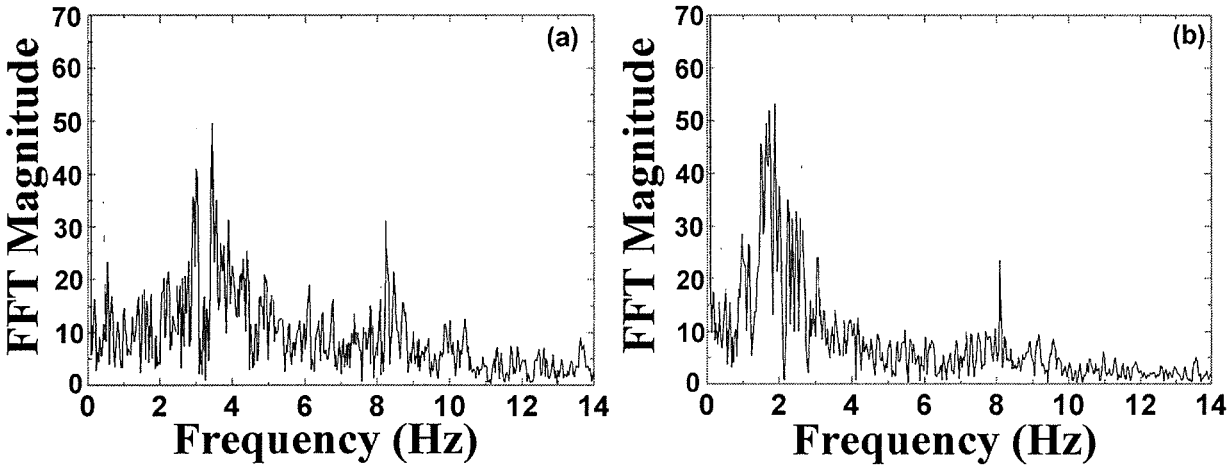

Figure 4.12. Effect of static bed height on bubble eruption frequency for H_o of (a) 0.10 m and (b) 0.20 m (Glass beads, V_p=0.0155 m^3, $U\text{-}U_{mf}$ = 0.037 m/s).

4.5 Summary

Orifice velocity fluctuations were measured by a custom-made hot-wire anemometer. Time-domain analysis showed that the amplitude of these velocity fluctuations decreased with decreasing plenum volume. Frequency-domain analysis revealed two peaks in the frequency spectrum. One of them represents the bubble formation, which decreases with increasing plenum volume. The other one appears to be related to bubble eruption at the surface of the bed, which depends on the static bed height as predicted by the Baskakov et al. (1986) model.

Chapter 5: Modeling of Bubble Formation

5.1 Introduction

Many physical and chemical processes involve the formation of gas bubbles in liquids or solid particles. The phenomena involved in bubble formation are extremely complicated, since many parameters influence the size, frequency and the shape of bubbles. Therefore, a somewhat simplified starting point has been common in describing the formation of bubbles at a single orifice, excluding the influence of bubbles being formed at neighbouring orifices. Although experimental studies of bubble formation at a submerged orifice have been conducted for some time, theoretical analysis has been less investigated, and those investigations have mostly been for gas-liquid systems. A general model applicable to the formation of babbles under all kinds of operating conditions is not yet available, possibly due to the complex nature of the problem.

Summing up published experimental results, Kupferberg & Jameson (1969) concluded that the most important factors governing bubble formation at a single upward orifice, submerged in a quiescent inviscid liquid, are gas flow rate, orifice radius and the volume of chamber beneath the orifice. Other parameters affecting bubble formation such as liquid density, surface tension, gas viscosity, gas density and depth of liquid above the orifice seem to be less important.

It is well known that bubble formation is gas-liquid systems can take place under constant flow or constant pressure conditions. In the former case, gas flows through an orifice into the liquid at a constant volumetric rate, so that the movement and growth of the bubble do not influence the gas flow rate. In this case, simple theory, based on a balance between the buoyancy force and the upward mass acceleration of the fluid surrounding the bubble, gives a rough estimation of the relationship between bubble volume and volumetric flow rate. This was firstly modeled by Davidson & Schuler (1960b) for low-viscosity liquids. According to their approach the equation of upward motion is:

$$V.g = \frac{d}{dt}\left(\frac{11}{16}V\frac{ds}{dt}\right) \tag{5.1}$$

where V is the volume of the bubble at time t after the start of bubble growth at the orifice, and s is the vertical distance of the center of the bubble above the point where the gas enters the liquid. There are several assumptions in deriving this equation:

1. The bubble is assumed to remain spherical during formation;
2. The effect of the orifice plate on the motion of the bubble is ignored;
3. Viscous forces are neglected;
4. The depth of the liquid on the plate is large compared with the bubble diameter;
5. The flow around the bubble is assumed to be irrotational and unseparated. Therefore, the drag coefficient is zero, known as D'Alembert's paradox. Davidson & Schuler (1960a) showed that for irrotational flow, when a spherical bubble is moving away from a wall, the volume of the liquid carried along with a bubble (its added mass) is 11/16 of the volume of the sphere.
6. Upward momentum of gas is negligible.

As the flow remains constant throughout bubble formation, the volume of the bubble at any time can be written:

$$V = G.t \tag{5.2}$$

where G is the volumetric flowrate. Equation 5.2 is substituted into Equation 5.1, and the latter is then integrated subject to the initial conditions:

$$\text{at } t = 0, \quad \frac{ds}{dt} = 0 \quad \textit{and} \quad s = 0 \tag{5.3}$$

Thus, the final bubble volume is given by:

$$V_b = 1.378\left(\frac{G^{6/5}}{g^{3/5}}\right) \tag{5.4}$$

Davidson & Schuler (1960b) suggested another equation which takes into account the residual bubble that forms the nucleus of the succeeding bubble. If this residual volume is V_o , then bubble volume can be calculated from:

$$V = G.t + V_o \tag{5.5}$$

Integrating Equation 5.1 with the same initial conditions leads to:

$$s = \frac{16g}{11}\left[\frac{t^2}{4} + \frac{V_o t}{2G} - \frac{V_o^2}{2G^2}\ln\left(\frac{Gt + V_o}{V_o}\right)\right] \tag{5.6}$$

The bubble is assumed to detach when its center has covered a distance equal to the sum of the radius of the final bubble and the radius of the orifice (i.e. $s = r+r_o$). Thus, the time of bubble formation can be achieved by plotting Equation 5.6 and $r+r_o$ as a function of time from Equation 5.5 on the same axes. Davidson & Harrison (1963) changed Equation 5.1 by using a value of 1/2 in the place of 11/16 for the virtual or added mass term when a tube extends into the dense phase, resulting in an equation similar to Equation 5.4, but with a constant of 1.138 instead of 1.378.

Ramakrishnan et al., (1969) proposed a more complicated model for bubble formation under constant flow conditions in a gas-liquid system. This model assumes two stages of bubble formation: an expansion stage and a detachment stage as shown in Figure 5.1. During the first stage, the bubble is assumed to expand while its base remains attached to the top of the orifice, whereas in the second stage the bubble base rises away from the tip, the bubble itself being in contact with the orifice through a neck. For each stage, the volume of the bubble can be evaluated by performing a force balance. This results in an iterative procedure for the estimation of bubble volume.

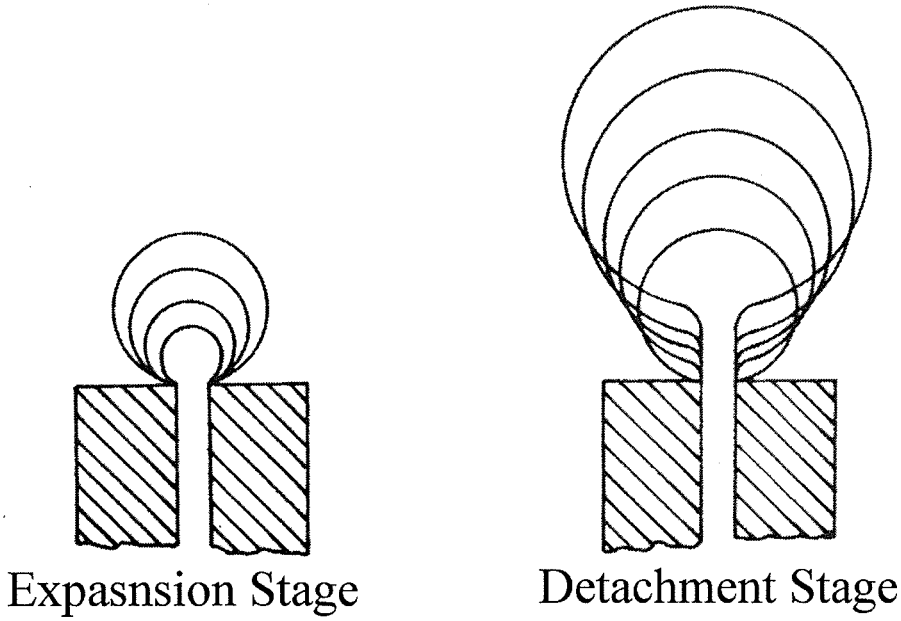

Figure 5.1. Two-stage mechanism of bubble formation.

For gas-solid fluidized beds, Equation 5.4 with the modified constant has been used to estimate the bubble volume. Nguyen & Leung (1972) investigated a two-dimensional fluidized bed and, after considering gas leakage through the bubble surface, suggested the following equation for bubbling in two-dimensional fluidized beds.

$$V_b = 0.74 \frac{G^{4/3}}{g^{2/3} a^{1/3}} \tag{5.7}$$

where a is the thickness of the fluidized bed and V_b is the final bubble volume.

Hsiung & Grace (1978) showed experimentally that the assumption of bubble formation under constant flow conditions is not always justified in fluidized beds. They evaluated the ratio of the pressure variation during formation to the pressure drop across the distributor approximately as $\left(d_{Bo}/2H_{mf}\right)/\left(\Delta P_{dist}/\Delta P_b\right)$. For high static bed heights $\left(d_{Bo} << H_{mf}\right)$ or large values of $\left(\Delta P_{dist}/\Delta P_b\right)$, the pressure variation during bubble formation is small, and constant flow conditions may be satisfied. However, for shallow fluidized beds and small $\Delta P_{dist}/\Delta P_b$, time-variation in flow tends to occur.

When bubbles form under variable flow conditions, another complication arises if the volume of the plenum chamber is comparable with that of the bubble being formed. In this case, the pressure in the plenum chamber oscillates during each cycle of bubble formation as the flow rate through the orifice varies. Hsiung & Grace (1978) titled this an "intermediate condition". On the other hand, for a large plenum volume ($V_p >> V_b$), the plenum pressure is almost constant and a "constant pressure condition" prevails.

In order to determine the regions for constant flow and constant pressure conditions, dimensional analysis has been performed by some researchers. Hughes et al. (1955) used an electrical analogy between bubble formation at a single orifice and an acoustic system leading them to define a dimensionless group called the capacitance number:

$$N_c = \frac{V_p g\left(\rho_l - \rho_g\right)}{\pi r_o^2 \rho_g c} \tag{5.8}$$

where c is the velocity of sound in the gas. Hughes et al. (1955) suggested constant flow conditions for $N_c < 1$ where the plenum chamber is small, and constant pressure conditions when $N_c > 1$ (i.e. large plenum volume). Tsuge & Hibino (1983) considered the pressure of the system and modified the capacitance number to:

$$N_c' = \frac{V_p g\left(\rho_l - \rho_g\right)}{\pi r_o^2 P_h} \tag{5.9}$$

where P_h is the hydrostatic pressure at the orifice plate. To determine constant flow or constant pressure conditions, similar constraints were suggested by Tsuge & Hibino (1983).

The constant pressure condition arises when the plenum volume is large (in practice, more than about one liter for a single orifice), and the pressure in the plenum chamber remains almost constant (Satyanarayan et al., 1969). As the pressure in the bubble varies during its formation, the pressure difference across the orifice also varies, bringing about a condition of varying flow rate. Davidson & Schuler (1960b) extended their analysis for constant flow conditions to constant pressure conditions by considering that the flow is now a function of the extent to which the bubble has formed. This was introduced into the constant flow equation (Equation 5.1) by an orifice equation which relates the volumetric gas flow rate through the hole to the pressure drop across the plate. McCann and Prince (1969) were among the first researchers to pay attention to the gas chamber beneath the single-hole perforated plate during bubble formation. They modeled the changing pressure in the plenum chamber by assuming adiabatic expansion of an ideal gas and applying the first law of thermodynamics to the gas in the chamber leading to:

$$\frac{dP_p}{dt} = \frac{\gamma}{V_p}\left(P_e Q_e - P_p Q_o\right) = \frac{c^2 \rho_g}{V_p}\left(Q_e - Q_o\right) \tag{5.10}$$

where γ is the ratio of specific heats and c is the velocity of sound in gas. McCann and Prince (1969) assumed bubbles to grow from a hemisphere, and then spherical bubble form, rising due to buoyancy. They also performed potential flow analysis to obtain an equation for pressure inside the bubble. The last two equations, together with the instantaneous orifice equation, were then solved simultaneously to obtain chamber pressure fluctuations. This model is in a good agreement with their experimental data for an air-water system.

Kupferberg & Jameson (1969) used also potential flow theory to derive equations for the motion of a spherical growing bubble, its radial expansion stage and the dynamic variation of pressure inside the bubble. The predicted size and frequency of formed bubbles were compared with experimental results from air-water and air-ethanol systems. Yang et al. (2000) used the same approach with the two-stage bubble formation assumption for high pressure liquid-solid suspensions. They concluded that this model can reasonably describe the initial bubble size under high-pressure conditions.

In the present study, the McCann and Prince (1969) approach was used for the first time in gas-solid systems to model bubble formation at a single-orifice distributor taking into account the influence of the plenum chamber. The next section describes the model formulation and the required modifications for a gas-solid fluidized bed.

5.2 Model Formulation

In this study, two-stage bubble formation was assumed for modeling, consistent with observations by previous researchers investigating formation of bubbles in low-viscosity liquids (Ramakrishnan et al., 1969, Tsuge & Hibino, 1983, and Kumar & Kuloor, 1970). The effective surface tension for the gas-solid fluidized bed is assumed to be zero. Immediately before the bubble formation it is assumed that there is no net pressure drop across the orifice and a horizontal gas-solid interface. As the chamber pressure increases, the bubble grows while retaining a spherical shape and remaining at the orifice as shown in Figure 5.2. The equations which describe this stage of bubble formation were formulated in the following manner:

The relationship between the difference of pressures in the plenum chamber, P_p, and in the bubble, P_{bubble}, and the gas flow rate through the orifice, Q_o, is assumed to be:

$$\left|P_p - P_{bubble}\right| = \left(\frac{Q_o}{k_o}\right)^2 \tag{5.11}$$

where k_o is the orifice "constant" which is a function of orifice gas flow rate, gas density, gas viscosity, orifice diameter, and orifice plate thickness. Considering the pressure drop due to the sudden contraction and enlargement at the orifice and the friction head loss, the following equations were proposed by McAllister et al. (1958) to calculate k_o:

$$k_o = \sqrt{\frac{2}{\rho_g C_g}} \left(\frac{\pi D_o^2}{4} \right) \tag{5.12}$$

where C_g can be obtained by the following equation if the flow of gas through the orifice is assumed to be laminar:

$$C_g = 1.5 + \frac{16\pi\mu_g L}{\rho_g Q_o} \tag{5.13}$$

Q_o can be related to the rate of volume change of bubble from:

$$Q_o = \frac{dV}{dt} + U_{tf}\pi r^2 = 4\pi r^2 \frac{dr}{dt} + U_{tf}\pi r^2 \tag{5.14}$$

where U_{tf} is the vertical component of velocity of gas flowing through the bubble boundary in the gas-solid fluidized bed. Davidson & Harrison (1963) predicted that for spherical bubbles in fluidized beds U_{tf} is three times the minimum fluidization velocity. But it was assumed here that $U_{tf} = U_{mf}$, since most evidence suggests that the Murray (1965) prediction of U_{tf} is more accurate.

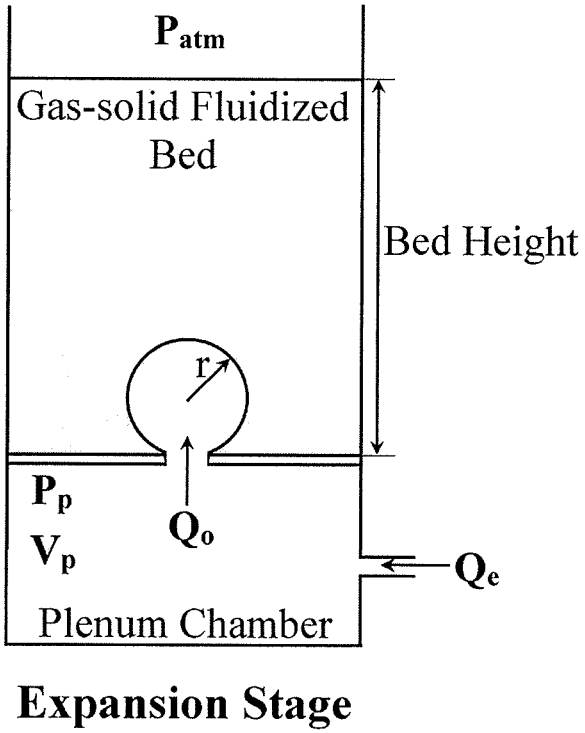

Figure 5.2. Schematic diagram of bubble formation during the expansion stage.

Assuming the ideal gas law for air inside the plenum chamber and adiabatic behaviour, the pressure in the chamber during the expansion stage and detachment stage can be expressed by Equation 5.10. Assuming a constant flow rate of gas entering the plenum chamber and equal pressure at the inlet and inside the plenum together with Equation 5.14 leads to:

$$\frac{dP_p}{dt} = \frac{\gamma P_p}{V_p}\left(Q_e - \left(4\pi r^2 \frac{dr}{dt} + U_{tf}\pi r^2\right)\right) \tag{5.15}$$

When the pressure inside the bubble becomes more than the average hydrostatic pressure, the bubble expands by this pressure difference. Kupferberg & Jameson (1969) used potential flow theory and the generalized Bernoulli equation derived by Lamb (1932) to derive an equation for the bubble pressure in an ideal liquid. Tsuge & Hibino (1983) noted that for a real liquid it is difficult to derive theoretically an accurate expression for bubble pressure, and they therefore suggested multiplying the inertial term for an ideal liquid by a viscosity-dependent factor. Ignoring surface tension in the gas-solid fluidized bed, the pressure inside the bubble can be estimated by the Kupferberg & Jameson (1969) procedure with the Tsuge & Hibino (1983) modification, giving

$$P_{bubble} = P_{atm} + \rho_{bulk} gH - \rho_{bulk} g\left(r - r_o\right) + \alpha\rho_{bulk}\left(\frac{3}{2}\left(\frac{dr}{dt}\right)^2 + r\frac{d^2r}{dt^2}\right) \tag{5.16}$$

On the right side of the above equation, r_o is included to satisfy the initial condition that when t=0, r= r_o and hydrostatic pressure at the bubble surface equals $P_{atm} + \rho_{bulk} gH$. In the above equation α, the viscosity-dependent factor, was estimated based on the Tsuge & Hibino (1983) correlation:

$$\alpha = 7.42 + 1.66\log\left(\mu_{bulk}\right) \tag{5.17}$$

where μ_{bulk} is the bulk viscosity in Poise. Even though, this equation was suggested for gas-liquid systems such as distilled water, 20% methanol water and 50% glycerine-water, it can be also used in gas-solid fluidized beds by defining an effective viscosity for the fluidized bed. Grace (1970) estimated the effective shear viscosity of fluidized beds by an empirical approach based on the shape of spherical-cap bubbles and included bubble angle. Different particles resulted in viscosities between 4 to 13 poise (0.4 to 1.3 Pa.s) for different particles, these values being comparable to those obtained by shear viscometers by earlier investigators.

The equations for the expansion stage, Equations 5.11, 5.15, and 5.16, can be solved simultaneously. Initial conditions for the expansion stage are:

$$@t=0 \;\Rightarrow\; r=r_o,\;\; \frac{dr}{dt}=0,\;\; P_p=P_{atm}+\rho_{bulk}gH=P_h \tag{5.18}$$

The expansion stage terminates when the sum of the buoyancy and the rate of gas momentum exceed the sum of the inertial force and viscous drag force, so that the bubble begins to rise. Thus

$$\left(\rho_{bulk}-\rho_g\right)Vg+\frac{4\rho_g Q_o^2}{\pi D_o^2}=\frac{d}{dt}\left(M\frac{dr}{dt}\right)+\frac{1}{2}C_D\rho_{bulk}\left(\frac{dr}{dt}\right)^2\pi r^2 \tag{5.19}$$

where M is the virtual mass for the ascending bubble, equal to $\left(11\rho_{bulk}/16+\rho_g\right)V_g$. To estimate the drag coefficient, Stokes law has been applied, since it was assumed that the velocity of the rising bubble, and correspondingly its Reynolds number, are small.

During the detachment stage of bubble formation, the bubble continues to grow while lifting up from the plate, but it is still connected to the orifice by a small gas column or neck, as shown in Figure 5.3. This stage ends when the neck breaks off and the bubble separates.

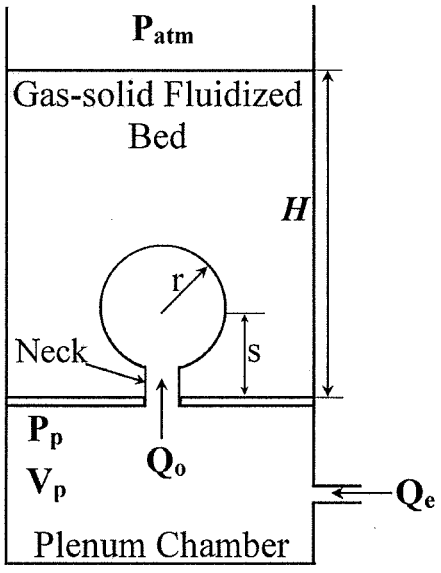

Detachment Stage

Figure 5.3. Schematic diagram of bubble formation during the detachment stage.

The equation of motion for the detachment stage can be written as follows, considering the inertial force, the net buoyancy force, rate of gas momentum and viscous drag force:

$$\frac{d}{dt}\left(M\frac{ds}{dt}\right)=\left(\rho_{bulk}-\rho_g\right)Vg+\frac{4\rho_g Q_o^2}{\pi D_o^2}-\frac{1}{2}C_D\rho_{bulk}\left(\frac{ds}{dt}\right)^2\pi r^2 \tag{5.20}$$

where s is the distance between the center of the bubble and the orifice plate. The equations for the detachment stage, Equations 5.11, 5.15, 5.16, and 5.20 can be solved with the final values from the expansion stage (denoted by subscript *fe*) as the initial conditions. Moreover, because of having an additional second order differential equation for the detachment stage compared with the expansion stage, the following initial conditions are added to the previous ones:

$$s=r_{fe} \qquad \frac{ds}{dt}=\left.\frac{dr}{dt}\right|_{fe} \tag{5.21}$$

As found experimentally by Kupferberg & Jameson (1969) and Tsuge & Hibino (1983), the neck breaks off when the length of the bubble neck becomes equal to the orifice diameter. Therefore, the detachment stage is assumed to end when the length of the bubble neck equals the diameter of the orifice.

The mathematical model was solved using MATLAB software. The simultaneous differential equations described above for each stage of bubble formation were solved numerically by using fourth order Runge-Kutta method. Appendix E includes the MATLAB program for this mathematical model. The following section presents predictions from this mechanistic model and compare them with experimental evidence.

5.3 Results and Discussion

By solving the above differential equations, the values of r, dr/dt, s, V, P_p and P_{bubble} were predicted as functions of time, t. Results from variation of P_p were used to characterize bubble formation and determine the bubbling frequency as suggested by McCann and Prince (1969), Yang et al. (2000), and Kupferberg & Jameson (1969). The typical plenum pressure variation is shown in Figure 5.4 (where P_h is the hydrostatic pressure at the orifice). Pressure variation inside the plenum versus time developed by the present model has the same trend as in the models of Yang et al. (2000) and Tsuge & Hibino (1983). Here only one cycle of bubble formation is shown. When the bubble detaches P_p-P_h is lower than zero level (initial condition).

Therefore, to start the next cycle of bubble formation a small step function is needed. Note that the lift-off line is based on the results from Figure 5.6 where s (dashed line) and r (bubble radius) diverge.

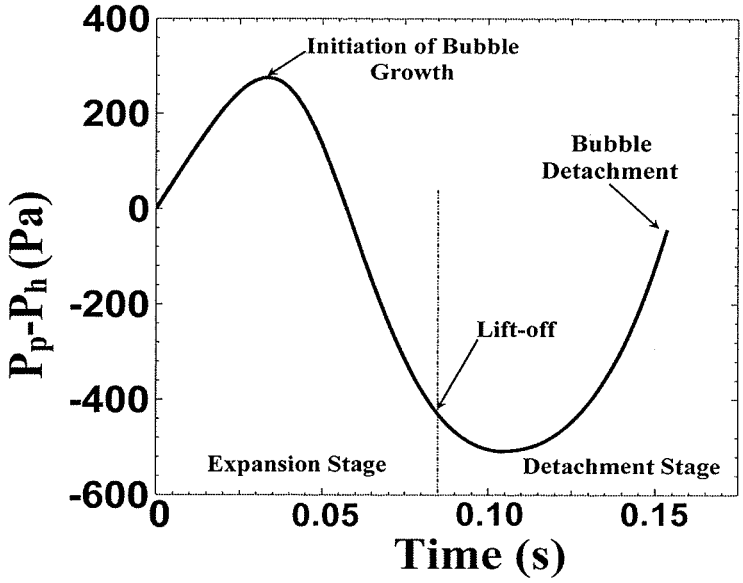

Figure 5.4. Typical variation of pressure inside the plenum predicted by the model, Glass beads, d_p=157 μm, U-U_{mf}= 0.037 m/s, H_o= 0.10 m, V_p=0.0425 m^3, D_o=0.012 m, μ_{bulk}=0.8 Pa.s, U_{mf}= 0.0279 m/s.

The present model was first solved for two limiting cases, very large and very small plenum volumes, to determine whether the model can predict accurately these two limiting conditions. For a very large plenum, bubble formation occurs under constant pressure conditions, so the pressure in the plenum chamber remains nearly constant, as shown in Figure 5.5a for a large plenum chamber volume of 0.1 m^3. On the other hand the instantaneous flow rate through the orifice becomes nearly constant with decreasing plenum volume because the volumetric gas flow rate entering the plenum chamber, Q_e, is assumed to be constant, so that, with decreasing plenum volume, the gas flow rate through the orifice, Q_o, and Q_e become identical as shown in Figure 5.5b.

Figure 5.6 shows the bubble radius as a function of time for an intermediate plenum chamber volume (0.0425 m^3). The radius of the bubble increases as it forms, but after a certain time it starts to level off. The distance between the centre of the bubble and orifice, which

always increases with time, is also shown in Figure 5.6. The results for bubble radius and distance of center of bubble above orifice are similar to those from Kupferberg & Jameson (1969).

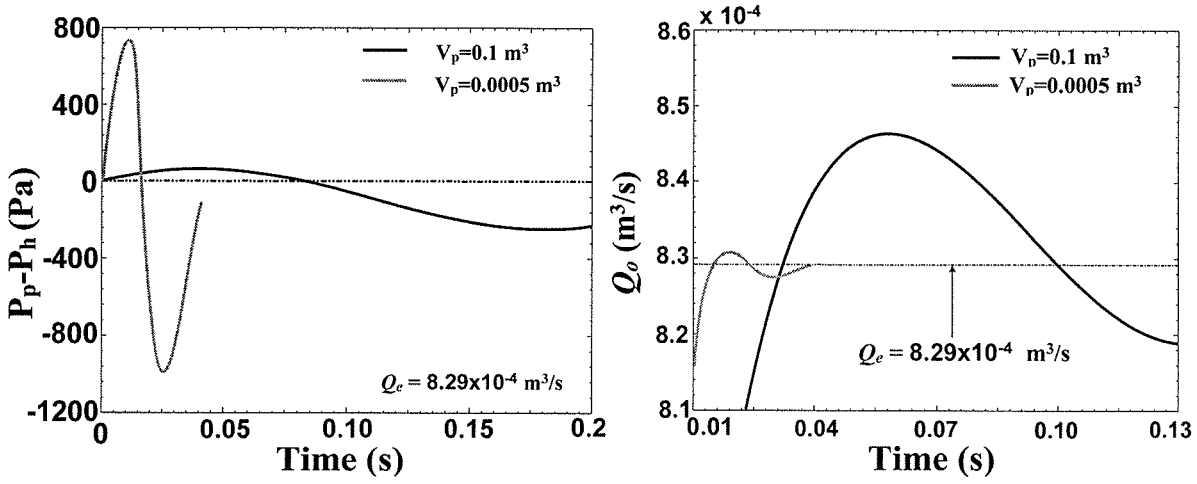

Figure 5.5. Model predictions for two limiting cases: large plenum volume, V_p=0.1 m^3 and small plenum volume V_p=0.0005 m^3. Glass beads, d_p=157 μm, U-U_{mf}= 0.037 m/s, H_o= 0.10 m D_o=0.012 m, μ_{bulk}=0.8 Pa.s, U_{mf}= 0.0279 m/s.

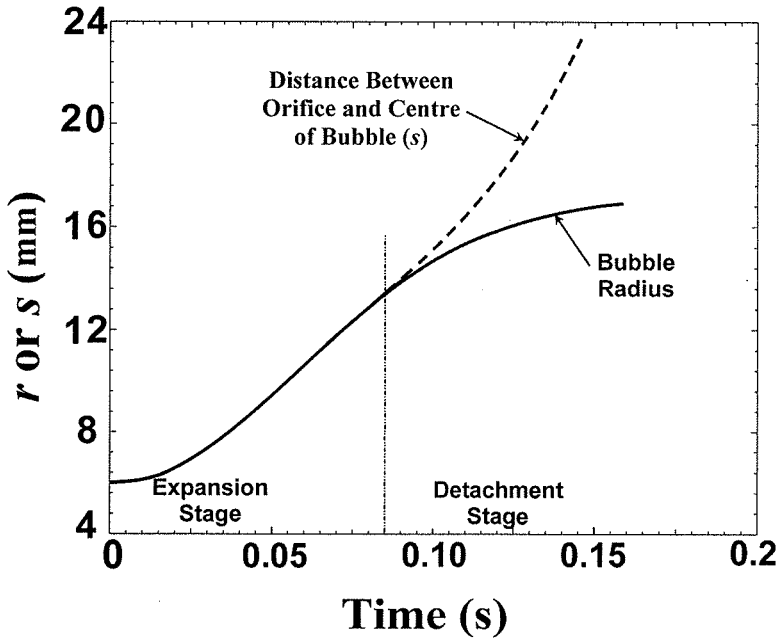

Figure 5.6. Typical variation of bubble radius and distance of centre of bubble above orifice as functions of time. Glass beads, d_p=157 μm, U-U_{mf}= 0.037 m/s, H_o= 0.10 m, V_p=0.0425 m^3, D_o=0.012 m, μ_{bulk}=0.8 Pa.s, U_{mf}= 0.0279 m/s.

The present model for bubble formation predicts increasing bubble volume with increasing plenum chamber volume as shown in Figure 5.7. This is consistent with pressure measurements in Chapter 3 where increasing plenum volume caused the bubble frequency to decrease. Therefore, for a given flow rate, the bubble volume increases with increasing plenum volume, also in agreement with theoretical models of McCann and Prince (1969, 1971), Kupferberg & Jameson (1969), Tsuge & Hibino (1983) and Yang et al. (2000) who studied bubble formation in gas-liquid systems. Figure 5.7 also shows the predicted dependence of the bubble volume on the gas flow rate. As expected, a higher gas flow rate through the plenum causes larger bubbles to form. Results from pressure measurements in Chapter 3 indicate a constant or slight decrease in bubbling frequency with increasing superficial gas velocity. Therefore, larger bubbles are generated with increasing superficial gas velocity. The model of McCann and Prince (1969, 1971) also predicts a monotonic increase of bubble volume with increasing orifice gas velocity.

Based on the results from the present model and also from pressure measurements (Chapter 3), it seems that for small windbox volumes, there is a failure in the procedure for estimating bubble size based on the incoherent pressure fluctuations suggested by Van der Schaaf et al. (2002), because the present model, consistent with gas-liquid systems, predicts smaller bubbles for a smaller plenum chamber, whereas the Van der Schaaf et al. (2002) approach estimates larger bubbles (Figures 3.8-3.10).

During the initial period of bubble formation, the pressure in the gas chamber increases first due to the inflow of gas to the plenum chamber and inertia of the dense phase. Due to this increase in pressure, the bubble begins to expand. When the flow into the expanding bubble exceeds the flow rate at which gas is supplied to the chamber, the amount of gas in the chamber and hence the pressure there begin to decrease. The bubble separates at approximately the same time as the pressure in the gas chamber reaches its minimum value, corresponding to the maximum volume of the bubble (Tsuge & Hibino, 1983). Figure 5.8 shows the effect of plenum volume on the pressure variation of the plenum chamber predicted by the model. Increasing plenum volume causes the period of bubble formation to increase resulting in a lower bubbling frequency. It also leads to a lower amplitude of pressure variation.

Figure 5.9 shows the predicted and experimental effect of plenum volume on bubbling frequency for glass beads and a 0.10 m static bed depth. Two different bulk viscosities (0.8 and 0.6 Pa.s) were used for glass beads to determine the effect of bulk viscosity on model predictions. Frequencies predicted by the model are relatively close to, but lower than, bubbling frequencies measured by the hot-wire anemometer. The model also underpredicts the frequencies measured from pressure fluctuations, but the margin in this case is larger, ~ 24% at most. The difference between velocity and pressure fluctuation measurements in Figure 5.9 might be due to the fact the upper port for differential pressure transducer was somewhat above the distributor (38.1 mm), so the differential pressure measurements were not completely localized.

The differences between the quantitative predictions and experimental values might be due to assumptions and simplifications in the present model. For example, the Basset force and particle-bubble collision force have been ignored in the force balance; low Reynolds number drag has been assumed for bubbles; and the suggested modification of Equation 5.16 proposed by Tsuge & Hibino (1983) was tested experimentally only in gas-liquid system, not in gas-solid system. Moreover, the viscosity of gas-solid fluidized bed was roughly estimated based on the Grace (1970) range.

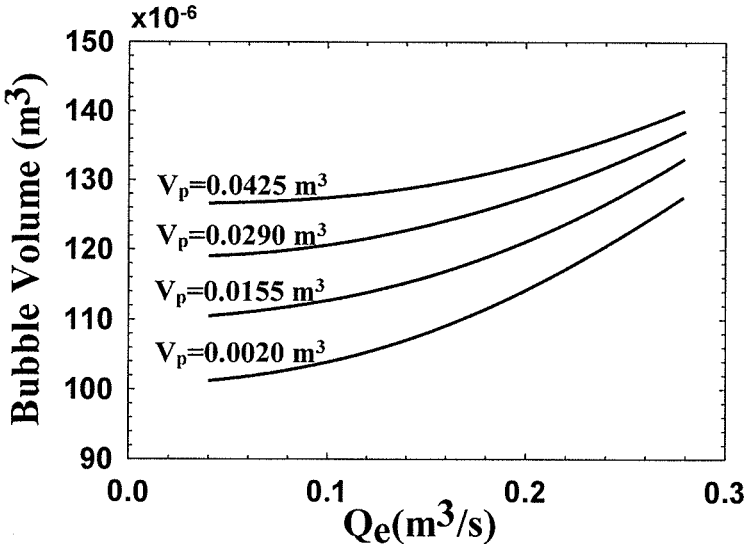

Figure 5.7. Effect of plenum volume and entering gas flow rate to plenum chamber on bubble volume predicted by the model (Glass beads, d_p=157 μm, H_o= 0.10 m, D_o=0.012 m, μ_{bulk}=0.8 Pa.s, U_{mf}= 0.0279 m/s.).

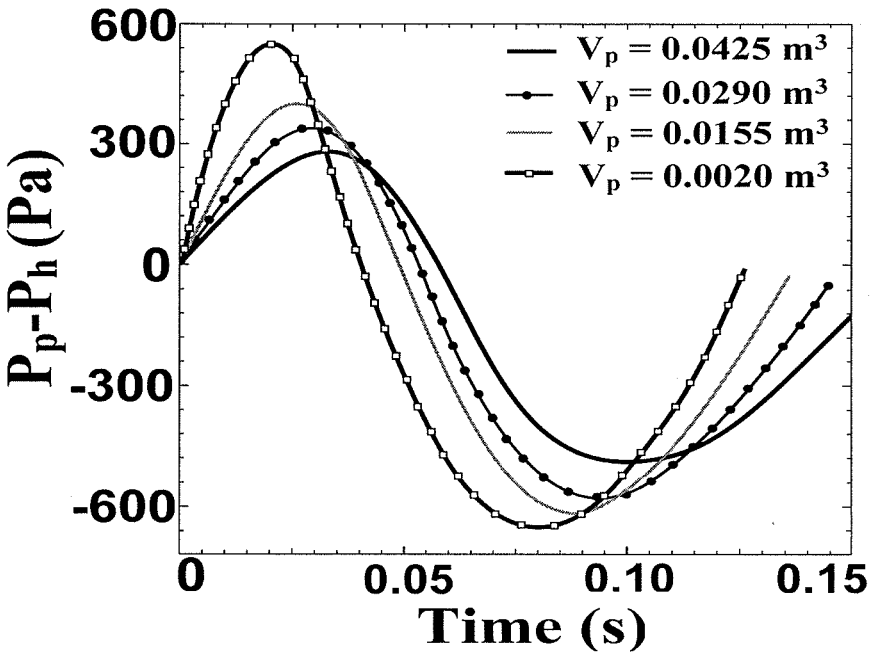

Figure 5.8. Effect of plenum volume on variation of the pressure in plenum chamber predicted by the model (Glass beads, d_p=157 μm, U-U_{mf}= 0.037 m/s, H_o= 0.10 m, D_o=0.012 m, μ_{bulk}=0.8 Pa.s, U_{mf}= 0.0279 m/s).

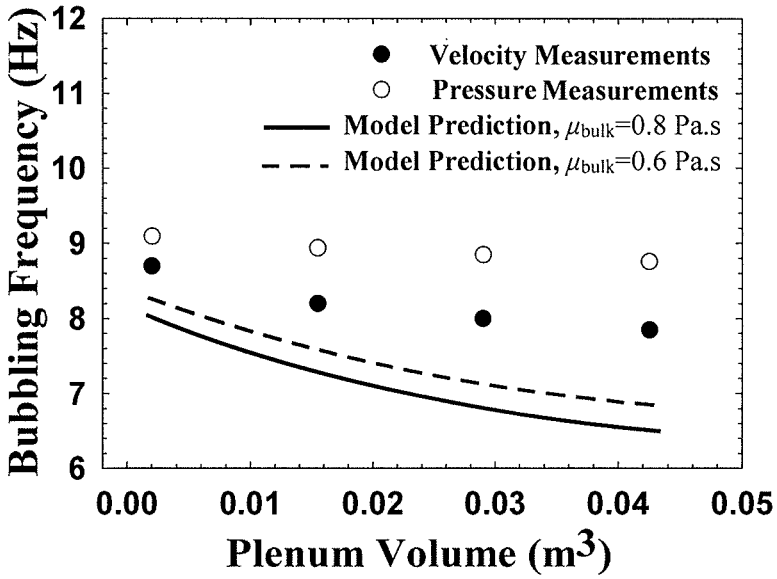

Figure 5.9. Effect of plenum volume on bubbling frequency predicted by the model (Glass beads, d_p=157 μm, U-U_{mf}= 0.037 m/s, H_o= 0.10 m, D_o=0.012 m, U_{mf}= 0.0279 m/s).

According to the model, the gas flow rate through the orifice, Q_o, varies with time. In the initial period of bubble growth, the gas flow rate through the orifice increases to a maximum, corresponding to the increase in plenum pressure during the expansion stage of bubble formation. After reaching a maximum, Q_o decreases gradually because the pressure inside the plenum decreases due to the rise in the centre of the bubble, and hence the pressure difference across the distributor, which causes the flow through the orifice, decreases (Equation 5.11).

Figure 5.10 shows the effect of the plenum volume on the variation of gas flow rate through the orifice with time during bubble formation. With increasing windbox volume, Q_o varies with higher amplitude and lower frequency. This was also observed from the hot-wire anemometer velocity-time signals measured inside the orifice (Figure 4.9) showing that for a large plenum volume, the velocity through the orifice changes with higher amplitude and lower frequency. On the other hand, decreasing plenum volume leads to a smaller variation in gas flow rate through the orifice and a higher frequency approaching one of the limiting cases of bubble formation, constant flow conditions.

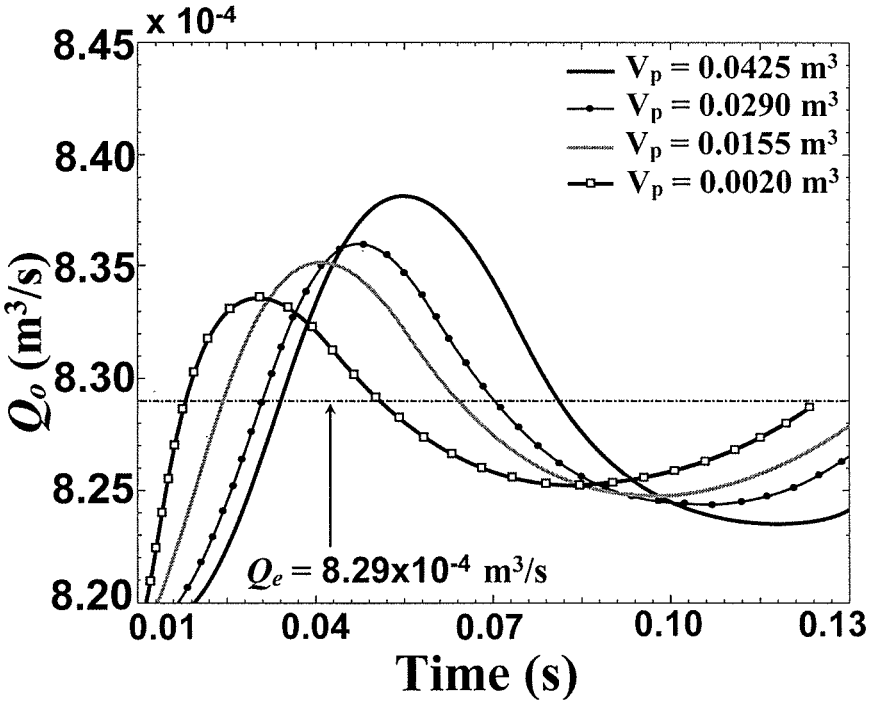

Figure 5.10. Effect of plenum volume on variation of gas flow rate through the orifice (Glass beads, d_p=157 μm, U-U_{mf}= 0.037 m/s, H_o= 0.10 m, D_o=0.012 m, μ_{bulk}=0.8 Pa.s, U_{mf}= 0.0279 m/s)

5.4 Summary

A two-stage mechanistic model (considering expansion and detachment stages) was developed for bubble formation at a single orifice submerged in a gas-solid fluidized bed. The model predicts the variation of plenum pressure, bubble volume, and orifice flow rate with time in a manner consistent to that previously reported for gas-liquid systems. For small plenum chambers, bubbles form with greater frequency and smaller detachment volumes compared with bubbles formed with larger plenum chambers. Decreasing plenum volume causes the gas flow rate through the orifice to vary with a lower amplitude and a higher frequency. The calculated variation of bubbling frequency with the volume of the gas chamber is in good qualitative agreement and quite good quantitative agreement, with the experimental results from hot-wire anemometer and pressure fluctuation measurements for a single orifice presented in Chapter 3.

Chapter 6: Conclusions and Recommendations

6.1 Conclusions

Experiments were carried out in a cylindrical fluidization column mounted on an axially symmetric, variable-volume plenum chamber to determine the effect of windbox volume on the hydrodynamics of fluidized beds of glass beads and FCC particles. Two low-pressure-drop distributors were used: one with a single orifice, and the other with 33 orifices having the same total open area as the single orifice.

Pressure and orifice velocity fluctuation measurements were preformed for the single-orifice distributor. The frequency spectrum of the distributor pressure drop fluctuations (differential pressure transducer) shows multiple peaks, as reported by Kage et al. (2000). The sharpest peak is believed to represent the bubbling frequency. As suggested by Nelson et al. (1993) to determine the bubbling frequency, the autocorrelation function also demonstrated strong periodicity corresponding to this peak.

Increasing superficial gas velocity caused a broadening of the sharp peak of bubbling frequency, indicating that at high orifice gas flow rates, bubbling did not occur at a single frequency. This is probably due to multiple bubble formation in the orifice. For a gas-liquid system, McCann and Prince (1969) reported that at high gas flows, pairs of bubbles coalesce close to the orifice. The merged bubbles rose only a small distance above the orifice before shattering into many small bubbles of varying sizes, leading to irregular bubbles. These authors also recorded video movies confirming pair formation in a gas-liquid system of high orifice flow rates. In the present study, a slight decrease in bubbling frequency with increasing orifice flow rate was observed, in agreement with observations of Nguyen and Leung (1972) for a two-dimensional fluidized bed and McCann and Prince (1969) for gas-liquid systems.

For the single-orifice distributor, the bubbling frequency increased slightly with decreasing plenum volume, in agreement with McCann and Prince (1969, 1971) and Kage et al. (2000). This can be explained by the damping effect of the plenum chamber; for a large windbox, the air withdrawn during the formation of each bubble is only a small fraction of the plenum chamber volume, so that a nearly constant pressure is maintained in the windbox. As a

result, depletion of gas in the plenum which is present for small windbox volumes no longer occurs, with the result that bubbles are larger, and hence the frequency is lower, for large plenum chambers at the same gas flowrate. Another effect of the plenum chamber volume was revealed by the autocorrelation function which determines the periodicity of pressure-time signals. With decreasing plenum volume, the autocorrelation revealed more periodic fluctuations in the plenum chamber. Moreover, by reducing the plenum volume, pressure signals from the plenum chamber matched the pressure fluctuations of the distributor pressure drop and at the bottom of the bed. This can be explained by relating the pressure fluctuations of the plenum chamber and bed suggested by Sierra and Tadrist (2000).

Increasing the bed depth resulted in a slight lowering of the bubble frequency, probably because of imposing more compression at the orifice, causing the air to enter the bed at a lower velocity for constant superficial gas velocity, determined at the bed surface.

In addition to the bubble frequency, a second sharp peak of lower frequency appeared in the frequency spectrum from the single-orifice distributor experiments. This frequency did not change significantly with varying plenum volume. On the other hand, increasing the bed height caused this frequency to decrease, whereas it appeared to be independent of the superficial gas velocity. It appeares likely that bursting bubbles at the surface of the fluidized bed were the source of these fluctuations. Quite good agreement was found between experimental results for this frequency and the model of Baskakov et al. (1986), which is based on an analogy between bubble eruption at the bed surface and oscillation of an ideal liquid in a U-tube of constant cross-sectional area.

A custom-made hot-wire anemometer measured orifice velocity fluctuations. Two peaks were found in the frequency spectrum from the orifice velocity fluctuations. One of these frequencies matched the bubbling frequency estimated from pressure fluctuations, decreasing with increasing plenum volume (the same trend as from the pressure fluctuation measurements). The second major peak in the frequency spectrum appeared to be related to bubble eruption at the surface of the fluidized bed since it migrated to lower frequency with increasing bed depth.

Effects of gas superficial velocity and bed depth on frequency spectra for the multi-orifice distributor were similar to those for the single-orifice distributor. Decreasing plenum volume caused the broad frequency spectrum of the plenum pressure fluctuations to move slightly towards higher frequencies. This may be related to the natural frequency of self-excited oscillations of gas in the plenum chamber. In addition, the frequency spectrum narrowed to a more specific frequency with decreasing plenum volume. It can be concluded that for small plenum chambers, coordinated or coherent in-phase bubbling occurs, compared with more random bubbling, leading to broader frequency spectra, for larger windbox volumes.

A two-stage mechanistic model was developed for bubble formation. This model predicted a decrease of bubble frequency at the distributor with increasing plenum volume. Variations of plenum pressure, bubble volume, and orifice flow rate with time are predicted to have similar trends as for gas-liquid systems. The model predicts that decreasing plenum volume leads to smaller and more frequent bubbles than for larger plenum volumes. Moreover, gas flow rate through the orifice varies with lower amplitude and higher frequency with decreasing windbox volume. The model predictions were in a reasonable agreement with pressure and velocity fluctuation measurements.

The Van der Schaaf et al. (2002) approach for estimating bubble size based on the incoherent part of pressure fluctuations has some defects when applied to beds of small plenum volume. This occurs due to several reasons. First, the bubbling frequency decreases with increasing plenum volume. As a result for the same superficial gas velocity larger bubbles are more probable for large plenum volume, whereas the Van der Schaaf et al. (2002) approach predicts larger bubbles for a small plenum volume. The other reason can be expressed by relating the plenum pressure fluctuations to the bed pressure fluctuations. For small plenum chambers, windbox pressure fluctuations match bed pressure fluctuations, so they are more coherent for small plenum chambers, as confirmed experimentally. But the Van der Schaaf et al. procedure predicts higher values of the incoherent part of pressure fluctuations for small plenum volumes, resulting in predicting larger bubbles. Moreover, the mechanistic model predicts decreasing bubble volume with decreasing plenum volume.

6.2 Recommendations

- In addition to time and frequency analysis of pressure fluctuations, state space (chaotic) analysis is needed to investigate pressure waves further in order to understand more fully the effects of the plenum chamber on fluidized bed hydrodynamics.

- Experiments with other types of bed materials, such as coarse particles of Geldart group D, and very fine particles corresponding to Geldart group C, are needed to determine whether the plenum chamber volume has the same effect on fluidized bed hydrodynamics over a broader spectrum of bed material properties.

- Other factors, ignored in the present model, such as the Basset force, drag force on particles surrounding the bubble, and particle-bubble collision force should be considered in the force balance in order to propose a more comprehensive model for bubble formation in gas-solid fluidized beds. Moreover, better estimation of bubble pressure would assist in finding a more applicable model. Considering more realistic bubble shapes rather than spherical boundaries might also lead to better predictions of bubble formation.

- Using an optical probe or capacitance probe is suggested for bubble size estimation in order to compare experimental results for various plenum volumes with the mechanistic model.

- Different types of distributor such as bubble cap and sparger should be investigated in similar experiments to understand whether the plenum volume influences fluidized bed hydrodynamics in the same manner as for the simple upward-facing horizontal orifices studied here. For constant superficial gas velocity and bed depth, testing distributors of similar geometry but different pressure drops should be used to find the limiting distributor pressure drop beyond which the fluidized bed and plenum chamber are decoupled.

References

Agarwal J. C., Davis W. L., and King D. T. (1962). Fluidized bed coal dryer. *Chemical Engineering Progress, 58*, 85-90.

Baeyens, J., & Geldart, D. (1974). An investigation into slugging fluidized beds. *Chemical Engineering Science, 29*, 255-265.

Baird, M. H. I., & Klein, A. J. (1973). Spontaneous oscillation of a gas-fluidised bed. *Chemical Engineering Science, 28*, 1039-1048.

Baskakov, A. P., Tuponogov, V. G., & Filippovsky, N. F. (1986). A study of pressure fluctuations in a bubbling fluidized bed. *Powder Technology, 45*, 113-117.

Bendat, J. S., & Piersol, A. G. (2000). *Random Data. Analysis and Measurements Procedures,* John Wiley and Sons, New York.

Bi, H. T. (2007). A critical review of the complex pressure fluctuation phenomenon in gas–solids fluidized beds. *Chemical Engineering Science, 62*, 3473-3493.

Brown, R. C., & Brue, E. (2001). Resolving dynamical features of fluidized beds from pressure fluctuations. *Powder Technology, 119*, 68-80.

Darton, R. C., La Nauze, R. D., Davidson, J. F., & Harrison, D. (1977). Bubble growth due to coalescence in fluidized beds. *Chemical Engineering Research and Design, 55*, 274-280.

Davidson, J. F. (1968). First session—introduction by rapporteur. *Inst.Chem.Eng.Symp.Ser, 30*, 3–11.

Davidson, J. F., & Harrison, D. (1973). *Fluidised Particles,* Cambridge University Press, Cambridge, U.K..

Davidson, J. F., & Schuler, B. O. G. (1960a). Bubble formation at an orifice in a viscous liquid. *Chemical Engineering Research and Design, 38*, 144-154.

Davidson, J. F., & Schuler, B. O. G. (1960b). Bubble formation at an orifice in an inviscid liquid. *Chemical Engineering Research and Design, 38*, 335-342.

Fan, L. T., Hiraoka, S., & Shin, S. (1984). Analysis of pressure fluctuations in a gas-solid fluidized bed. *AIChE Journal, 30*, 346-349.

Fan, L. T., Tho-Ching Ho, Hiraoka, S., & Walawender, W. P. (1981). Pressure fluctuations in a fluidized bed. *AIChE Journal, 27*, 388-96.

Geldart, D. (1986). Introduction in D. Geldart (Ed.), *Gas Fluidization Technology.* Chichester, U.K. ; John Wiley & Sons.

Geldart, D., & Baeyens, J. (1985). The design of distributors for gas-fluidized beds. *Powder Technology, 42*, 67-78.

Geldart, D., & Kelsey, J. R. (1968). The influence of the gas distributor on bed expansion, bubble size and bubble frequency in fluidized beds. *Fluidization: I.Chem.E.Symposium Series No. 30,* 114-125.

Grace, J. R. (1970). The viscosity of fluidized beds. *Canadian Journal of Chemical Engineering, 48,* 30-33.

Grace, J. R. (1986). Contacting modes and behaviour classification of gas-solid and other two-phase suspensions. *Canadian Journal of Chemical Engineering, 64*, 353-363.

Harrison, D., & Leung, L. S. (1961). Bubble formation at an orifice in a fluidized bed. *Chemical Engineering Research and Design, 39*, 409-414.

Hauptmann, E. G. (1968). A simple hot wire anemometer probe. *Journal of Scientific Instruments (Physics E), 1,* 874-875.

Hay, J. M., Nelson, B. H., Briens, C. L., & Bergougnou, M. A. (1995). The calculation of the characteristics of a chaotic attractor in a gas-solid fluidized bed. *Chemical Engineering Science, 50,* 373-380.

Hiby, J. W. (1964). Critical minimum pressure drop of the gas distribution plate in fluidized bed units. *Chemical Engineering & Technology, 36*, 228.

Hiby, J. (1967). Periodic phenomena connected with gas-solid fluidization. *Proc.Int.Symp.On Fluidization,* 99-111.

Hsiung, T. P. & Grace, J. R. (1978). Formation of bubbles at an orifice in fluidized beds. *IEEE Conference Record of Annual Pulp and Paper Industry Technical Conference,* 19-24.

Hughes, R. R., Handlos, A. E., Evans, H. D., & Maycock, R. L. (1955). Formation of bubbles at simple orifices. *Chemical Engineering Progress, 51*, 557-563.

Johnsson, F., Zijerveld, R. C., Schouten, J. C., van den Bleek, C. M., & Leckner, B. (2000). Characterization of fluidization regimes by time-series analysis of pressure fluctuations. *International Journal of Multiphase Flow, 26*, 663-715.

Johnsson, F., Larsson, G., & Leckner, B. (2002). Pressure and flow fluctuations in a fluidized bed-interaction with the air-feed system. *Chemical Engineering Science, 57*, 1379-1392.

Kage, H., Agari, M., Ogura, H., & Matsuno, Y. (2000). Frequency analysis of pressure fluctuation in fluidized bed plenum and its confidence limit for detection of various modes of fluidization. *Advanced Powder Technology, 11*, 459-475.

Kage, H., Iwasaki, N., & Matsuno, Y. (1993). Frequency analysis of pressure fluctuation in plenum as a diagnostic method for fluidized beds. *AIChE Symp.Ser, 89*, 184-190.

Kage, H., Iwasaki, N., Yamaguchi, H., & Matsuno, Y. (1991). Frequency analysis of pressure fluctuation in fluidized bed plenum. *Journal of Chemical Engineering of Japan, 24*, 76-81.

Karri, S. B. R., & Werther, J. (2003). Gas distributor and plenum design in fluidized beds, Chapter 8. In W. C. Yang (Ed.), *Handbook of Fluidization and Fluid-Particle Systems* (pp. 155-170). Pittsburgh, Pennsylvania, U.S.A.: Marcel Dekker.

Kato, K., & Wen, C. Y. (1969). Bubble assemblage model for fluidized bed catalytic reactors. *Chemical Engineering Science, 24*, 1351-1369.

Kehoe, P. W. K., & Davidson, J. F. (1973). Pressure fluctuations in slugging fluidized beds. *AIChE Symposium Series, 69*, 30-40.

King, L. V. (1914). On the convection of heat from small cylinders in a stream of fluid: Determination of the convection constants of small platinum wires with applications to hot-wire anemometry. *Philosophical Transactions of the Royal Society of London. Series A, 214*, 373-432.

Kumar, R., & Kuloor, N. R. (1970). The formation of bubbles and drops. *Advances in Chemical Engineering, 8*, 255-368.

Kunii, D., & Levenspiel, O. (1969). *Fluidization Engineering, 2nd.* New York: John Wiley & Sons.

Kupferberg, A., & Jameson, G. J. (1969). Bubble formation at a submerged orifice above a gas chamber of finite volume, *Chemical Engineering Research and Design, 47*, 241-250.

Lamb, H. (1932). *Hydrodynamics*. London, U.K.: Cambridge University Press.

Lirag, R. C. J., & Littman, H. (1971). *Statistical study of the pressure fluctuations in a fluidized bed, AIChE Symp.Ser, 67*, 11-22.

Lomas, C. G. (1986). *Fundamentals of Hot Wire Anemometry*. Cambridge, UK: Cambridge University Press.

McAllister, R. A., McGinnis, P. H., & Plank, C. A. (1958). Perforated-plate performance. *Chemical Engineering Science, 9*, 25-35.

McCann, D. J., & Prince, R. G. H. (1969). Bubble formation and weeping at submerged orifice. *Chemical Engineering Science, 24*, 801-814.

McCann, D. J., & Prince, R. G. H. (1971). Regimes of bubbling at a submerged orifice. *Chemical Engineering Science, 26*, 1505-12.

Moritomi, H., Mori, S., Araki, K., & Moriyama, A. (1980). Periodic pressure fluctuations in a gaseous fluidized bed. *Kagaku Kogaku Ronbushu, 6*, 392-396.

Morris, S. C., & Foss, J. F. (2003). Transient thermal response of a hot-wire anemometer. *Measurement Science and Technology, 14*, 251-259.

Murray, J. D. (1965). On the mathematics of fluidization, part 2. steady motion of fully developed bubbles. *Journal of Fluid Mechanics, 22*, 57-80.

Nelson, B. H., Briens, C. L., & Bergougnou, M. A. (1993). Pressure fluctuations at individual grid holes of a gas-solid fluidized bed. *Powder Technology, 77*, 95-102.

Nguyen, X. T., & Leung, L. S. (1972). A note on bubble formation at an orifice in a fluidised bed. *Chemical Engineering Science, 27*, 1748-1750.

Peirano, E., Delloume, V., Johnsson, F., Leckner, B., & Simonin, O. (2002). Numerical simulation of the fluid dynamics of a freely bubbling fluidized bed: Influence of the air supply system. *Powder Technology, 122*, 69-82.

Perry, A. E. (1982). *Hot-Wire Anemometry*. New York: Oxford University Press.

Pianarosa, D. L. (1996). Hydrodynamic studies of spouted and spout-fluid beds. (M.A.Sc Thesis, Chemical & Biological Engineering Department, University of British Columbia).

Qureshi, A. E., & Creasy, D. E. (1979). Fluidised bed gas distributors. *Powder Technology, 22*, 113-119.

Ramakrishnan, S., Kumar, R., & Kuloor, N. R. (1969). Studies in bubble formation—I bubble formation under constant flow conditions. *Chemical Engineering Science, 24*, 731-747.

Roy, R., Davidson, J. F., & Tuponogov, V. G. (1990). The velocity of sound in fluidized beds. *Chemical Engineering Science, 45*, 3233-3245.

Sasic, S., Johnsson, F., & Leckner, B. (2004). Interaction between a fluidized bed and its air-supply system: Some observations. *Industrial and Engineering Chemistry Research, 43*, 5730-5737.

Sasic, S., Leckner, B., & Johnsson, F. (2005). Fluctuations and waves in fluidized bed systems: The influence of the air-supply system. *Powder Technology, 153*, 176-195.

Sasic, S., Leckner, B., & Johnsson, F. (2007). Characterization of fluid dynamics of fluidized beds by analysis of pressure fluctuations. *Progress in Energy and Combustion Science, 33*, 453-496.

Sathiyamoorthy, D., & Sridhar Rao, C. (1977). Gas distributors in fluidized bed. *Powder Technology, 20*, 47.

Sathiyamoorthy, D., & Sridhar Rao, C. (1981). The choice of distributor to bed pressure drop ratio in gas fluidised beds. *Powder Technology, 30*, 139-143.

Satyanarayan, A., Kumar, R., & Kuloor, N. R. (1969). Studies in bubble formation—II bubble formation under constant pressure conditions. *Chemical Engineering Science, 24*, 749-761.

Sierra, C., & Tadrist, L. (2000). About frequency coupling between riser and plenum in a gas fluidized bed. *Comptes Rendus de l'Academie des Sciences, Series IIB, Mechanics Physics Astronomy, 328*, 323-328.

Sun, J. G., Chen, M. M., & Chao, B. T. (1994). Modeling of solids global fluctuations in bubbling fluidized beds by standing surface waves. *International Journal of Multiphase Flow, 20*, 315-338.

Svensson, A., Johnsson, F., & Leckner, B. (1996). Fluidization regimes in non-slugging fluidized beds: The influence of pressure drop across the air distributor. *Powder Technology, 86*, 299-312.

Tamarin, A. I. (1964). The origin of self-excited oscillations in fluidized beds. *Int.Chem.Eng, 4*, 50-54.

Tsuge, H., & Hibino, S. I. (1983). Bubble formation from an orifice submerged in liquids. *Chemical Engineering Communications, 22*, 63-79.

Van der Schaaf, J., Schouten, J. C., Johnsson, F., & van den Bleek, C.M. (1999). Multiple modes of bed mass oscillation in gas–solids fluidized beds. *Proceedings of the 15th International Conference on Fluidized Bed Combustion ASME, New York, Paper No.FBC99-0201.*

Van der Schaaf, J., Schouten, J. C., Johnsson, F., & van den Bleek, C. M. (2002). Non-intrusive determination of bubble and slug length scales in fluidized beds by decomposition of the power spectral density of pressure time series. *International Journal of Multiphase Flow, 28*, 865-880.

Van der Schaaf, J., Schouten, J. C., & van den Bleek, C. M. (1998). Origin, propagation and attenuation of pressure waves in gas—solid fluidized beds. *Powder Technology, 95*, 220-233.

Van Ommen, J. Ruud, Schouten, J. C., vander Stappen, Michel L.M., & van den Bleek, Cor M. (1999). Response characteristics of probe-transducer systems for pressure measurements in

gas-solid fluidized beds: How to prevent pitfalls in dynamic pressure measurements. *Powder Technology, 106*, 199-218.

Verloop, J., & Heertjes, P. M. (1974). On the origin of bubbles in gas-fluidized beds. *Chemical Engineering Science, 29*, 1101-1107.

Welch, P. D., (1967). The use of fast Fourier transform for the estimation of power spectra. *IEEE Transactions on Audio Electroacoustic, AU-15*, 70-73

Whitehead, A. B. (1971). Some problems in large scale fluidized bed. In J. F. Davidson, & D. Harrison (Eds.), *Fluidization* (pp. 781-814). London: Academic Press.

Williams, J. (1984). Thermal techniques in measurement and control circuitry. *Linear Applications Handbook* (pp. 7-8) Linear Technology.

Wong, H. W., & Baird, M. H. I. (1971). Fluidisation in a pulsed gas flow. *Chemical Engineering Journal, 2*, 104-113.

Xie, H. , & Geldart, D. (1997). Response time of pressure probes. *Powder Technology, 90*, 149-151.

Yang, G. Q., Luo, X., Lau, R., & Fan, L. S. (2000). Bubble formation in high-pressure liquid-solid suspensions with plenum pressure fluctuation. *AICHE Journal, 46*, 2162-2174.

Appendix A

LabVIEW Program to Acquire Pressure Signals

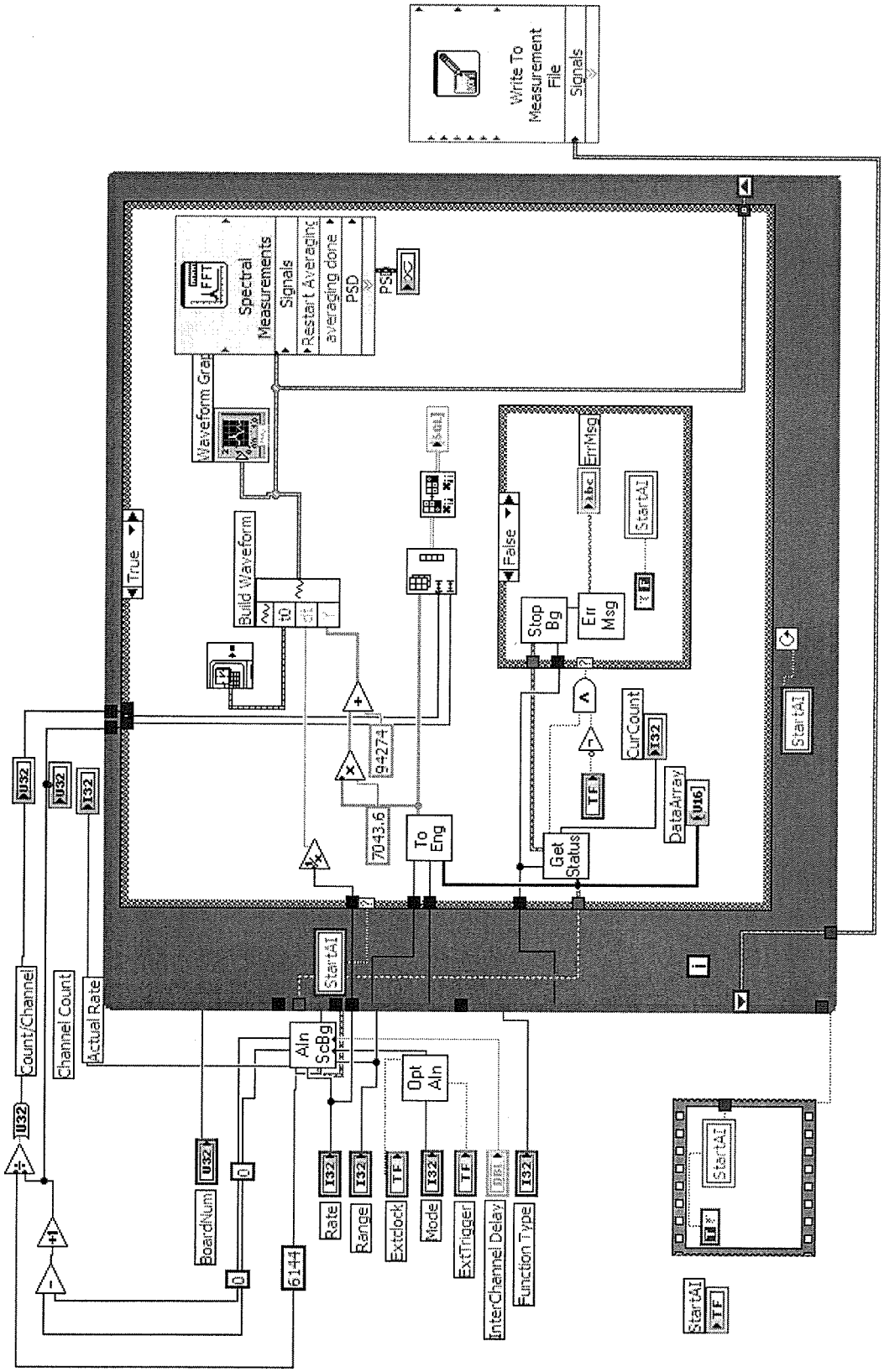

Appendix B

Welch's Procedure for Direct Computation of Power Spectral Density FFT

An infinite range Fourier transform of a real valued or complex-valued record, x(t), is defined by the complex-valued quantity:

$$X(f) = \int_{-\infty}^{+\infty} x(t) e^{-j2\pi ft}\, dt \tag{A.1}$$

By restricting the limits to finite time interval 0 to T, the finite-range Fourier transform is:

$$X(f,T) = \int_{0}^{T} x(t) e^{-j2\pi ft}\, dt \tag{A.2}$$

Assuming that $x(t)$ is sampled at N equally spaced intervals, Δt, where Δt has been selected to produce a sufficiently high cut-off frequency, then the sampling times are $t_n = n\,\Delta t$, and the samples are $x_n = x(n\,\Delta t)$ with $n=0,1,2\ldots,N-1$. Therefore, the finite range Fourier transforms can be expressed as

$$X(f,T) = \Delta t \sum_{n=0}^{N-1} x_n \exp[-j2\pi fn\Delta t] \tag{A.3}$$

The normal selection of the discrete frequency values for the computation of $X(f,T)$ is

$$f_k = \frac{k}{T} = \frac{k}{N\Delta t}, \qquad k = 0,1,2,\ldots,N-1, \tag{A.4}$$

At these frequencies, the transformed values give the Fourier components defined by

$$X_k = \frac{X(f_k,T)}{\Delta t} = \sum_{n=0}^{N-1} x_n \exp\left[-j\frac{2\pi kn}{N}\right], \qquad k = 0,1,2,\ldots,N-1, \tag{A.5}$$

The power spectral density function can be calculated as

$$S_{xx}(f) = \frac{1}{n_d \Delta T} \sum_{i=1}^{n_d} \frac{|X_k(f,T)|^2}{N}, \qquad k = 0,1,2,\ldots,N-1, \tag{A.6}$$

where $|X_k(f,T)|^2 / N$ is often called a periodogram.

Welch (1967) has introduced a simple procedure for direct computation of the power spectral density using Fast Fourier Transform (FFT) with suitable resolution and confidence. Assuming a set of data, $x(n)$ with $0 \le n \le N$, divided into $K=N/M$ segments of M samples each:

$$x^{(i)}(n) = x(n + iM - M) \qquad 0 \le n \le M-1 \qquad 1 \le i \le K \tag{A.7}$$

Window $W(n)$ is next applied directly to the data segments before computing the periodograms.

$$J_M^{(i)}(\omega) = \frac{1}{MU}\left|\sum_{n=0}^{M-1} x^{(i)}(n)\omega(n)e^{-j\omega n}\right|^2 \qquad i = 1,2,...,K \tag{A.8}$$

where $\omega(n)$ is the applied window, i.e., inverse Fourier transform of spectrum window $W(e^{j\omega})$, with

$$U = \frac{1}{M}\sum_{n=0}^{M-1}\omega^2(n) \tag{A.9}$$

$$\omega(n) = \frac{1}{2\pi}\int_{-\pi}^{\pi} W(e^{j\omega})e^{j\omega}d\omega \tag{A.10}$$

The spectrum estimate is defined as:

$$B_{xx}^{\omega}(\omega) = \frac{1}{K}\sum_{i=1}^{K} J_M^{(i)}(\omega) \tag{A.11}$$

FFT provides an efficient means of computing an estimate for the power spectrum at equally spaced intervals ($\omega=(2\pi/M)K$). Therefore, a spectrum can be estimated at equally spaced frequencies by averaging the periodograms in the Welch's method by:

$$B_{xx}^{\omega}(\frac{2\pi}{M}k) = \frac{1}{K}\sum_{i=1}^{K} J_M^{(i)}(\frac{2\pi}{M}k), \qquad k = 0,1,2,...,M-1, \tag{A.12}$$

where

$$J_M^{(i)}(\frac{2\pi}{M}k) = \frac{1}{MU}\left|\sum_{n=0}^{M-1} x^{(i)}(n)\omega(n)e^{-2(2\pi/M)kn}\right|^2, i = 1,2,...,K \qquad k = 0,1,2,...,M-1,$$

(A.13)

$$J_M^{(i)}(\frac{2\pi}{M}k) = \frac{1}{MU}\left|X_M^i(k)\right|^2 \tag{A.14}$$

with

$$X_M^i(k) = \sum_{n=0}^{M-1} x^{(i)}(n)\omega(n)e^{-2(2\pi/M)kn}, \qquad k = 0,1,2,...,M-1 \tag{A.15}$$

The spectrum can be estimated by first computing $X_M^i(k)$ with an appropriate FFT algorithm and then computing $J_M^{(i)}(2\pi k/M)$ from Equation (A.14) for each section. When all K estimates are accumulated, Equation (A.12) is used to compute this estimate. This simple procedure

results in a direct estimate of the power spectral density function, which will always be non-negative.

Appendix C

LabVIEW Program to Estimate CPSD and Bubble Size

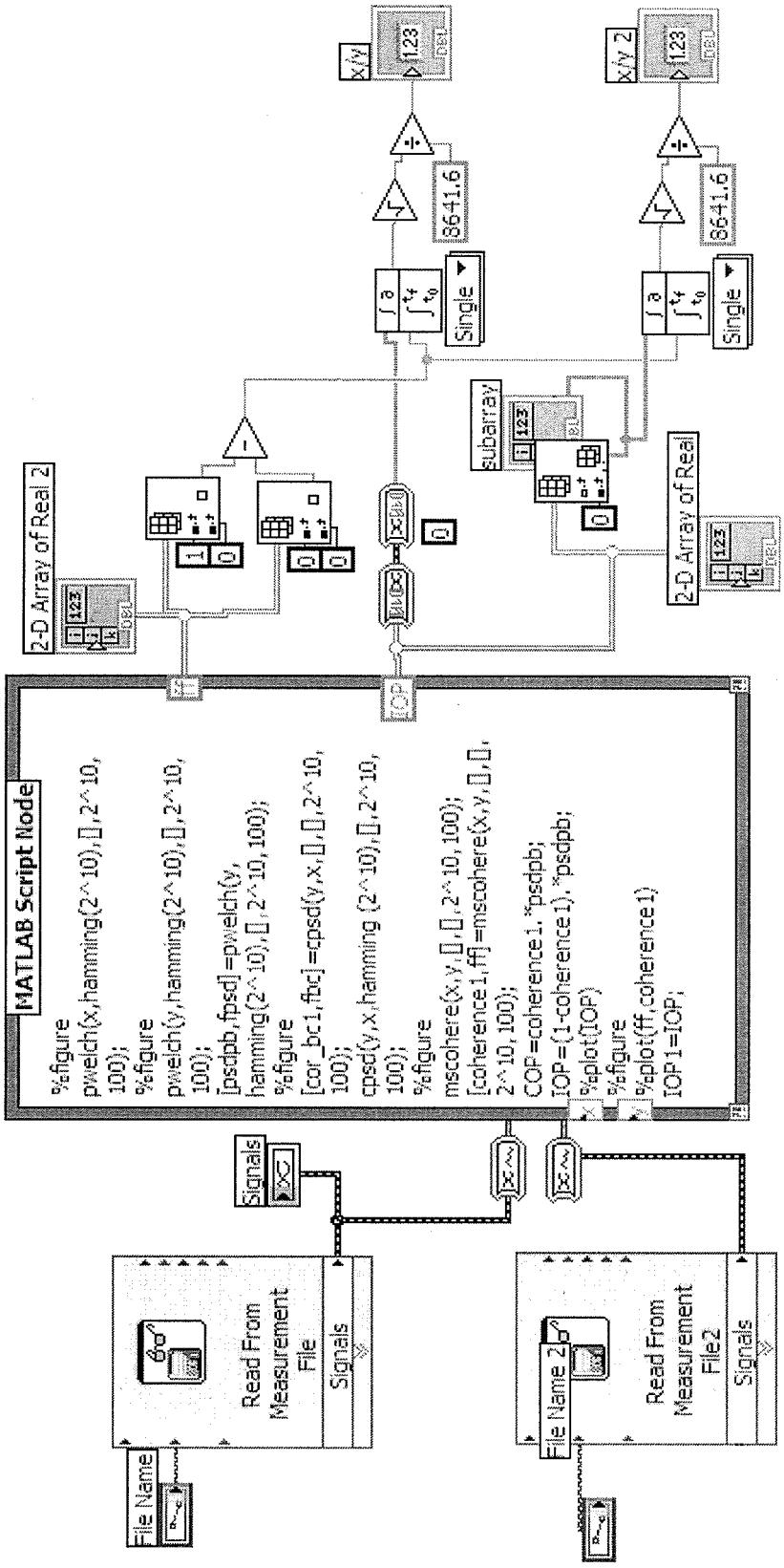

Appendix D

LabVIEW Program to Calculate PSD and Autocorrelation Function

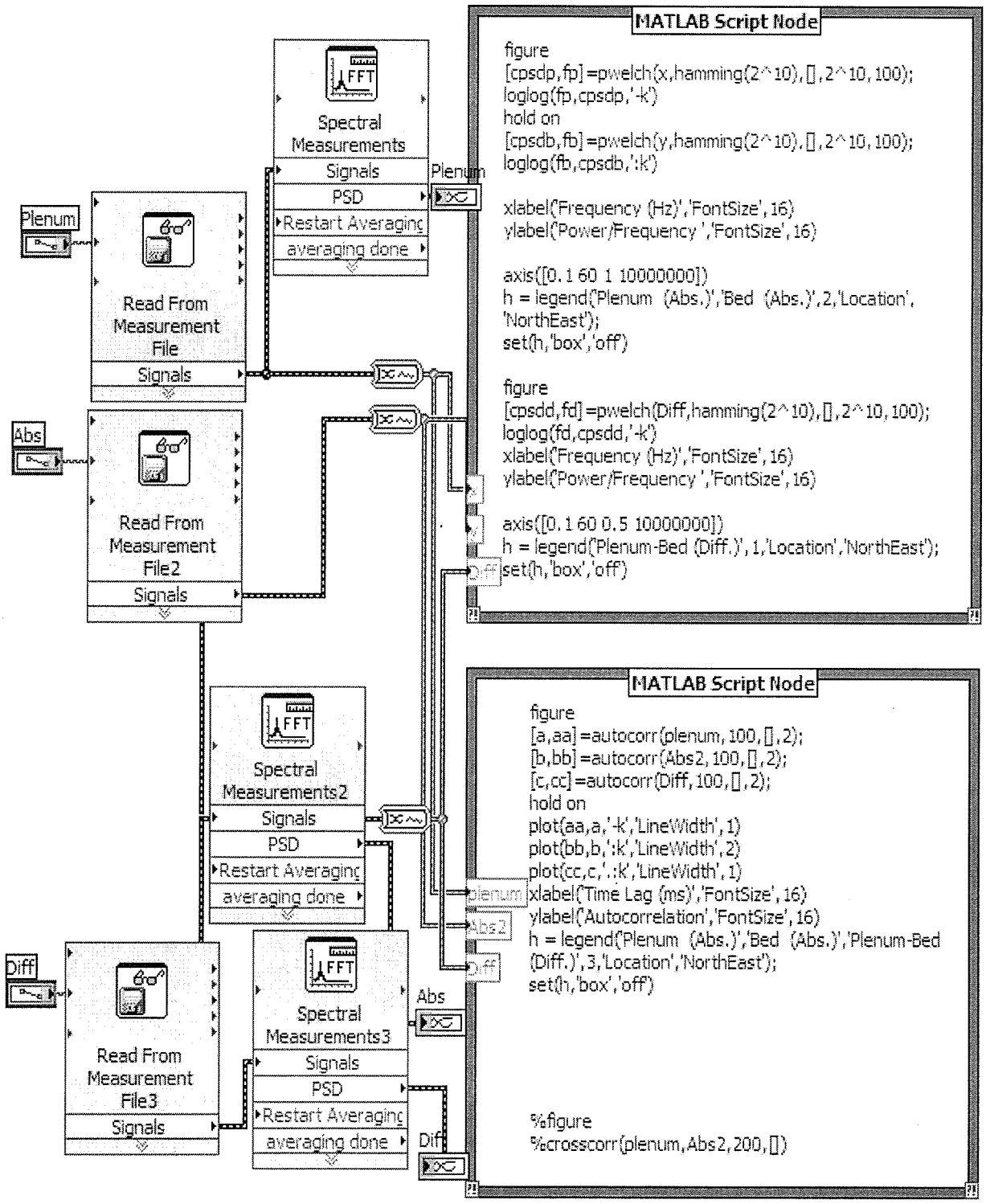

Appendix E

Computer Program for Modeling of Bubble Formation

```
% This program was used to model the bubble formation at a single orifice
% in  a gas-solid system by considering two stages of bubble formation:
% Expansion and Detachment stages. Fourth order Runge-Kutta method was used
% to solve the differential equations for each stage.
clc
t0=2;
N=100;
gravity=9.82;
bulk_density=1125.66;                          % glass beads
%bulk_density=720;                             % FCC
gas_density=1.205;
gas_viscosity=1.73*1e-5;
Patm=101325;
r0=0.006;
D0=0.012;
gama=1.4;
Qg=8.29e-4;                                    % glass beads
%Qg=2e-4;                                      % FCC
Umf=0.0279;
Utf=Umf;
Vp=0.0425;
height=0.10;
L=0.0095;
bulk_viscosity=8;                              % glass beads
%bulk_viscosity=4;                             % FCC

          Kuttaa_expansion(0, t0, N, [0.006;102430.4;0])
```

```
function Kuttaa_expansion(a, b, N, alpha)

% This function solve related equations for expansion stage
gravity=9.82;
bulk_density=1125.66;                          % glass beads
%bulk_density=720;                             % FCC
gas_density=1.205;
gas_viscosity=1.73*1e-5;
Patm=101325;
r0=0.006;
D0=0.012;
gama=1.4;
Qg=8.29e-4;                                    % glass beads
%Qg=2e-4;                                      % FCC
Umf=0.0279;
Utf=Umf;
Vp=0.0425;
heiht=0.10;
L=0.0095;
bulk_viscosity=8;                              % glass beads
%bulk_viscosity=4;                             % FCC
w(1,1)=0.006;
```

```
w(2,1)=102430;
w(3,1)=0;
cg=1.5+(16*pi*gas_viscosity*L/gas_density).*1./Qg;
K0=(2./(gas_density.*cg)).^0.5.*(pi.*r0.^2);

m = size(alpha,1);
if m == 1
   alpha = alpha';
end

h = (b-a)/N;          %the step size
t(1) = a;
w(:,1) = alpha;       %initial conditions

for i = 1:N

        k1 = h*f(t(i), w(:,i));
        k2 = h*f(t(i)+h/2, w(:,i)+0.5*k1);
        k3 = h*f(t(i)+h/2, w(:,i)+0.5*k2);
        k4 = h*f(t(i)+h, w(:,i)+k3);
        w(:,i+1) = w(:,i) + (k1 + 2*k2 + 2*k3 + k4)/6;
        t(i+1) = a + i*h;
        t

   if abs(4/3.*pi.*(bulk_density-
gas_density).*w(1,i).^3.*gravity+(gas_density./(pi.*r0.^2)).*(4.*pi.*w(1,i).
^2.*w(3,i)+Utf.*pi.*w(1,i).^2).^2-
(4/3.*pi.*(11/16.*bulk_density+gas_density).*(3.*w(3,i).^2.*w(1,i).^2+w(1,i)
.^3.*((1./w(1,i)).*((w(2,i)-
((1./K0).*(4.*pi.*w(1,i).^2.*w(3,i)+Utf.*pi.*w(1,i).^2)).^2-
Patm)./bulk_density-gravity.*height+gravity.*(w(1,i)-r0)-
1.5.*w(3,i).^2)))+6.*pi.*0.8.*w(1,i).*w(2,i)))<0.001

      [tt wd]=Kuttaa_detachment(t(i), b, N,
[w(1,i);w(2,i);w(3,i);w(1,i);w(3,i)]);
       t;
       tt=tt';
       wd=wd';
       wd1=wd(1,:);
       wd2=wd(2,:);
       wd3=wd(3,:);
       wdd=vertcat(wd1,wd2,wd3);
      time=horzcat(t,tt);
      result=horzcat(w,wdd);

% [t' w'];
time=time';
result=result';
p=result(:,2);
r=result(:,1);
plot(time,p,'r')
figure
plot(time,r,'g')

   break
```

```
   end

end
time=t';
result=w';
p=result(:,2);
p=p-Patm-bulk_density.*gravity.*height;
r=result(:,1);
Vb=4/3.*pi.*r.^3;
Q=pi*Utf.*r.^2+4*pi.*r.^2.*result(:,3);
plot(time,p)
figure
plot(time,Vb)
figure
plot(time,Q)
figure
plot(time,r)
-----------------------------------------------------------------------

function dy = f(t, y)

% This function contains equations for the Expansion stage
gravity=9.82;
bulk_density=1125.66;                          % glass beads
%bulk_density=720;                             % FCC
gas_density=1.205;
gas_viscosity=1.73*1e-5;
Patm=101325;
r0=0.006;
D0=0.012;
gama=1.4;
Qg=8.29e-4;                                    % glass beads
%Qg=2e-4;                                      % FCC
Umf=0.0279;
Utf=Umf;
Vp=0.0425;
height=0.10;
L=0.0095;
bulk_viscosity=8;                              % glass beads
%bulk_viscosity=4;                             % FCC
cg=1.5+(16*pi*gas_viscosity*L/gas_density).*1./(4.*pi.*y(1).^2.*y(3)+Utf.*pi
.*y(1).^2);
K0=(2./(gas_density.*cg)).^0.5.*(pi.*r0.^2);

dy = [y(3);
      (gama.*y(2)./Vp).*(Qg-(4.*pi.*y(1).^2.*y(3)+Utf.*pi.*y(1).^2));
      (1./y(1)).*((y(2)-
((1./K0).*(4.*pi.*y(1).^2.*y(3)+Utf.*pi.*y(1).^2)).^2-
Patm)./(8.919.*bulk_density)-gravity.*height./8.919+gravity.*(y(1)-
r0)./8.919-1.5.*y(3).^2)];
-----------------------------------------------------------------------

function [tt wd]=Kuttaa_detachment(a, b, N, alpha)

mm = size(alpha,1);
if mm == 1
```

```
   alpha = alpha';
end

h = (b-a)/N;         %the step size
tt(1) = a;
wd(:,1) = alpha;      %initial conditions

for ii = 1:N
      k1 = h*ff(tt(ii), wd(:,ii));
      k2 = h*ff(tt(ii)+h/2, wd(:,ii)+0.5*k1);
      k3 = h*ff(tt(ii)+h/2, wd(:,ii)+0.5*k2);
      k4 = h*ff(tt(ii)+h, wd(:,ii)+k3);
      wd(:,ii+1) = wd(:,ii) + (k1 + 2*k2 + 2*k3 + k4)/6;
      tt(ii+1) = a + ii*h;
      if abs(wd(4,ii)-(wd(1,ii)+D0)<1e-6
            tt=tt';
            wd=wd';
            [tt wd];
            break
      end
end
tt=tt';
wd=wd';
[tt wd];
--------------------------------------------------------------------------

function dy = ff(t, y)

% This function contains equations for the Detachment stage
gravity=9.82;
bulk_density=1125.66;                          % glass beads
%bulk_density=720;                               % FCC
gas_density=1.205;
gas_viscosity=1.73*1e-5;
Patm=101325;
r0=0.006;
D0=0.012;
gama=1.4;
Qg=8.29e-4;                                    % glass beads
%Qg=5.7e-4;                                      % FCC
Umf=0.0279;
Utf=Umf;
Vp=0.0425;
height=0.1;
L=0.0095;
bulk_viscosity=8;                              % glass beads
%bulk_viscosity=4;                             % FCC
cg=1.5+(16*pi*gas_viscosity*L/gas_density).*1./(4.*pi.*y(1).^2.*y(3)+Utf.*pi
.*y(1).^2);
K0=(2./(gas_density.*cg)).^0.5.*(pi.*r0.^2);


dy = [y(3);
      (gama.*y(2)./Vp).*(Qg-(4.*pi.*y(1).^2.*y(3)+Utf.*pi.*y(1).^2));
      (1./y(1)).*((y(2)-
((1./K0).*(4.*pi.*y(1).^2.*y(3)+Utf.*pi.*y(1).^2)).^2-
```

```
Patm)./(8.919.*bulk_density)-gravity.*height./8.919+gravity.*(y(1)-
r0)./8.919-1.5.*y(3).^2);
      y(5);
(1./y(3).^3).*((1./(4/3.*pi.*(11/16.*bulk_density+gas_density))).*((bulk_den
sity-
gas_density).*4/3.*pi.*y(1).^3.*gravity+gas_density./(pi.*r0.^2).*(4.*pi.*y(
1).^2.*y(3)+Utf.*pi.*y(1).^2+pi.*r0.^2.*(y(5)-y(3))).^2-
6.*pi.*0.8.*y(1).*y(5))-3.*y(1).^2.*y(5).*y(3))];
```